7-9-2009

Modeling riparian groundwater depth as a function of river flow for the Rio Grande at Albuquerque, NM

Kelly Isaacson

Kelly Isaacson
Candidate

Civil Engineering
Department

This thesis is approved, and it is acceptable in quality and form for publication:

Approved by the Thesis Committee:

Julie Coonrod, Chairperson

Venkatesh Merwade

JShormont

MODELING RIPARIAN GROUNDWATER DEPTH AS A FUNCTION OF RIVER FLOW FOR THE RIO GRANDE AT ALBUQUERQUE, NM

BY

KELLY ISAACSON

B.S. ENGINEERING PHYSICS, TAYLOR UNIVERSITY, 2006

THESIS

Submitted in Partial Fulfillment of the
Requirements for the Degree of

Master of Science
Civil Engineering

The University of New Mexico
Albuquerque, New Mexico

May, 2009

ACKNOWLEDGEMENTS

First, I must thank God for the gift of life and leading me here to study such an interesting field. If God were not full of mercy, I would never have made it to the beginning of this program, much less the end.

My gratitude to Dr. Julie Coonrod is beyond words. She made my graduate work possible, inspired me in her dedication to her family and her work, and has provided many opportunities for professional development. In addition to being the best advisor in the department, Julie has been one of the most important mentors of my life and has listened, encouraged, and supported me way beyond the call of duty, and I am privileged to call her a friend.

Dr. John Stormont and Dr. Venkatesh Merwade were extremely supportive committee members who supplied their technical expertise .

I would like to thank my family for their support. Thanks to my mother Gerri for investing her life in mine in – I am the person I am today in a large part because of you. Thanks to my daddy Steve for all the late night talks in the kitchen, for knowing a little about everything and always being willing to share, and for all your assistance on all problems math, boy, Excel, or computer related. Shout out to my siblings Stephanie, Timothy, Mandy, and Sven. Thanks for loving me despite myself and for reminding me not to take life so seriously. I love you all.

I also need to thank several people who have assisted me in various ways with this project. Andy MacLeod kindly answered many Geo-RAS questions and provided his expertise. Jungseok Ho and Christian LeJeune spent lots of time with me in the field. George Seiber of the USGS spent hours of his time explaining their procedures, providing data, and reviewing Chapter Three. Mark Roark and Dale Rankin at the USGS also provided technical expertise and data. Dr. Tim Ward graciously provided very instructive comments on Chapter Three that improved clarity and development. Jed Frechette has spent many hours with me writing and debugging the Python code used in Chapter Four, and Steve Isaacson wrote the VB program used to process the groundwater data. I am also grateful to Ben Swanson, James Cleverly, Jen Tichy, Carolyn Donnelly, Nabil Shafike, Cliff Wilke, Isaiah Pedro, Bruce Thomson, Dean Djokic, Amit Sinha, and Raghavendra Vemula for field assistance or technical support.

Many people have made this journey bearable, and I am indebted to them for their encouragement and support: Iphigenia Kerfoot, Scott Emerson, Ryan Schnalzer, Emily and James Price, Kim Kerfoot, Josh Goldman, Odell Lee, Elizabeth Field, Alandren Etlantus, Sarah Tuite, Christina Leibner, Scott Sadlon, Kirill Trapeznikov, Kerry Howe, Barbara Kimbell, Luke Smith, Todd Marti, Nelson Bernardo, Belle Rehder, Yolanda Sanchez, and Phyllis Taylor.

The US Army Corps of Engineers funded this research through the Arid Regions/Urban Flood Reduction and Channel Restoration Program.

MODELING RIPARIAN GROUNDWATER DEPTH AS A FUNCTION OF RIVER FLOW FOR THE RIO GRANDE AT ALBUQUERQUE, NM

BY

KELLY ISAACSON

ABSTRACT OF THESIS

Submitted in Partial Fulfillment of the
Requirements for the Degree of

Master of Science
Civil Engineering

The University of New Mexico
Albuquerque, New Mexico

May, 2009

MODELING RIPARIAN GRONDWATER DEPTH AS A FUNCTION OF RIVER FLOW FOR THE RIO GRANDE AT ALBUQUERQUE, NM

by

Kelly Isaacson

B.S., Engineering Physics, Taylor University, 2006
M.S., Civil Engineering, University of New Mexico, 2009

ABSTRACT

Riparian corridor ecological health is strongly tied to river streamflow. As climate change threatens to significantly reduce monthly streamflows in semi-arid regions, riparian groundwater will be similarly reduced, impacting native and non-native flora. This paper presents a geographic information system (GIS) based approach for creating comprehensive riparian water surfaces from point surface water and groundwater measurements. These water surfaces are used to calculate depth to groundwater as a function of river discharge for the study reach in Albuquerque, NM, USA. A one dimensional hydraulic model, calibrated with USGS streamflow data, was used to interpolate streamflow measurements throughout the study reach and provide the river water surface elevation for the entire river. The limitations of streamflow measurements in sand bed rivers are presented along with guidance on using stage-discharge curve data to calibrate hydraulic models.

A GIS model that combines groundwater measurements and interpolated river water surfaces to produce comprehensive water surfaces for the entire riparian corridor is presented. Groundwater gradient from the river is calculated to interpolate the riparian water surface between well sites. For the study reach, the groundwater gradient is determined to be approximately linear on each side of the river and primarily controlled by urban groundwater pumping. Depth to groundwater is calculated by subtracting the water surface from the terrain. The impact of river discharge on depth to groundwater is

analyzed. The reduction in depth to groundwater for a given discharge on the falling side of the hydrograph versus the rising side of the hydrograph is quantified. Native and non-native riparian species have different tolerances for groundwater depth: the impact of different flow rates on the ability of species to survive is presented. The depth to groundwater grids as a function of discharge provide a baseline model that can be used to predict climate change altered depth to groundwater. Future reductions in streamflow are correlated to new depth to groundwater grids. Although the model and analysis are demonstrated for the study reach, the approach may be utilized for any river system with a similar dataset available.

Table of Contents

List of Figures

List of Tables

1 Introduction

1.1 Motivation

In many water scarce regions, water resources are already over-allocated (Jackson et al 2001, Vörösmarty 2008). This over-allocation results in declining groundwater levels (McAda and Barroll 2002) and rivers that dry up before they reach their historic destinations (i.e. the Rio Grande in North America). Water managers acknowledge the need for improved understanding of the many components of water accounting to try to balance the plethora of ecological, municipal, agricultural, and industrial demands on water systems (Dahm et al. 2002).

An example of taxed water resources is the city of Albuquerque, New Mexico, USA. For most of its history, Albuquerque has relied on groundwater as its sole source of municipal water supply. New research in the early 1990s indicated that the aquifer was being depleted at rates significantly higher than recharge rates, resulting in groundwater mining (McAda and Barroll 2002). This discovery led to a new water supply plan that involved surface water diversion. In the 1960s, the City of Albuquerque acquired water rights to the San Juan River and built a series of tunnels to divert that water from the San Juan River to the Chama River, which is a Rio Grande tributary. This water has traditionally been leased to other users. As of December 2008, the diverted water is taken from the Rio Grande in Albuquerque then treated and distributed as the major portion of municipal water supply. Approximately half of the water diverted will be returned to the Rio Grande at the Southside Water Reclamation plant (www.abcwua.org). This diversion is likely to impact both surface water and groundwater levels in the basin.

Within this context, climate change may significantly alter the water resource regimes of water scarce regions, changing the timing and magnitude of surface runoff and altering evaporation rates (AR4 2007, Seager et al. 2007). These hydrologic changes have significant implications for water resource management strategies. Understanding how climate change may impact freshwater availability can help water managers make informed decisions about current management practices as well as prepare and plan for future conditions.

1.2 Objective

The purpose of this work is to create a tool that predicts groundwater elevation everywhere in a riparian area as a function of river flow rate. This is accomplished by use of two computer software packages: ESRI's ArcGIS and the United States Corps of Engineers' (USACE) Hydraulic Engineering Center's River Analysis System (HEC-RAS). The goal is to utilize a process that takes a digital terrain model, Manning's *n* values, and volumetric flow rate as inputs, then predicts groundwater elevations. First, a hydraulic model is created and calibrated with measured river stage. The surface water elevations are then correlated to measured groundwater levels. This provides a relationship between surface water elevation and groundwater gradients that can be used to predict depth to groundwater for any given flow rate.

In this thesis, the process is utilized to produce comprehensive river-ground water surfaces that correlate river discharge and groundwater gradient. These water surfaces are used to study diversion-dam induced impacts to groundwater levels in the immediate vicinity of the dam. This tool is also used to study management alternatives in the event of altered flow regimes in rivers. This is demonstrated by identifying areas of increased depth to groundwater given a climate change scenario.

The second chapter of this thesis presents a literature review of topics relevant to this research. Chapter Three was written as technical note for submission to American Society of Civil Engineers (ASCE)'s *Hydraulic Engineering*. The fourth chapter was written as a journal article for Water Resources Research. Thus, some information is repeated within the first four chapters. Model utilizations is presented in Chapter Five. Chapter Six ties the five previous chapters together; Chapter Seven presents future work.

1.3 Study Area

The Middle Rio Grande (MRG), for water budgeting purposes, stretches from the Otowi gauge just downstream of Cochiti Dam to the Elephant Butte Dam gauge (Figure 1-1) in the state of New Mexico, USA. This stretch of river is approximately 320 km and drains an approximate area of 39,220 km^2 (Dahm et al. 2002). The semi arid northern portions of the basin receive an average of thirty one cm of precipitation per year, while the arid south receives an annual average of 20 cm (Dahm et al. 2002).

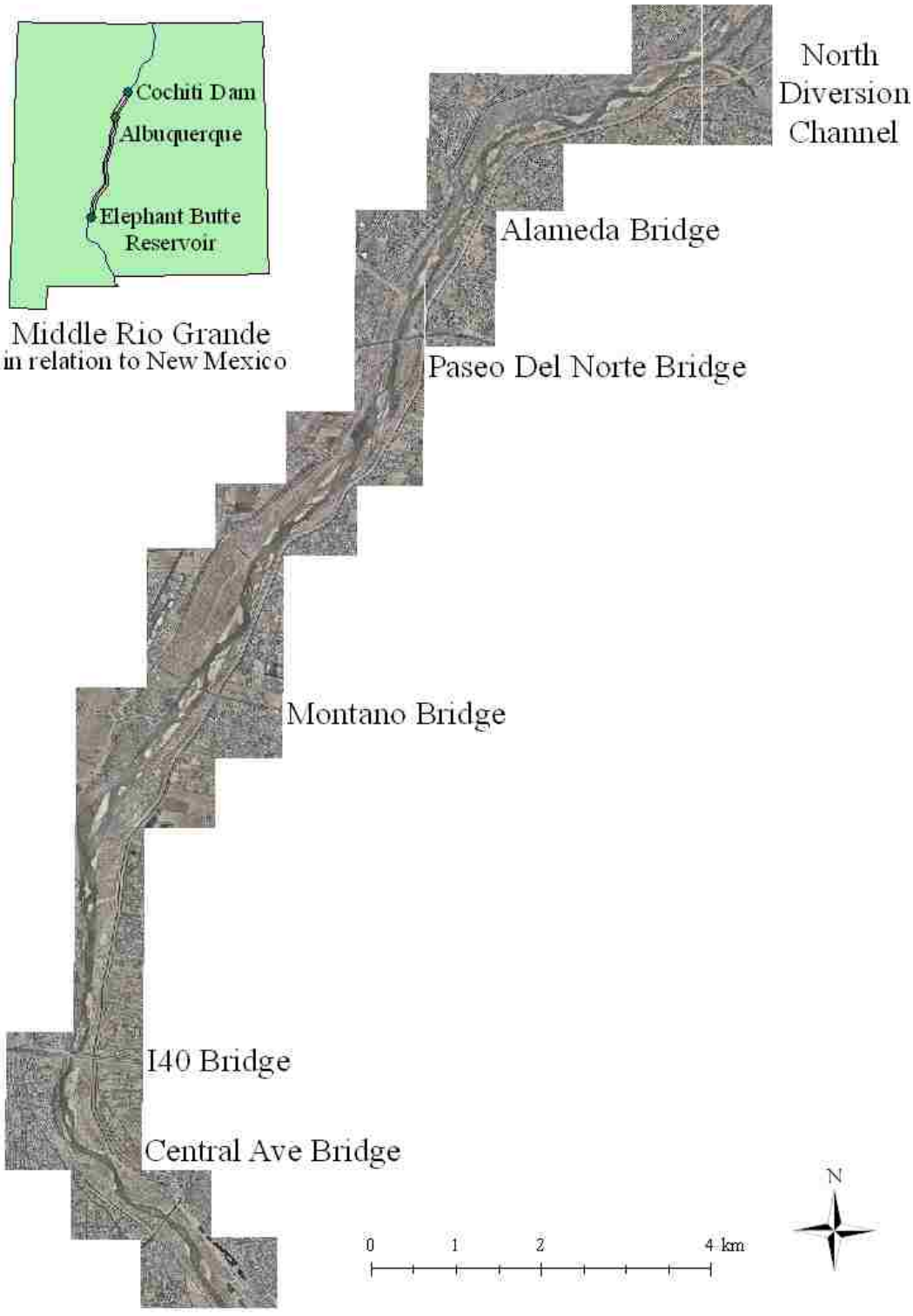

Figure 1-1 The Rio Grande through a portion of Albuquerque, NM, USA

This study considered a portion of the Albuquerque Reach of the MRG from the confluence of the North Diversion Channel with the Rio Grande to 1.2 km downstream of Central Bridge (Figure 1-1). The North Diversion Channel drains a significant portion of the northeast quadrant of Albuquerque and primarily transports precipitation event runoff. The new low-head diversion dam for the San Juan-Chama drinking water project is located in the Rio Grande approximately 500 m south of Alameda Bridge (Figure 1-2). The dam consists of twenty four gates that span the 183 meter width of the Rio Grande; each gate can be individually raised and lowered. The dam was designed to maintain an upstream water depth of approximately one meter while allowing sediment movement through the system. The dam pool is collected by an intake structure on the east bank of the river and transported to a pumping station near the river where is it pumped to a new water treatment plant to be treated for drinking water use.

The diversion dam was completed in January 2006 but was placed down and left inactive until summer 2007. Dam operations testing in summer and fall 2007 focused on optimizing sediment transport through the dam and minimizing sediment intake at the intake structure. The pump station at the river was completed in 2007 and the water treatment plant began trial runs in early fall 2008. Purified river water was first introduced to the water utility distribution system in December 2008. The treated surface water will not eliminate the need for continued aquifer pumping; it is intended as a supplement to reduce groundwater mining. Groundwater is blended with the treatment plant effluent in city reservoirs and then is distributed throughout the system.

The Bosque Ecological Monitoring Program (BEMP) maintains 20 shallow wells in the area of the dam (Figure 1-2). The wells were originally monitored by supervised middle school students on a periodic basis as part of an outreach program. With funding from the USACE, in summer 2006 twelve of the wells were equipped with Solinst Model 3001 Gold Pressure Transducers (Solinst Canada Ltd, Ontario Canada) that record water depth every 15 minutes. By the fall of 2007, the remaining wells were also outfitted with pressure transducers. As part of a large scale project to establish groundwater and surface water elevations in the Middle Rio Grande, the United States Geological Survey (USGS) has established several cross sections in the Albuquerque Reach of the Rio

Grande, including one near Montano Bridge. Wells have been placed near the river, in the middle of the Bosque, and bracketing the riverside drains at each cross section.

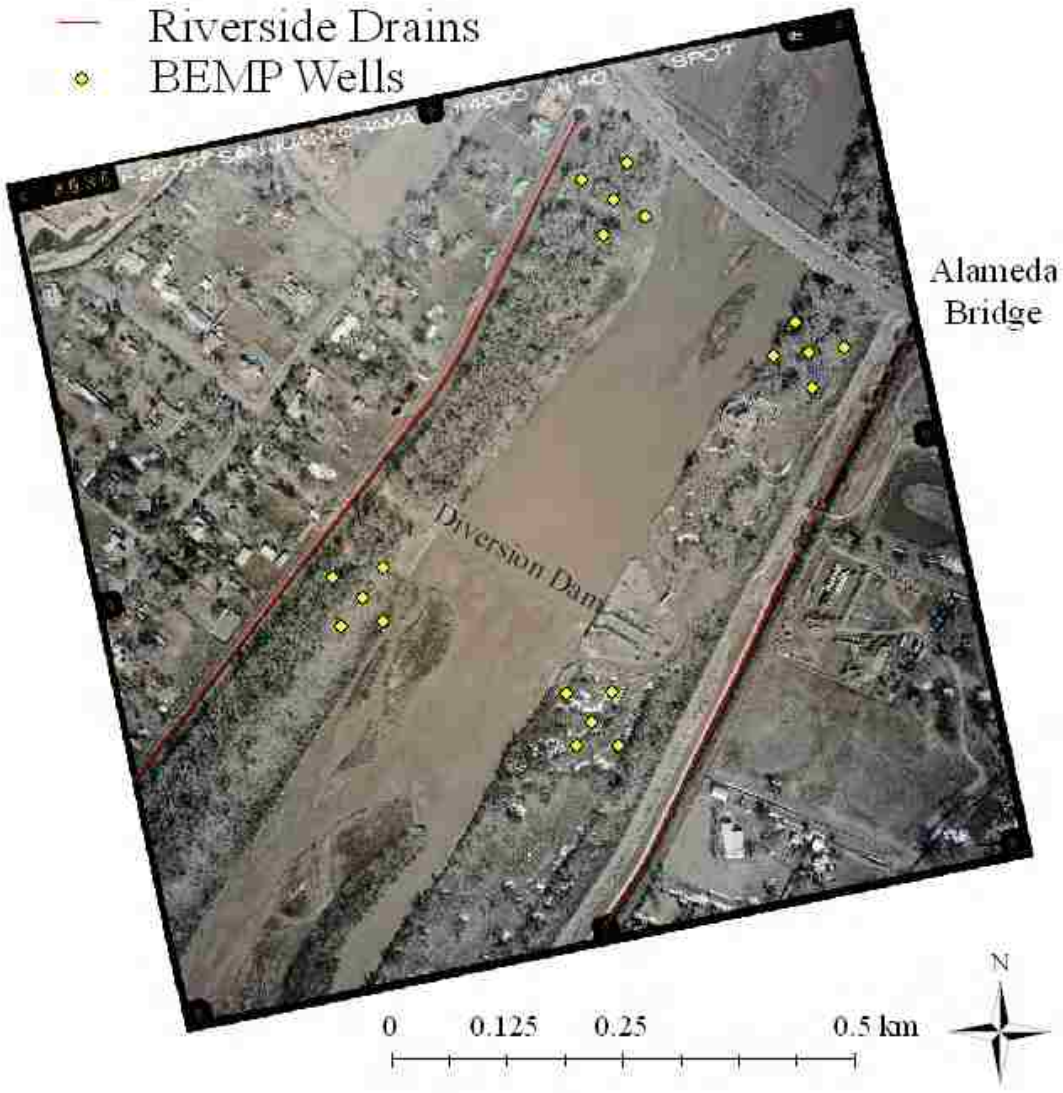

Figure 1-2 BEMP well locations in relation to the diversion dam

This study reach was selected for several reasons. First, the reach encompasses areas impacted by the diversion dam so that dam impacts on groundwater and surface water levels can be quantified. Secondly, detailed groundwater data availability in the area made this reach an excellent study location. Thirdly, the area encompasses three (USGS) continuous stage measurement sites on the Rio Grande that provide a basis for model calibration. The first gage, 3.25 km from the northernmost extent of the study

reach, is “Rio Grande at Alameda Bridge at Alameda, NM.” The second gage, “Rio Grande near Alameda, NM” is located on the Paseo del Norte Bridge 1.8 km downstream from the Alameda Bridge. “Rio Grande at Albuquerque, NM” is on the Central Bridge 1.2 km upstream of the southernmost extent of the study reach. The gages on the Alameda and Paseo del Norte Bridges have similar names because the USGS naming convention for gage sites relates the gage name to the nearest post office name, with ‘at’ or ‘near’ designating relative distance to the post office (personal communication USGS personnel, Aug 2008).

2 Literature Review

2.1 Terrain Models

Traditionally, terrain models were constructed from topographic maps and field surveys. Recent significant advances in surveying technology have eliminated the need for many of the complicated field survey techniques, replacing them with automated data collection, allowing "all-digital data collection and processing" (Buckley et al. 2008). One of the most important advances in terrain imaging has been the development of light detection and ranging (LiDAR), which has become a "routine practice" for many surveying companies (Buckley et al. 2008).

LiDAR systems measure the distance between the sensor and a surface by calculating the difference between emitted and received light pulses (Wehr and Lohr 1999). LiDAR sensing units can be ground based or airborne. Both systems have common components: a laser ranging unit (which emits laser signal and receives reflected laser signal), a position and orientation system (consisting of a differential Global Positioning System (GPS) and an inertial measurement unit (for airborne)), and a control/recording unit (Wehr and Lohr 1999). Airborne LiDAR systems may also have a downward-looking digital camera on board to aid in data processing and interpretation (Wright and Brock 2002).

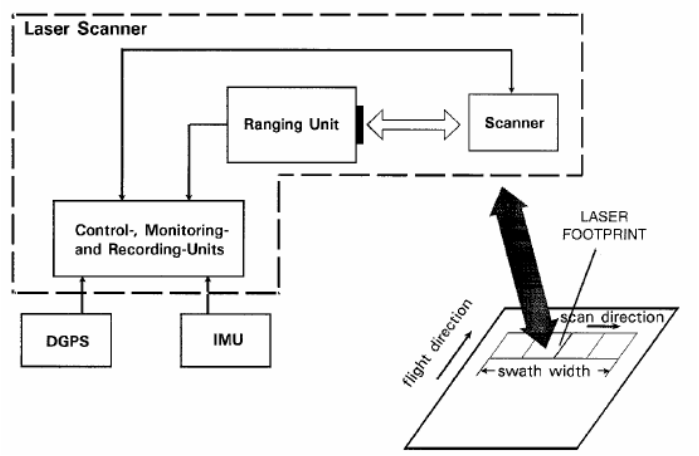

Figure 2-1 Schematic of airborne LiDAR system components (Wehr and Lohr 1999)

The configuration of an airborne laser scanner (ALS) is shown in Figure 2-1. A simple model of a pulsed signal emitter (Figure 2-2) correlates the time difference between the emitted signal and received signal (t_L) to the distance between the sensor and surface by

$$t_L = 2\frac{R}{c} \qquad \text{Eq 2.1}$$

where
c = speed of light (m/sec)
R = distance between the ranging unit and the object surface (m)

The range resolution is linearly related to the time resolution by

$$\Delta R = 0.5c\Delta t_L \qquad \text{Eq 2.2}$$

where
ΔR = range resolution (m)
Δt_L = time resolution = time interval measurement (sec)

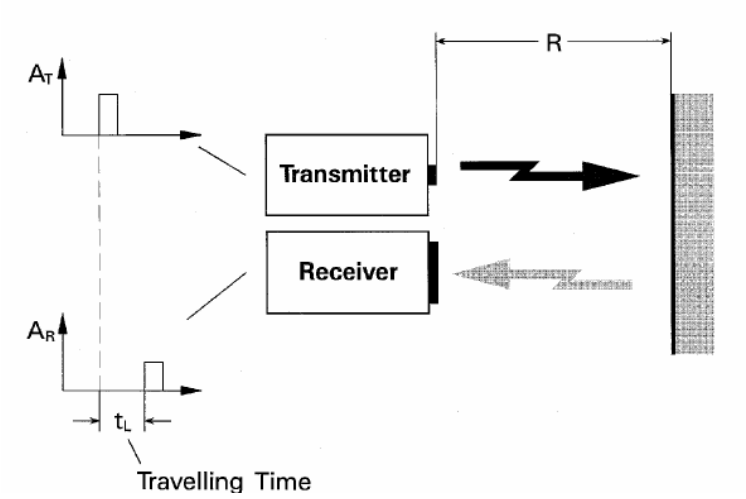

Figure 2-2 Time of flight conceptual model (Wehr and Lohr 1999)

Sinusoidal signals may be used by continuous signal emitters. Because the period T of the signal is known, the travel time is directly related to the phase difference (φ) between the sent and received signals. Period is inversely proportional to frequency (f, sec^{-1}), so the range resolution can be derived similarly to Eq 2.2 as

$$\Delta R = \frac{1}{4}\frac{c}{f}\Delta\varphi \qquad \text{Eq 2.3}$$

This equation demonstrates that higher range resolution can be achieved by increasing the frequency of the emitted signal (Wehr and Lohr 1999). A small spectral laser signal is advantageous because the received signal can be filtered to a narrow range to remove background radiation such as backscattered sunlight. The wavelength of light used should be tailored to the surface being scanned, as different surfaces (sand, water, trees) have different wavelength-dependent backscattering properties (Wehr and Lohr 1999).

The distance to the surface must be recorded simultaneously as the position and orientation of the sensor so the surface may be computed in a coordinate system. Post-scan data processing helps reduce noise and clarify objects such as buildings. Systems that record multiple echoes per emitted signal allow the vertical profile of the surface to be recorded with better clarity (i.e. trees, which have a tree crown but also a trunk length) (Wehr and Lohr 1999). The processed LiDAR points are often converted to three dimensional (3D) digital terrain models (DEM) or triangulated irregular networks (TIN) that represent the scanned surface (Merwade et al. 2008).

A recent advance in LiDAR technology is 'Green LiDAR' which yields bathymetry data. Experimental Advanced Airborne Research LiDAR (EAARL), developed by the National Aeronautics and Space Administration (NASA), utilizes blue/green lasers to achieve water penetration, hence the name 'Green LiDAR' (Wright and Brock 2002). Although specialized algorithms are needed to interpret bathymetric surfaces, green LiDAR measurement of bedforms in shallow, sand-bed rivers has been demonstrated by Kinzel et al. (2007).

Green LiDAR has not been extensively demonstrated and is a relatively new technology. Therefore, LiDAR data is currently predominately used to develop a terrain model for un-submerged regions while the river channel shape is determined from other techniques, most commonly cross section surveys or echo-sounder with GPS measurements (Merwade et al. 2008). Cross section surveys are used to delineate the bathymetric surface at specific locations but often need to be interpolated and are difficult to integrate with terrain models (Merwade et al. 2005). More recently, depth-sounding measurements taken concurrently with GPS locations have been combined with LiDAR data to create comprehensive terrain models containing bathymetric data (Merwade et al.

2005). Methods for creating a meaningful, well interpolated channel bottom surface from a cloud of bathymetry points that accounts for anisotropic spatial considerations are presented by Merwade et al. (2005, 2006). Using cross sectional measurements of the channel shape as the basis for interpolation of a channel bottom surface are given in Merwade et al. (2008). Integrating an interpolated channel bottom surface with the surrounding terrain model requires careful consideration and interpolation techniques to maintain an accurate representation of the channel boundary; Merwade et al. (2008) outline a procedure for integrating these two surfaces.

Terrain models in geographic information systems (GIS) are stored as raster data (gridded cells that have one value for the parameter per grid cell) or as vector data (points, lines, and polygons). These terrain models are often used to generate the geometry for hydraulic and groundwater models, and the water surfaces generated by the hydraulic models can be combined with the original terrain models to examine flood inundation extents (Merwade et al. 2008, Yang et al. 2006). The improvements in terrain model building and associated spatial data processing have been hailed as "by far the most significant new technology from the standpoint of simulation modeling" by Camp, Dresser and McKee (2001), who state that GIS has "revolutionized the task of designing models and interpreting and reporting results of model applications."

2.2 Populus Species

Populus spp., commonly called cottonwood (Figure 2-3), is a tree species native to many Western riparian forests (Beauchamp and Stromberg 2007). Facultative phreatophytes, Populus species have fast growth rates, high inundation or sedimentation tolerance, and low shade tolerance (Beauchamp and Stromberg 2007). Cottonwoods reproduce by clonal reproduction (sprouting from roots of established trees) (Lines 1999) or by seed germination (Lines 1999, Beauchamp and Stromberg 2007). Seed dispersal is wind driven (Beauchamp and Stromberg 2007); seeds only maintain viability for a few weeks (Bhattacharjee et al. 2006). Magnitude, timing, and duration of flooding controls regeneration: sufficient water is required to create germination beds yet drawdown must occur slowly enough that seedlings have access to moist soils until they develop root systems that tap the capillary fringe (Lines 1999, Beauchamp and Stromberg 2007).

Seedling survival is dependent on shallow soil moisture (Bhattacharjee et al. 2006) while mature cottonwoods rely on groundwater that has moved upward through the capillary fringe to the unsaturated zone rather than shallow infiltration from precipitation (Lines 1999). Cottonwood leaf area index (LAI) ("an excellent indicator of overall health of trees" (Lines 1999)) has a strong linear correlation to depth to groundwater. Some research indicates that cottonwoods stress when soil moisture potential is greater than five MPa (Lines 1999). This work was refined by Horton et al. (2001), which measured cottonwood crown dieback at depth to groundwater greater than three meters, and cottonwood mortality at groundwater depths greater than five m.

Figure 2-3 ***Populus deltoides***

Engineered changes to the timing and magnitude of river flows have negatively impacted cottonwood reproduction. Early riparian restoration efforts focused on cottonwood pole plantings but current efforts often emphasize an ecosystem approach. An ecosystem approach recognizes the importance of fluvial dynamics and often works to simulate historic hydrologic regimes, including the re-introduction of flood pulsing (Middleton 2002, Beauchamp and Stromberg 2007, Bhattacharjee et al. 2006). Managing dam releases to create spring flooding has proved effective at increasing cottonwood recruitment in some studies (Middleton 2002). Work by Ellis et al. (1999) suggests that a decade of annual flooding of riparian forest may be used to return forest floor organic

debris levels to pre-disturbance levels. Leaf litter and woody debris prevent moisture from getting to the soil surface, where microbial activity is able to decay organic debris back to nutrients essential for plant sustenance (Ellis et al. 1999). Clear forest floors (therefore bare seed beds) are "essential" for cottonwood forest restoration (Bhattacharjee et al. 2006).

2.3 Evapotranspiration

Evapotranspiration (ET) is the term used to designate the combined effects of evaporation and transpiration, two forms of water loss. Evaporation generally refers to the process of water changing from a liquid state to a gaseous state; here it specifically refers to water that is lost from water surfaces (rivers, lakes) or bare soil (liquid water in the soil converts to a gas and is lost to the atmosphere). Transpiration is a specific form of evaporation where water is lost from plant tissue, generally through plant stomata (Burt et al. 2005).

Water underground exists in the unsaturated zone or the saturated zone; the interface of the two zones is called the water table (Webb et al. 2007). The term "depth to groundwater" denotes the vertical distance below the ground surface at which the water table is reached.

Depth to groundwater and ET are interrelated. Decreased water availability from declining water tables negatively impacts mature riparian trees (Horton et al. 2001). Specifically, photosynthesis and stomatal aperture (which impact ET) are sensitive to depth to groundwater in Populus species (Horton et al. 2001). Conversely, ET rates impact depth to groundwater. Transpiration is a result of photosynthesis, which requires light. Therefore, ET rates are higher during the day and lower (or zero) at night, thus the demand on groundwater is higher in the day and lower at night. ET induced daily fluctuations in depth to water table can be seen in Figure 2-4 below from Dahm et al. (2002). Dahm addresses the difference between the two years of data presented in the figure (2002).

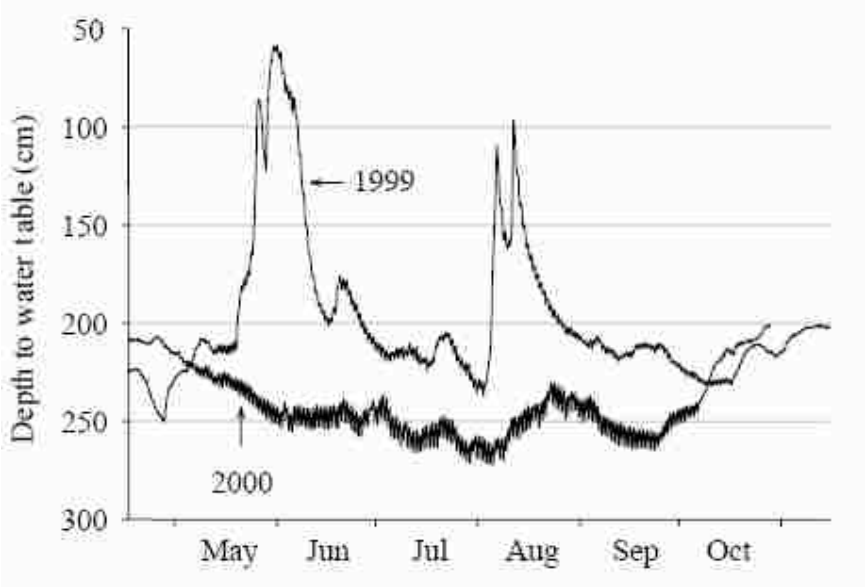

Figure 2-4 30 min pressure transducer measurement of depth to water table at Bosque del Apache, NM, USA (Dahm et al. 2002). Used with permission.

Soil water table evaporation is often estimated by Gardner's equation (Torrez, 2007). Flow in unsaturated soil is given by Gardner (1958) as

$$\frac{\partial \theta}{\partial t} = \nabla \cdot k \nabla \phi \qquad \text{Eq 2.4}$$

where

θ = volumetric water content

k = capillary conductivity (unsaturated soil hydraulic conductivity)

ϕ = water potential function, sum of the pressure or suction potential (ψ), and a gravitational potential

The maximum evaporation rate (E, m/day) can be found by solving this equation at steady state, given in Jury et al. (2004) as

$$E = K_s \left(\frac{-a\pi}{LN \sin\left(\frac{\pi}{N}\right)} \right)^N \qquad \text{Eq 2.5}$$

where

K_s = saturated hydraulic conductivity (m/day)

a = empirical Gardner's soil parameter (m)

N = empirical Gardner's soil parameter (dimensionless)

L = depth to water table (m)

A study conducted by the USGS in Nevada and California on phreatophytic shrubs whose primary source of water was groundwater indicated that there is a "strong correlation" between plant cover (measured via plant density and LAI) and groundwater evapotranspiration. A "weaker" but significant correlation between groundwater evapotranspiration and depth to groundwater was determined, which "strongly suggest that plant cover is the major factor in determining groundwater ET by phreatophytes in areas of shallow groundwater" (Nichols 2000). Nichols found that the relationship between ET and depth to groundwater was best described by a linear equation of the form

$$ET = \alpha + \beta Z_W \qquad \text{Eq 2.6}$$

For Z_W < 10ft

where

ET = mean daily May-September, mean daily October-April, annual mean daily or annual total groundwater ET

Z_W = depth to groundwater, in feet

α, β = empirical coefficients that are derived from field measurements

Riparian ET can comprise significant portions of total water lost in a river system (Dahm et al. 2002). Quantification of ET losses is particularly important in arid and semi-arid regions so that accurate water budgets can be developed to improve water resource management (Dahm et al. 2002). Better estimates of depth to groundwater will refine ET estimates, improving water budgets thereby facilitating better management practices.

2.4 Groundwater – Surface water Interaction

Historically, renewable groundwater and surface water were considered separately in both the scientific and legal communities. This attitude is changing as research has highlighted the importance of groundwater-surface water interaction in water supply and water quality (Jackson et al. 2001). Groundwater pumping from aquifers hydraulically connected to a river can significantly deplete stream flow and water available for plants (Webb et al. 2007). Rassam et al. (2008) discuss the importance of bank storage and groundwater movement through riparian zones in significantly improving surface water quality, especially by reducing nitrogen loads. The connectivity of groundwater and surface water is particularly important in arid and semi arid regions (Jackson et al. 2001).

Groundwater recharge that occurs through the river banks and bed is called transmission loss. Water can also seep from the saturated zone through the bed and banks into the river, increasing channel flow. Seepage rates exhibit inter-annual variability, dependent on a variety of factors including river discharge, riparian and groundwater conditions, and climate (SSPA 2002). The impact of river discharge on groundwater in wells in a riparian corridor can be seen in Figure 2.4, where spring snowmelt (May-June) and monsoonal derived (July-Aug) increases in river discharge in 1999 are starkly contrasted with the drought conditions in 2000 where spring snowmelt and monsoons were mild (Dahm et al. 2002).

A variety of approaches to modeling groundwater surface water interaction exist, including conceptual, empirical, and physically based models (Ivkovic et al. 2009). Each approach has different strengths and weakness that result in different models to be appropriate for different situations. Physical models are frequently hard to calibrate and validate due to lack of the detailed parameters required as model input data. They also tend to be computationally prohibitive due to the complexity of the model (Ivkovic et al. 2009). Modeling groundwater-surface water interaction has a variety of challenges. To incorporate rapid hydrologic changes surface water models often require short computational intervals, such as minutes or days whereas groundwater models simulate longer time periods (weeks, months) to capture changes. This conflict in required computational time step must be resolved in order to combine these two processes in one model (Ivkovic et al. 2009). Spatial discretization required to properly model river hydraulics may be significantly different from that required to properly represent small scale processes like bank storage (Werner et al. 2005). Another issue with fully coupled stream-aquifer models is the difference in "flow and head variability in surface and subsurface flow systems and their respective mathematical representations" (Werner et al. 2005).

Models of groundwater-surface water interaction have improved with increasing computational and software capabilities. A plethora of groundwater models have been developed, although USGS's MODFLOW is commonly used because it is freely available and fairly rigorous. MODFLOW models have been used to study transmission losses and riparian restoration options (Wilcox et al. 2007, MacClune et al 2006, McAda

and Barroll 2002). Wilcox et al. (2007) utilized MODFLOW to study management options regarding a low flow conveyance channel. Rodriguez et al. (2008), acknowledging the limitations of MODFLOW's water surface elevation calculation in the Drain Module, present an iterative process that utilizes HEC-RAS generated water surface elevations to refine a MODFLOW model. MODFLOW calculates the groundwater movement into a river as a linear function of the hydraulic head between the drain water elevation and the groundwater elevation. Therefore, HEC-RAS generated water surface elevations are used to refine the MODFLOW model and MODFLOW determined groundwater movement as lateral inflows are used to refine the HEC-RAS model until the models converge. This iterative procedure helps better define the hydraulic gradient, allowing a better estimation of groundwater movement (Rodriguez et al. 2008).

MIKE SHE is a software package developed to model "fully coupled surface water and groundwater flow and transport processes" with the additional ability to incorporate hydrologic processes (Hughes and Liu, 2008). Reviewers suggest the data requirements for MIKE SHE are similar in nature and complexity to those required for HEC-RAS/HEC-HMS and MODFLOW models (Illangasekare 2001), but there is no need to iterate between surface water and groundwater models as both computations are handled within the MIKE SHE software. MIKE SHE has been shown to effectively model complex hydrologic conditions and surface water interactions with saturated or unsaturated soils in semi-arid environments. Camp Dresser and McKee (2001) review nine models on thirteen criteria, including cost, regulatory acceptance, GIS integration, model limitations, and ease of use. MIKE SHE received the highest ranking of the nine software packages analyzed, although it received low marks in the categories of expandability and cost (indicating it has a high cost). The second highest ranking software package was MODFLOW, although it received low marks for GIS integration and service and support. Both MIKE SHE and HEC-RAS/MODFLOW models of groundwater-surface water interaction require substantial data acquisition and time investment for model development and calibration. The cost associated with data collection and time required to develop and calibrate these types of groundwater –

surface water models encourages exploration into less computationally and data intensive methods of predicting groundwater levels.

Conceptual models of groundwater –streamflow interaction can utilize considerably fewer input parameters and require less calibration effort, but may need to be adjusted each time a new level of detail is required (Bari and Smettem 2004). Bari and Smettem develop a conceptual model to predict streamflow and groundwater recharge for semi-arid regions in Australia, but at a monthly time step. Another conceptual model is presented by Ivkovic et al. (2009) to specifically address how groundwater pumping impacts streamflow. The model is utilized to demonstrate that groundwater pumping near streams impacts the timing, frequency, and magnitude of streamflow, especially baseflow. Based on model results, the authors make specific recommendations for limits of groundwater pumping rates from various aquifers within the study area, and quantify what pumping rates are likely to cause permanent stream – aquifer disconnection.

This thesis presents an empirical model for estimation of groundwater levels over substantial spatial and temporal scales based on streamflow data and well groundwater measurements. Previous work has applied linear regression to well data to estimate groundwater elevation as a function of land surface elevation (Kuniansky et al. 2009, based on Williams and Williamson 1989). This method is demonstrated for aquifers that are not being used for large scale water supply, and is not considered appropriate for use on aquifers that are subject to substantial pumping. Numerical methods have been used to estimate groundwater levels throughout space and time (Sorooshian and Gupta 1995, but these models are data intensive and complicated. Integrated Time Series (ITS) and Back-Propagation Artificial Neural Networks (BPANN) are proven to accurately fit historic groundwater data to create predictive models by Yang et al (2008), but application requires an understanding of advanced mathematics. These methods have not been demonstrated in the literature to correlate surface water and groundwater levels.

Quantification of groundwater-surface water exchange in its spatial and temporal variability is important for optimal water management decisions. Water budgets are "critical components" of water management in arid and semi-arid regions (Dahm et al. 2002), e.g. dam releases. Knowledge of localized groundwater-surface water movement can aid in the selection of restoration sites that target water quality improvement or native species rehabilitation (Rassam et al. 2008).

2.5 Climate Change

The Intergovernmental Panel on Climate Change (IPCC) has been reporting on climate change since the early 1990s. In the IPCC's latest assessment report, AR4 (2007), climate change is defined as "a change in the state of the climate that can be identified (e.g. using statistical tests) by changes in the mean and/or the variability of its properties, and that persists for an extended period, typically decades or longer". This definition encompasses natural and anthropogenic causes of climate change. Numerous reports document the measured indications of significant climate change (IPCC AR4 2007) and increasingly more literature has focused on the impact of climate change on water resources (Vörösmarty et al. 2000).

AR4 (2007) reports with high confidence (confidence level "used to express the assessed chance of a finding being correct" is about 8 out of 10) that hydrological systems are already impacted in the following ways: "increased runoff and earlier spring peak discharge in many glacier- and snowfed rivers, and warming of lakes and rivers in many regions, with effects on thermal structure and water quality." Mass loss from glaciers and reduced snow pack due to increasing temperatures (Figure 2-5) will reduce the quantity of water available in systems that depend on this freshwater source. Precipitation is predicted to increase in humid and higher latitude regions but decrease in semi-arid and arid environments (Figure 2-6). Timing of precipitation is also projected to change, resulting in changes in runoff patterns (Figure 2-7). Rising temperatures will likely increase rates of ET, causing an increase in the water required by riparian vegetation and agriculture for the same productivity (AR4 2007, Hurd and Coonrod 2007).

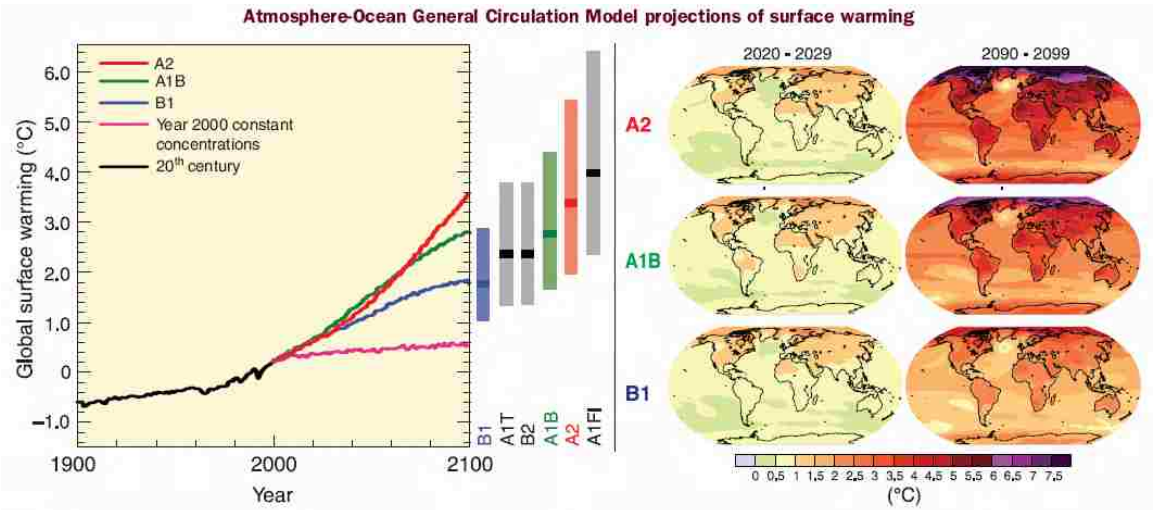

Figure 3.2. ***Left panel:*** *Solid lines are multi-model global averages of surface warming (relative to 1980-1999) for the SRES scenarios A2, A1B and B1, shown as continuations of the 20th century simulations. The orange line is for the experiment where concentrations were held constant at year 2000 values. The bars in the middle of the figure indicate the best estimate (solid line within each bar) and the likely range assessed for the six SRES marker scenarios at 2090-2099 relative to 1980-1999. The assessment of the best estimate and likely ranges in the bars includes the Atmosphere-Ocean General Circulation Models (AOGCMs) in the left part of the figure, as well as results from a hierarchy of independent models and observational constraints.* ***Right panels:*** *Projected surface temperature changes for the early and late 21st century relative to the period 1980-1999. The panels show the multi-AOGCM average projections for the A2 (top), A1B (middle) and B1 (bottom) SRES scenarios averaged over decades 2020-2029 (left) and 2090-2099 (right). {WGI 10.4, 10.8, Figures 10.28, 10.29, SPM}*

Figure 2-5 Projected temperature changes (AR4 2007)

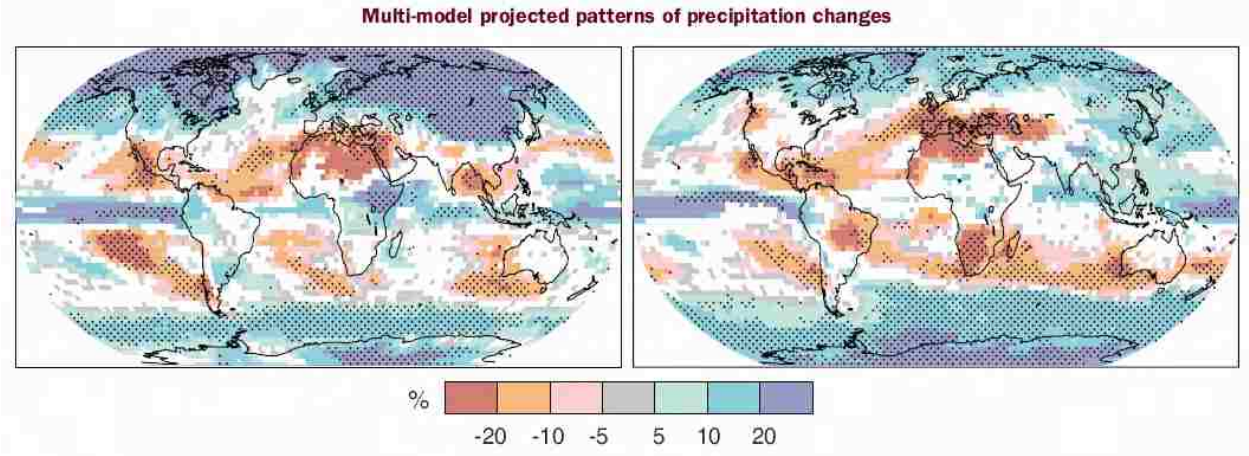

Figure 3.3. Relative changes in precipitation (in percent) for the period 2090-2099, relative to 1980-1999. Values are multi-model averages based on the SRES A1B scenario for December to February (left) and June to August (right). White areas are where less than 66% of the models agree in the sign of the change and stippled areas are where more than 90% of the models agree in the sign of the change. {WGI Figure 10.9, SPM}

Figure 2-6 Predicted precipitation changes (AR4 2007)

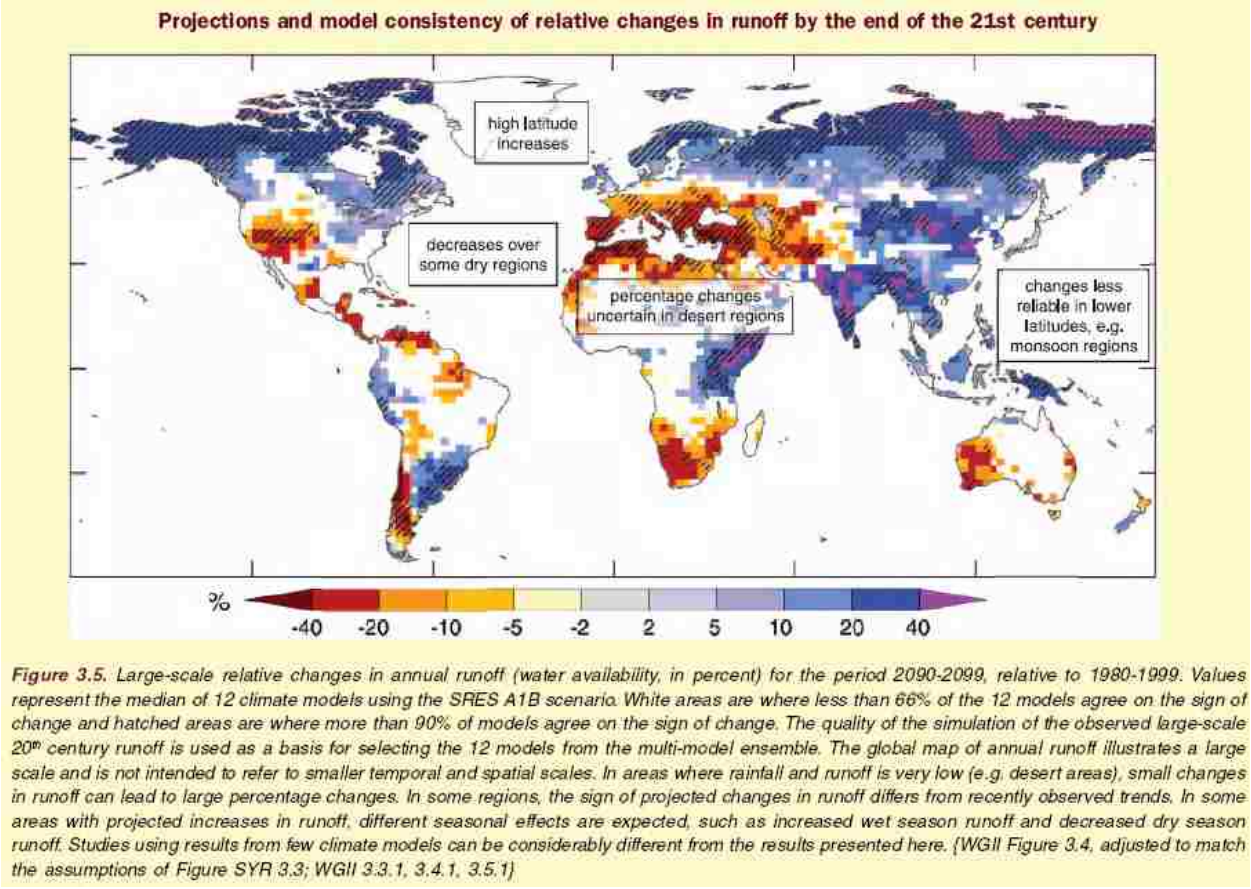

Figure 3.5. Large-scale relative changes in annual runoff (water availability, in percent) for the period 2090-2099, relative to 1980-1999. Values represent the median of 12 climate models using the SRES A1B scenario. White areas are where less than 66% of the 12 models agree on the sign of change and hatched areas are where more than 90% of models agree on the sign of change. The quality of the simulation of the observed large-scale 20th century runoff is used as a basis for selecting the 12 models from the multi-model ensemble. The global map of annual runoff illustrates a large scale and is not intended to refer to smaller temporal and spatial scales. In areas where rainfall and runoff is very low (e.g. desert areas), small changes in runoff can lead to large percentage changes. In some regions, the sign of projected changes in runoff differs from recently observed trends. In some areas with projected increases in runoff, different seasonal effects are expected, such as increased wet season runoff and decreased dry season runoff. Studies using results from few climate models can be considerably different from the results presented here. {WGII Figure 3.4, adjusted to match the assumptions of Figure SYR 3.3; WGII 3.3.1, 3.4.1, 3.5.1}

Figure 2-7 Predicted runoff changes (AR4 2007)

Global freshwater resources are already stressed at the current climatic conditions and human population, and non sustainable water management practices are presently in effect (i.e. groundwater mining) (Jackson et al. 2001, Vörösmarty et al. 2000, Postel 2000). This stress is demonstrated by river discharge-demand models (Vörösmarty et al. 2000) and the current trends towards desalination and potable wastewater reuse (Marks 2006). Changes in climate and population may be beyond the capacity of many water systems that have been designed for the current climate (Jackson et al. 2001), resulting in significant challenges to water infrastructure and services in the future (Vörösmarty et al. 2000). Human uses of freshwater resources extend beyond simply water for drinking, agriculture, and industry. In-stream uses include hydroelectric power, transportation, recreation, flood control, and waste disposal and processing (Jackson et al. 2001). Decreased water availability as a result of climate change will impact all of these uses.

This myriad of human demands upon and use of freshwater resources have significant implications for freshwater ecological systems, especially regarding climate change induced water scarcity. Alterations by water engineers to river networks (damming, levee construction) in the last century rarely considered the consequences of the changes made to fundamental stream processes (i.e. sediment transport) and characteristics (i.e. temperature) (Postel 2000). There is a multiplicity of examples where damming and diversion have negatively impacted native plants, animals, and habitat (Postel 2000), yet decreased water resources and increasing human demand will only strengthen the tension between human and ecological needs. A decrease in the quantity of water available (due to decreased precipitation and increased evaporation) may result in increased concentrations of nutrients and salts, which often negatively impact native species within river systems and their receiving bodies (Jackson et al. 2001). According to the Nature Conservancy, water-based life is more at risk than land-based life due to habitat degradation or destruction (Postel 2000).

In AR4, nineteen climate models were used to predict precipitation and evaporation in the 21st century. Up to twenty percent reduction in precipitation from 1950-2000 levels in semi-arid to arid regions is predicted (AR4 2007). For the American Southwest, the models predict a transition to Dust Bowl conditions as the new climate of the region on time scales of years to decades (Figure 2-8) (Seager et al. 2007). Other models echo these results: increased water scarcity in arid and semiarid regions, with rapidly expanding cities (i.e. Albuquerque, NM) experiencing the most scarcity (Vörösmarty et al. 2000).

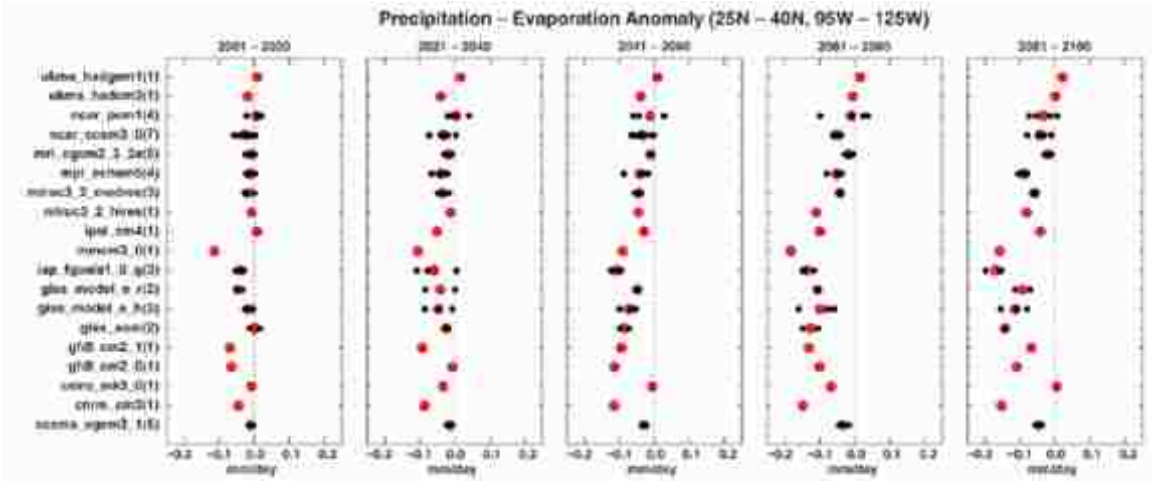

Fig. 2. The change in annual mean $P - E$ over the American Southwest (125°W to 95°W and 25°N to 40°N, land areas only) for 19 models (listed at left), relative to model climatologies from 1950–2000. Results are averaged over 20-year segments of the current century. The number of ensemble members for each projection is listed by the model name at left. Black dots represent ensemble members (where available), and red dots represent the ensemble mean for each model.

Figure 2-8 Predicted precipitation and evaporation changes for the American Southwest (Seager et al. 2007)

3 Calibrating Hydraulic Models of Sand Bed Rivers with USGS Data

3.1 Introduction

Sand bed rivers represent some of the most economically important and potentially destructive rivers in the United States (i.e the Mississippi River, Rio Grande, and Des Moines River). For a variety of economic, ecological, and flooding studies, sand bed rivers are increasingly analyzed with computer models. To calibrate these models, discharge and stage hydrographs are required. United States Geological Survey (USGS) data is frequently used to calibrate one, two, and three dimensional hydraulic models (Castellarin et al. 2009, van der Sande et al. 2003).

During an effort to calibrate a one dimensional model of the Rio Grande through Albuquerque, close examination of the fifteen minute USGS gage data revealed discrepancies in timing and magnitude of discharges at gages in close proximity which lead to concerns regarding data quality. In the most extreme case, a 241 m^3/s peak discharge was registered at a gage 1.8 km downstream from a gage that registered a 152 m^3/s peak discharge. With travel time and all tributaries accounted for, there was no feasible source of the 89 m^3/s difference (155%) between the gage measurements. This sizeable difference led to extensive discussion with USGS personnel as well as a literature review on gaging sand bed rivers. From this research, several practical guidelines on the use of USGS gage data in modeling sand bed rivers were determined and are outlined in this chapter.

3.2 Study Area

This study considers an 18.7 km reach of the Rio Grande within Albuquerque, NM, USA. This reach encompasses the river from the confluence of the North Diversion Channel to the Central Bridge (Figure 3.1). Within this reach there are three USGS gages on the main stem of the Rio Grande. The first is at the Alameda Bridge, located 3.25 km from the northernmost edge of the study reach. One point eight km downstream from the Alameda gage is the Paseo del Norte Bridge gage, referred to here as the Paseo gage.

The river traverses 12 km before it encounters the gage at the Central Bridge, which is located 1.2 km from the southernmost part of the study area. There are two significant tributaries to the Rio Grande in this reach. The North Diversion Channel, at the beginning of the study reach, drains approximately 284 km^2 of the northeast quadrant of Albuquerque. The Calabacillas Arroyo, which drains 90 km^2 of the northwest quadrant of Albuquerque, is located between the Alameda and Paseo del Norte bridges, 540 m upstream of the Paseo del Norte Bridge. Both of these storm water conveyance channels are gaged by the USGS, North Diversion Channel (NDC) (USGS gage number 08329900) in fifteen minute intervals and Calabacillas Arroyo (USGS gage number 08329926) in five. The three main stem gages and the NDC gage daily data are available online at waterdata.usgs.gov. The fifteen minute stage measurements and computed discharges are available upon request; some of the more recent years are available in an online archive at ida.water.usgs.gov/ida/index. The Calabacillas gage is operated for a client and that data is not available on the internet but was obtained from USGS personnel.

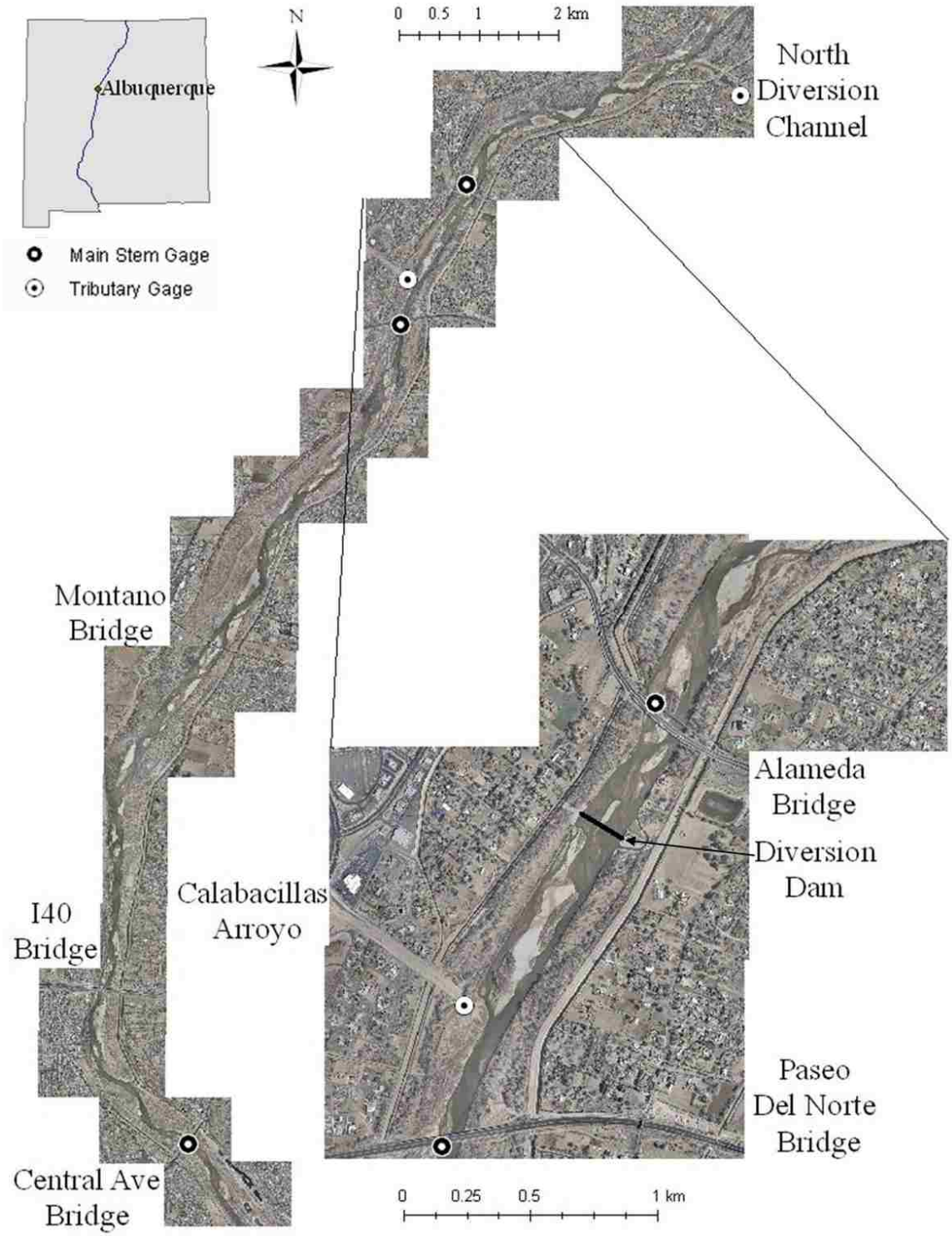

Figure 3-1 Study Area

3.3 Site Selection for Stream Gaging Stations

To fully understand gage data quality, it is important to first understand the importance of gage location. The USGS guidance on stream gaging is outlined in Geological Survey Water Supply Paper 2175, a two volume document titled "Measurement and Computation of Streamflow." A list of qualifications of an "ideal" gaging site is given in Table 3-1 (WRP 2175 1982). For the three gages on the Rio Grande in Albuquerque, it is determined whether the criteria are met.

Table 3-1 USGS criteria for an ideal gaging site

	Criteria Met at Site? Yes or No		
Criteria	Alameda	Paseo	Central
General course of the stream is straight for about 100 m upstream and downstream from the gage site.	Yes	Yes	Yes
The total flow is confined to one channel at all stages, and no flow bypasses the site as subsurface flow.	No	Yes	Yes
The streambed is not subject to scour and fill and is free of aquatic growth.	No	No	No
Banks are permanent, high enough to contain floods, and are free of brush.	No	No	No
Unchanging natural controls are present in the form of a bedrock outcrop or other stable riffle for low flow and a channel constriction for a high flow – or a falls or cascade that is unsubmerged at all stages	No	No	No
A pool is present upstream from the control at extremely low stages.	No	No	No
The gage site is far enough upstream from the confluence with another stream or from tidal effect to avoid any variable influence the other stream or the tide may have on the stage at the gage site. (Figure 3.1)	Yes	Yes	Yes
A satisfactory reach for measuring discharge at all stages is available within reasonable proximity of the gage site.	No	Yes	Yes
The site is readily accessible for ease in installation and operation of the gaging station.	Yes	Yes	Yes

In the chapter on selection of gaging-station sites, the authors recommend locating gages away from flow obstructions such as bridges, as they "tend to intensify scour and fill" (WRP 2175 1982, pg 6).

There are often other motivating factors that determine gage placement such that stream gages are not always placed in ideal locations. Gages may be placed for ease of accessibility, desire to monitor impacts of hydraulic structures, or for regional hydrologic studies. Flawed gaging sites must at times be accepted, thus the data from these gages may frequently fail to be "good", defined by the USGS to be within five percent of the actual streamflow. Gage locations on sand bed rivers are likely to be problematic based on the criteria listed in Table 3-1. Mobile bed channels are subject to scour and fill and typically have no natural controls. Ensuring a pool upstream of the control is difficult if sand bars form immediately upstream of the stage measurement location. Major flow events can cause significant sediment movement; and steady flows can generate dune movement that creates variable channel configuration.

3.4 Stage – Discharge Curve Development

In the preface to WRP 2175 1982, the authors acknowledge that stream gaging is part science and part art (pg III). The scatter of measurements used to create rating curves underscores the fact that the stage – discharge relationship for mobile bed channels is difficult to obtain with certainty.

Stream gaging is accomplished through two different approaches. In the first, point flow velocities and corresponding cross-sectional areas are measured in the field across the channel, multiplied, then added together to arrive at a discharge rate. The result of this process is called a measured discharge. This method requires field personnel every time a measurement is needed, which can be expensive, time consuming, and at times dangerous (Sahoo and Ray 2006).

In the second method, measured river stage is used to estimate discharge via a site specific relationship, resulting in what is called a computed discharge. Computed discharges rely on measured discharges and the corresponding stages (a water surface elevation at some location relative to a fixed datum measured at the same time as the discharge) to establish a relationship between stage and discharge. This relationship is called a discharge rating curve or the stage – discharge curve (Figure 3-2). At the selected gage location, an arbitrary datum below the river bottom is chosen as the gage

datum (stage = 0) (Figure 3-3). This gage datum is defined by assigning permanent markers (e.g. survey benchmarks, bolts on bridge pilings, bolts on power line poles) an elevation within the gage coordinate system (e.g. from Paseo gage: USGS bronze disk set on the west end of the bridge deck, elevation= 20.519 ft gage datum). The gage datum is may not be assigned a value in a vertical datum referenced to mean sea level by the USGS, but the gage datum value in a vertical datum may be determined if the elevation of one or more of the reference marks can be accurately established. Once a gage datum is established, a device is installed to record the water surface elevation relative to the gage datum. This stage measurement is used to calculate the discharge via a rating curve.

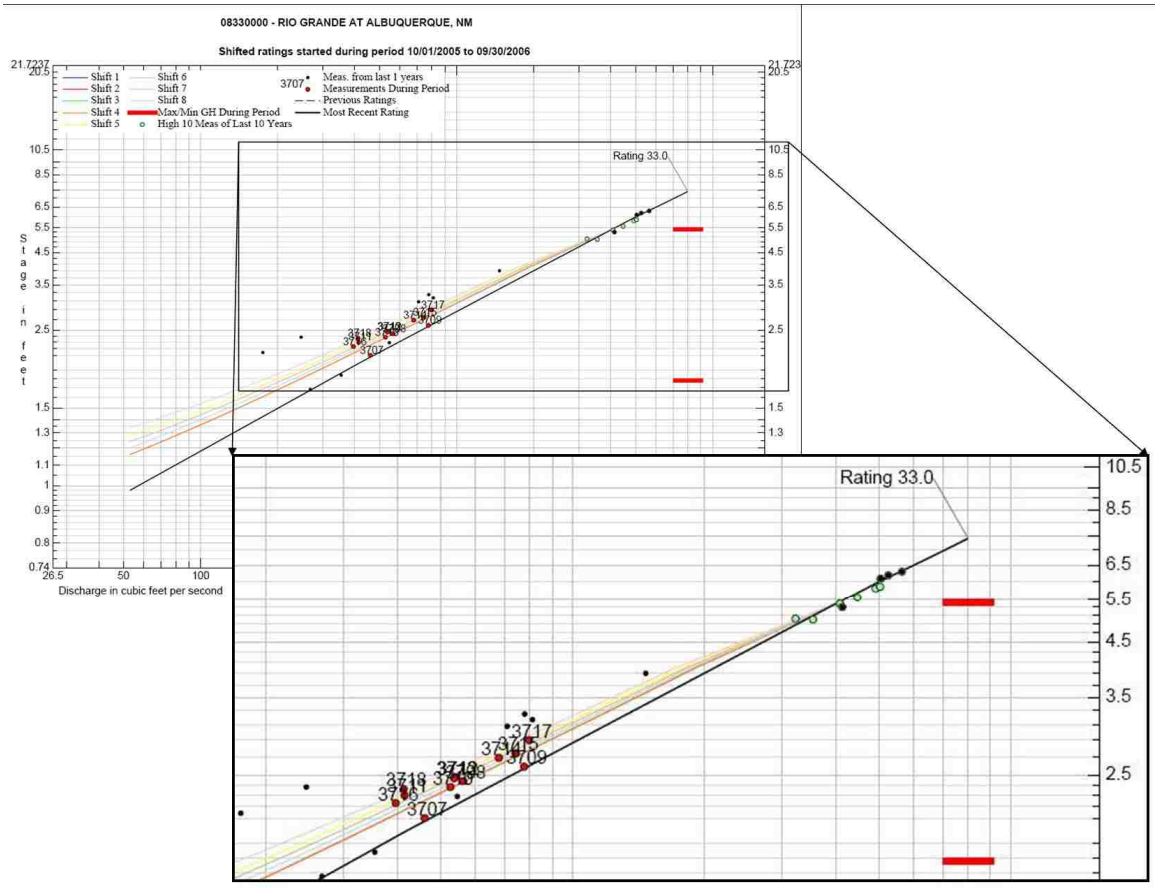

Figure 3-2: Example USGS Central gage stage-discharge curve

The general equation given by USGS to describe a rating curve is

$$Q = p(G - e)^N \qquad 3.1$$

where

Q = discharge

(G-e) = head or depth of water on the control

G = gage height

e = gage height of zero flow or effective zero flow

p = constant

N = coefficient of the rating curve

Alternatively, the equation can be written in log-log space as

$$\log(Q) = \log(p) + N \log(G - e) \qquad 3.2$$

The values of p and N are determined by simple linear regression of the data pairs of Q and G optimized on the value of e. Non-linear regression can be used as well and may be a better approach for the three parameter model of Eq 3.1. Once their values are established, stage measurements (frequently automated) are used to calculate the discharge.

There are several problems with this approach. Most importantly, Eq 3.1 assumes that the rating curve is a singular function of stage, but the stage – discharge relationship is seldom a function of stage alone (Rantz et al 1982). Assuming singularity ignores the hysteresis of unsteady hydrographs, e.g., for a given stage, the discharge is higher on the rising limb of the hydrograph than the falling limb for a system where diffusion and local and convective accelerations affect the friction slope. Eq 3.1 does not accommodate this variation. Additionally, stage may be a function of sediment concentration or water temperature (USGS WSP 2175 1982) because both may impact sediment transport and thus scour and fill. Furthermore, discharge may be a function of stage and time when overbanking occurs as water returns to the river on the falling limb, resulting in a looped rating curve.

This introduces the second problem with the rating curve approach: p, N, and e are all assumed to be constant between measurements. Automatic measuring devices record only G for Eq 3.1; therefore changes in other variables are not documented. The rating curve is sensitive to bedforms because moving bedforms change e in Eq 3.1 (see Figure

3-3). Sand bed rivers may experience dune formation and movement in both high and low flow regimes. Dune movement can cause a wide spread of stage measurements for a constant discharge, a problem which requires frequent stage – discharge measurements (up to once a day in some rivers) (USGS WSP 2175 1982). Installation of control structures at the gage site is recommended "if at all feasible" (USGS WSP 2175 1982), especially to assist with low flow measurements. To track these changes in the stage – discharge relationship, the USGS recommends measuring the stage and discharge at least 10 times a year (USGS WSP 2175 1982). The stage discharge measurements are available online as part of the site information (http://waterdata.usgs.gov). The stages and discharges at gages in the study reach are measured on average ten times per year.

It should be noted that different segments of a rating curve have different confidence intervals. At low flows, measurements are easier and safer to obtain, so there tend to be more stage – discharge measurements. For a stable river bottom, that redundancy increases the confidence in the rating curve. However, for sand bed channels, the stage measurement is sensitive to bedform movement at low flows: a sediment bar moving into a cross section reduces the cross sectional area for the same flow rate, which increases the stage. Thus, the higher incidence of calibration measurements does not increase confidence in the low flow part of the rating curve for sand bed rivers. In all river types, it is frequently more difficult to measure the area and velocity at high flows thus high discharge measurements are rare. For stable channels, fewer measurements decrease the confidence in the rating curve for high flows relative to low flows. For mobile bed channels, at high flows the stage measurement is less sensitive to bedform movement, thus despite the relatively fewer measurements, confidence in the rating curve might be greater at high flows because the stage – discharge relationship is stable (personal communication with USGS personnel, July 2008). This confidence assumes that channel bed change is similar for all high discharges flow events: presumably, a calibration measurement taken at a high discharge accounts for some river scour due to the high flow fluidizing the channel bed. Thus, the rating curve would assume a certain amount of channel bed change for a give discharge, which may or not accurately reflect reality. For both mobile and stable river channels, the highest discharges calculated are

commonly extrapolated from the rating curve because the automated stage measurement is higher than any calibration stage measurement.

After a stage – discharge calibration measurement is taken; shifts may be applied to the discharge calculation. The USGS reports stage as measured, with no shifts applied. However, depending on whether the river has scoured or filled (determined when a calibration measurement is taken); the stage value may be increased or decreased before it is used in Eq 3.1. Figure 3-3 shows how the stage may remain constant while the actual depth of water varies. This is essentially accounting for a changing *e* value in Eq 3.1. A negative shift indicates the cross section filled, a positive shift indicates scour. The approved data that USGS releases has undergone data processing to determine to what magnitude and direction a shift should be applied, if at all. Shifts are not uniformly applied to all discharges, they are stage dependent. High stage/high discharges may have one shift applied because the river control at high discharge may be the banks. However, at low flows the stage will primarily be influenced by bathymetric changes, so a different magnitude shift may be applied to the stage measurement. Therefore, the published computed discharge is a product of not only a measurement but also experienced opinion. The HEC-RAS Version 4.0 User's Manual (2008) comments that the quality of the record produced from rating curves "depends on the frequency of discharge measurements and the skill of the hydrologist" (pg 8-43).

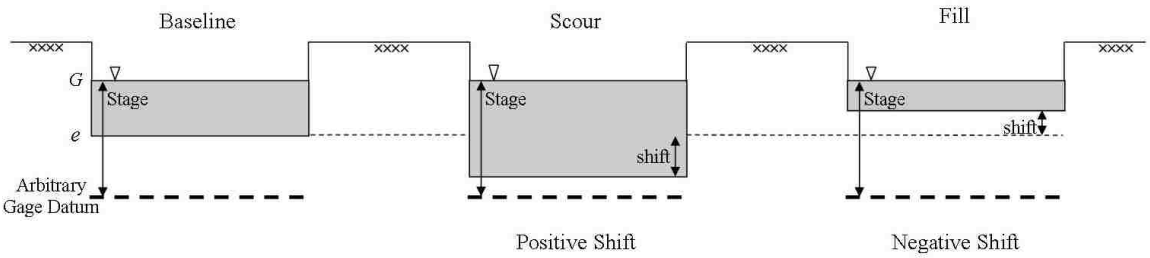

Figure 3-3 Stage and shift explanation, with *G* and *e* indicated from Eq (3.1)

Determining the appropriate magnitude and direction of a shift is not done at each gage in a river network independently, according to members of the USGS Albuquerque Office (personal communication, July 2008). Measurements from one gage are likely to be compared to the measurements of the gages immediately upstream and downstream of

the gage under consideration. If a gage demonstrates an anomaly compared to its closest neighbors that cannot be explained by tributaries, a shift is likely to be applied to that gage to make the peak discharge and volume consistent with the other gages. Thus the data is amended, often giving preference to readings from gages where the stage – discharge curve is deemed more reliable and giving less weight to measurements at newer or more sensitive gages. Discharge measurements published for a given series of gages may be thought of as a compilation of measurements along a river, rather than exact truth for each gage location. This system provides a degree of quality control to remove false peaks but requires professional judgment in determining the computed discharge.

An example of this can be taken from the three gages considered in this study. Of the three gages, the Alameda gage has the shortest period of record as well as the most sensitive rating curve. Therefore, if an abnormal discharge occurs at the Alameda gage that is not consistent with the nearest upstream gage, the Paseo gage, and the North Diversion Channel gage, a shift may be applied to the Alameda measurement to make the volume of water passing the gages comparable. Similarly, members of the Albuquerque USGS office (personal communication, July 2008) indicated that stage – discharge calibration measurements at high discharge are easier to obtain at the Paseo gage than the Alameda gage, so Paseo measurements may be used to refine the Alameda rating curve.

If a sufficiently significant alteration occurs to the gaging site (e.g., a large scour or fill event or significant lateral river movement) such that the current rating curve is no longer considered descriptive of river conditions, a new rating curve may be developed. The new curve will likely use a few historic data points but will mainly rely on newer measurements. The Central gage, established in 1942, is currently on the thirty-third version of the rating curve, while the Paseo curve (re-established in 1989) is on the fourth version for that site.

3.5 Detailed Gage Descriptions

3.5.1 USGS Gage 08329918: Rio Grande at Alameda Bridge at Alameda, NM

The Alameda gage is mounted to the northern edge of the old Alameda Bridge, which is now a pedestrian walkway (Figure 3-4). The old Alameda Bridge is 23 meters directly upstream of the new Alameda Bridge. This station has been operated since July 2003. The gage is a radar level gage that sends a microwave signal to the river surface which is reflected back to the gage sensor. The gage sensor applies a filter to the return signals to determine the greatest distance between the sensor and river surface. Wind induced waves on the river surface complicate this measurement, and may cause a false low reading of river stage. This sensitivity to wind patterns requires monitoring of gage data to evaluate whether sudden low discharge measurements are reflected in the Paseo gage or if they are due to wind-induced waves.

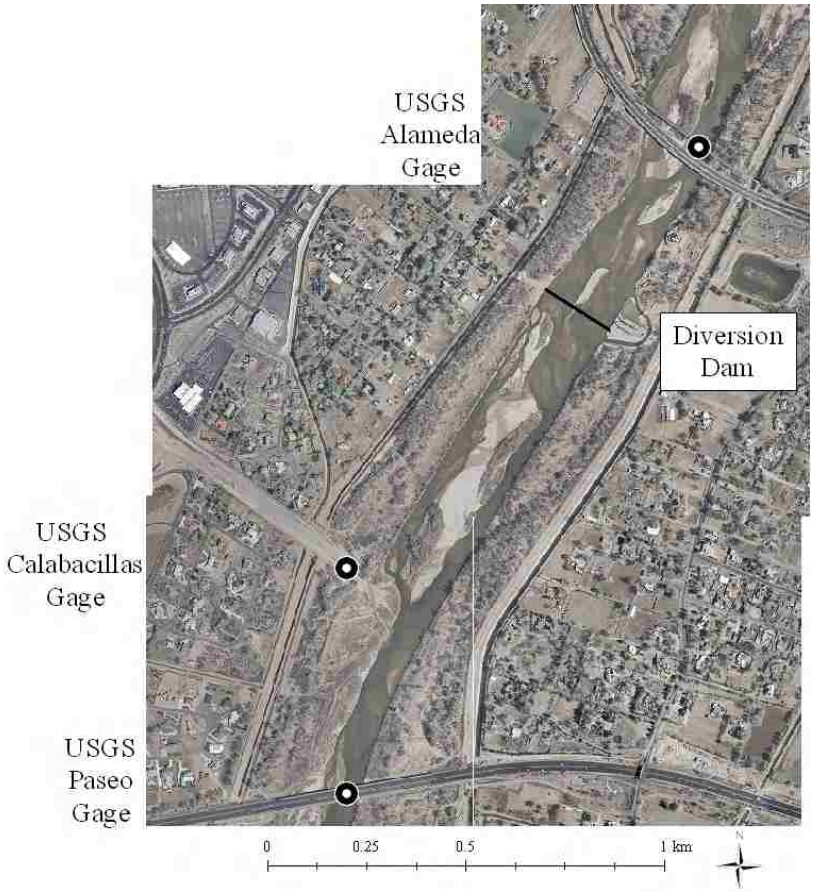

Figure 3-4 Diversion dam in relation to Alameda and Paseo Bridges

The stage – discharge measurements for the Alameda gage exhibit little scatter. However, the curve is particularly flat, with a small value of N in Eqs (1) and (2). A small value of N indicates a sensitive curve, which is proved by taking the natural logarithm of both sides of Eq (1) Assume $G\text{-}e = H$ (stage).

$$\ln Q = \ln p + N \ln H \qquad 3.3$$

Using the chain rule, the derivative of Q with respect to H is:

$$\frac{d(\ln Q)}{dH} = \frac{[dQ/Q]}{dH} \qquad 3.4$$

The derivative of the right hand side of Eq (3) with respect to H is

$$\frac{d(\ln p + N \ln H)}{dH} = \frac{d \ln p}{dH} + \frac{dN \ln H}{dH} = 0 + N \frac{d \ln H}{dH} = \frac{b}{H} \qquad 3.5$$

Replacing these equivalents in Eq (3) yields

$$\frac{1}{Q}\frac{dQ}{dH} = \frac{N}{H} \qquad 3.6$$

Rearranging Equation (6):

$$\frac{dQ}{Q} = N\frac{dH}{H} \qquad 3.7$$

The magnitude of N indicates the sensitivity of the gage: $N>1$ magnifies the fractional change in Q due to a fractional change in stage; $N < 1$ gives a smaller fractional change in Q due to change in stage. Therefore, large N values imply sensitive gages: a small change in stage corresponds to a large change in discharge. Stage discharge curves are frequently plotted with stage as the dependent variable so the slope of the line is $1/N$. Thus a sensitive gage can be identified by a rating curve with a flat slope.

There are several issues with the Alameda gage affecting the accuracy of the gage measurements. First, a very long vegetated island exists in the middle of the river stretching 280 meters upstream and 80 meters downstream from the bridge. The island splits the channel in two with the potential of different water surface elevations in each. Additionally, the Upper Corrales Main Drain (operated by the MRGCD) empties into the Rio Grande 24 meters upstream of the old Alameda Bridge. The vegetated island prevents this inflow from being included in the Alameda measurement further making this an undesirable site for a stream gage. Sixty stage-discharge measurements have been

made to calibrate the Alameda rating curve during its period of record. Only six of the sixty measurements have indicated that the rating curve computes a discharge within five percent of the actual streamflow. Four of the measurements indicated that the rating curve computed discharge differs from actual streamflow by greater than eight percent.

3.5.2 *USGS Gage 08329928: Rio Grande near Alameda, NM*

This gage is located under the Paseo del Norte Bridge (Figure 3-4) within the river, and is referred to here as the Paseo gage. The gage record exists from March 1989 through September 1995, and from June 2003 to the present. The nitrogen-fed pressure transducer and data logger are located on the west bank of the river inside the gaging station. A pipe with a nitrogen feed line from the pressure transducer on the bank to near the middle bridge pier terminates with an orifice that has a constant stream of nitrogen bubbles exiting. Changes in water depth cause a change of pressure on the stream of nitrogen coming from the orifice. This change in pressure is transmitted through the nitrogen gas in the line to the pressure transducer. Pressure is correlated to a height of water (stage) in the river and recorded. This stage measurement technique is particularly susceptible to corruption by sediment movement, as the pressure transducer can become buried in sediment which invalidates the pressure reading.

In March 1989, the river flowed on the west side of the bridge. Since then, the river has migrated to the east side of the bridge, a distance of approximately 61 meters. This movement is probably due in part to bank erosion and in part to sediment contributions from the Calabacillas Arroyo on the west side of the river. Because of this, the rating curve at Paseo today is significantly different than it was twenty years ago.

3.5.3 *USGS Gage 08330000: Rio Grande at Albuquerque, NM*

Located beneath the Central Bridge on Historic Route 66, this gage is referred to as the Central gage. It was started in March 1942 and has been operating continuously, although it was temporarily relocated in the early 1990s during the reconstruction of the bridge. The gage is similar to that at Paseo with a pressure transducer on the banks reading the change in pressure on an orifice line in the water. The USGS considers this gage to have the most reliable rating curve in the Albuquerque reach, primarily because

of the length of the record but also because of the stability of the channel and therefore the rating curve.

3.5.4 Gages Discussion

In 2005, two consecutive large releases from the upstream Cochiti Reservoir caused a significant amount of scour (magnitude of feet) in the entire study reach. The scour altered the river so significantly that both Paseo and Central gages required new rating curves based on post-2005 data.

In addition, a new low head inflatable diversion dam was completed in early 2006 located 400 m downstream from Alameda Bridge (1400 m upstream of Paseo Bridge). Prior to dam completion, the shifts applied to the rating curves at both locations were both positive, indicating that the reach was scouring. The dam was installed and was left down (flat on the river bottom) for the rest of 2006. For this period, the shifts were consistently negative. The dam was impacting the river even though it was not operational.

As previously mentioned, confidence in the rating curves are limited to the range of discharges for which measurements were taken. Thus the rating curve must be extrapolated for any stage measurements beyond what has been measured in a calibration measurement. This can be a challenge especially for the Rio Grande that at times receives high intensity, short duration storm runoff events from urban areas. These events appear as very high but short lived spikes in river discharge. The surface water specialist in the Albuquerque USGS office considers the rating curve for the "real flashy stuff not real good for the upper end" and considers high flow events to be "a whole new ballgame" compared to stable periods of flow (personal communication, July 2008). Albuquerque USGS personnel have repeatedly emphasized that the rating curve may be descriptive prior to a large event, but river changes during high flow events can change the river significantly (personal communication, Sept 2008). In fact, the rating curve may be significantly different after a high flow event in the mobile bed channel. Even if the river returns to the same rating curve relationship after a large event, what occurred during the event may have been completely different.

The problems with extrapolating the rating curve and appropriately applying shifts is demonstrated by considering a storm event on July 8, 2006. Figure 3-5 plots the calculated (from the rating curves) discharge at the three gages, shifted to account for travel time between the locations. The significant difference in calculated flow between the Alameda and Paseo gages (Figure 3-4) is not attributed to the Calabacillas Arroyo or the other outfalls in the area.

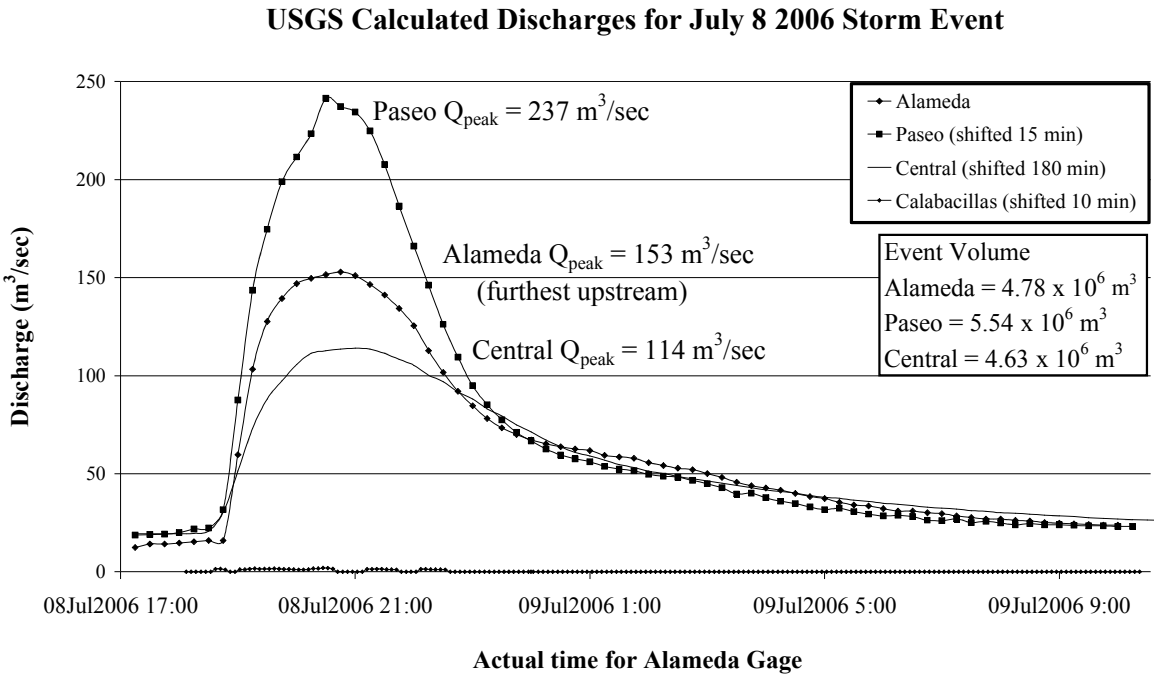

Figure 3-5: USGS Gage Measurements for July 8 2006 Storm Event

The stage height at the Paseo gage for the peak discharge was 2.07 meters at 21:00. However, the highest stage at which a calibration measurement occurred was 1.99 meters in 2005 with a discharge of 195 m^3/sec. In fact, on July 8th seven consecutive stage measurements registered higher than 1.99 m (20:30 to 22:00). This means that the July 8 peak computed discharge was extrapolated, which may be part of the reason that this likely artificial high discharge occurs. The problematic discharge reading may also have its roots in the shift that was applied to calculate discharge. It is impossible to determine if extrapolation beyond measured stage – discharge values or incorrect shift application – or a combination of the two – is the source of the huge discharge anomaly.

3.5.5 Gage Datums

To compare HEC-RAS calculated water surface elevations (WSE) to the measured WSEs, the stage measurement was added to the gage datum. The USGS published gage datums for each gage are listed in Table 3-2. The gage datums at Alameda and Paseo were estimated from a twenty foot topographic map. The gage datum at Central was surveyed in the 1950s. In the early 1980s, Central Ave over the Rio Grande was consolidated to one bridge. Multiple reference marks are assigned elevations relative to the gage datum. The reference mark elevations were obtained from the National Geodetic Surveying or via measurement by both real-time centimeter accuracy global navigation satellite system measurement and traditional leveling. The gage datum elevation was determined by subtracting the reference mark's gage datum height from the reference mark elevation (Table 3). The extreme difference at the Alameda gage is likely due to estimation from a topographic map that was interpolated in the wrong direction. The difference at Paseo comes from the resolution of surveying versus estimating from a topographic map. The Central gage datum, having been previously surveyed, was found to be consistent with the published value.

Table 3-2 Gage datums for study reach gages

Gage	USGS Published (NGVD29) (m)	USGS Published (NAVD88) (m)	Measured (NAVD 88) (m)	Difference (m)
Alameda	1539.24	1539.85	1519.25	20.60
Paseo	1520.95	1521.87	1519.72	2.15
Central	1507.59	1508.40	1508.42	-0.02

3.6 Methods

In the study reach, the Alameda gage is considered to be the most questionable, primarily due to the channel geometry issues mentioned previously. At similar dual channel cross sections in other rivers, continuously monitoring a gage's accuracy may be difficult. In this study, the proximity of the Paseo gages allows evaluation of the quality of the Alameda gage.

To study the impact different hydrographs have on a model, an unsteady HEC-RAS model of the study reach was created. The model was calibrated and validated (see Chapter Four and Appendix A for detailed description) using the Paseo calculated

discharge as the upstream boundary condition and the Central stage measurement as the downstream boundary condition. Four time periods (two to three days each) were selected to represent different seasonal flows in the Rio Grande (Table 3-3). For each time period, the calculated discharge hydrographs for Paseo and Alameda were used as the upstream boundary conditions then the calculated WSE at each cross section was compared for the two cases.

Table 3-3 HEC-RAS Input hydrograph characterization

	Paseo Discharge Hydrograph (all values m^3/sec)			Alameda Discharge Hydrograph (all values m^3/sec)		
	Average	Maximum	Minimum	Average	Maximum	Minimum
Fall	11	12	10	10	12	9
Winter	24	27	21	26	30	24
Spring	78	95	68	103	117	99
Summer	48	60	34	59	68	39

The maximum water depth at each cross section was calculated by subtracting minimum channel elevation from the calculated WSE for every time step in the Paseo hydrograph input case. The average of the maximum depth at each time step is presented in Table 3-4 for each cross section. The difference between the WSE calculated from the Paseo hydrograph and the WSE calculated from the Alameda hydrograph was determined for each cross section. This difference was averaged over all the time steps (Table 3-4).

Table 3-4 HEC-RAS calculated water surface elevation (WSE) comparisions

	Bridge	Average Paseo WSE - Alameda WSE (m)	Average Max Depth at the Cross Section (m)	%	Maximum Paseo WSE - Alameda WSE (m)	Corresponding Maximum Water Depth (m)	%
Fall	Alameda	0.01	0.22	3.9	0.03	0.25	13.3
	Paseo	0.01	0.29	4.5	0.04	0.45	9.5
	Central	0.01	0.23	5.4	0.04	0.29	13.5
Winter	Alameda	-0.02	0.38	-4.8	-0.03	0.36	-7.7
	Paseo	-0.03	0.60	-4.5	-0.04	0.61	-7.0
	Central	-0.03	0.42	-6.3	-0.04	0.42	-8.8
Spring	Alameda	-0.07	0.55	-12.6	-0.21	0.73	-29.0
	Paseo	-0.08	0.84	-10.0	-0.21	1.05	-20.0
	Central	-0.08	0.63	-13.1	-0.22	0.85	-26.1
Summer	Alameda	-0.15	0.73	-20.8	-0.11	0.52	-21.5
	Paseo	-0.15	1.05	-14.6	-0.13	0.80	-16.7
	Central	-0.16	0.84	-18.7	-0.13	0.60	-21.8

Table 3-4 shows the percentage of the maximum depth that the difference between the Paseo hydrograph derived WSE and the Alameda hydrograph derived WSE represents. For lower flows, the difference between the calculated WSE for the Alameda and Paseo inputs is minimal (less than 0.05 m). However, at higher flows the difference between the calculated WSEs can be significant, and represent a significant portion of the total water depth. That the difference between the calculated water surfaces can be 30% of the maximum water depth illustrates the importance of the input hydrographs.

3.7 Conclusions

USGS streamflow data is an extremely valuable resource for understanding sand bed rivers. However, when using this data, modelers should consider the following points.

1. Know the limitations of the gaging site. Sites such as the Alameda site with dual channels will probably never have reliable stage – discharge curves. Whenever possible, these gages should be avoided as boundary conditions in models.
2. Understand the limitations of the stage - discharge curve development and maintenance at each gage site used.
3. Unsteady high computed discharges should be used with extreme caution to calibrate models, due to the high probably of bed change that will not be accounted for in the rating curve.
4. Flood events are likely to be unsteady flows where lots of bed movement occurs, and the stage discharge relationship is questionable. Therefore, consider calibrating to the actual stage measurement in addition to peak discharge and volume, especially if high water marks are not available. This will not be possible for daily data.
5. For models where the water surface elevation is important (i.e. a flood inundation study) and will be transferred to other programs, confirm that the value of the gage datum has been surveyed.
6. Do not consider a single gage in isolation from the system. Whenever possible, plot upstream and downstream gages for the time period of interest to check for potentially mis-applied shifts.

There are many modeling issues that are not addressed in this discussion – changing Manning's *n* as a function of discharge, loop rating curves that account for overbanking, etc. This paper is not intended to address all model calibration issues, but to ensure awareness about the limitations and challenges of working with USGS streamflow data. Gaging sand bed rivers is a challenging task and a modeler should make every effort to use streamflow data appropriately.

4 Coupling GIS and HECRAS to Create Comprehensive Riparian Water Surfaces

4.1 Introduction

Historically, groundwater and surface water have been considered separately in both the scientific and legal communities. This attitude has changed as research highlighted the importance of groundwater-surface water interaction in water supply and water quality (Jackson et al. 2001). Quantification of groundwater-surface water exchange in its spatial and temporal variability is important for optimal water management decisions. Thus, the connectivity of groundwater and surface water is particularly important in arid and semi arid regions that have limited water resources (Jackson et al. 2001) that are highly regulated, engineered, and managed. Water budgets are "critical components" of water management in arid and semi-arid regions (Dahm et al. 2002).

Quantifying the magnitude and timing of groundwater – surface water exchange may be extremely important for proper water accounting, depending on the river system. However, simple numbers and flow rates may be hard to use to help decision makers understand complicated groundwater-surface water systems (i.e. should a new well be permitted?). This is especially true with groundwater surfaces, where it is physically impossible to view the entire surface at a point in time. Therefore, visualization tools that create pictures of what we cannot see facilitate better understanding of these complex systems. Coupling the surface water and groundwater in one image may provide additional insight into the groundwater-surface water relationship.

The purpose of this study is to create a tool that predicts depth to groundwater in the riparian corridor as a function of river discharge. This tool can be used to study management alternatives for dam releases, restoration projects, and climate change studies in the Albuquerque Reach of the Rio Grande. The process outlined in this paper can be used to create similar models for other areas to aid in management and climate change studies. The other purpose of this study is to create visualization tools that will graphically demonstrate the connectivity of the river and shallow groundwater. The

visualization tool can also be used to help stakeholders understand how different management techniques affect the groundwater and in turn can affect consumptive losses.

4.2 Study Area

The study is focused on a portion of the Albuquerque Reach of the Middle Rio Grande, from the North Diversion Channel confluence to the Central Bridge. There are three main stem United States Geological Survey (USGS) gages in this reach: Rio Grande at Alameda Bridge at Alameda, NM, Rio Grande near Alameda, NM, and Rio Grande at Albuquerque, NM. They are 3.2 km, 5 km, and 17 km, respectively from the beginning of the study reach. All of these gages are mounted on bridges: 'at Alameda' is on the Alameda Bridge; 'near Alameda' is located on the Paseo del Norte Bridge; and 'at Albuquerque' is on the Central Ave Bridge. These gages will be referred to as: Alameda, Paseo, and Central.

Within the study reach, there are two major tributaries. The concrete lined North Diversion Channel (NDC) drains 284 km^2 of Albuquerque and only flows for precipitation events on the city itself or on the western face of the mountains due east of the city. The NDC is the northern boundary of the study reach. The mostly sand bed Calabacillas Arroyo begins in the desert west of the city and drains 90 km^2 of Albuquerque. It also is a storm water conveyance channel that is extremely flashy in nature with a high sediment load because of its partial sand bottom. The Calabacillas Arroyo enters the Rio Grande between the Alameda and Paseo Bridges, 540m upstream of the Paseo Bridge.

The primary source of water for this stretch of the Rio Grande varies seasonally, although actual streamflow is controlled by Cochiti dam year round. Cochiti is located approximately 80 km upstream of Albuquerque. The entire Rio Grande traditionally experiences its highest streamflow in springtime (March-May) as a result of melting snowpack within the watershed. Irrigation diversions begin March 1 every year. The summer streamflow is maintained in large part by irrigation water being passed through the system, although brief high streamflows result from monsoonal rain throughout July and August. September and October traditionally have the lowest average streamflow.

October 31 is the end of irrigation season, so there is usually a marked increase in streamflow on November 1 as all irrigation diversions are closed.

In 2006, construction was completed on a low head dam in the Rio Grande between the Alameda and Paseo del Norte Bridges (Figure 4-1). The dam is part of the Albuquerque - Bernalillo County Water Utility Authority (ABCWUA) San Juan Chama Drinking water project, in which the primary water supply for Bernalillo County changed from groundwater to surface water. The low head dam, constructed in 24 gates that can be individually raised and lowered, will continuously divert 3.7 m^3/sec to be treated and blended with groundwater for municipal supply.

The Bosque Ecological Monitoring Program (BEMP) maintains 20 shallow wells in the area of the dam (Figure 4-1). The wells were originally monitored by middle school students on a periodic basis. With funding from the USACE, during the summer of 2006 twelve of the wells were equipped with Solinst Model 3001 Gold Pressure Transducers (Solinst Canada Ltd, Ontario Canada) that record water depth every 15 minutes. By the fall of 2007, the remaining wells were also outfitted with pressure transducers. Just upstream of the Montaño Bridge the USGS has fourteen groundwater wells that record depth to groundwater and temperature every hour. These wells are arranged in transects across the river with a well located at the east riverside drain, one in the middle of each riparian zone, a well on each side of the river, and a pair of wells bracketing the west riverside drain (Figure 4-1). These two sets of groundwater data were used to estimate the groundwater table in the riparian corridor.

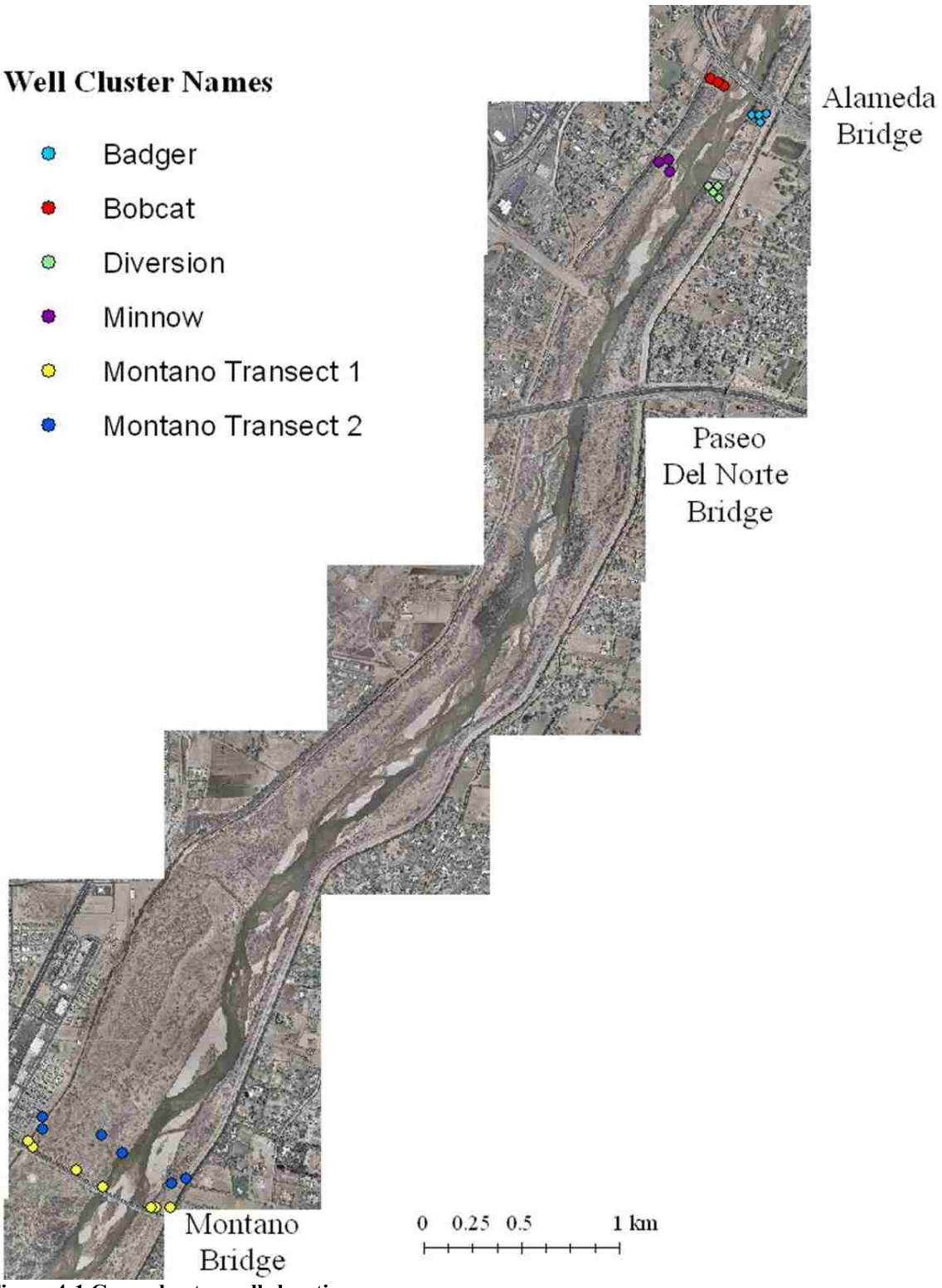

Figure 4-1 Groundwater wells location map

4.3 Groundwater Data Analysis

4.3.1 Groundwater Data

The initial concept was to take only the point surface water measurements (interpolated with HEC-RAS), and the groundwater well points to define a comprehensive water surface for the riparian corridor. However, when combining these data sets it became evident that there needed to be some boundary condition that defined the gradient from the river because the riparian water surface became less meaningful with increasing distance from the wells. The riverside drains were a logical boundary condition, as their current primary purpose is to intercept river water lost to groundwater. The idea that the water surface elevation in the riverside drains would serve as a boundary condition for flow from the river became the working conceptual model.

The groundwater data was plotted with the appropriate HEC-RAS cross section in Excel to visualize depth to groundwater and gradient (Figures 4-2 to 4-6). The HEC-RAS cross section is plotted looking downstream, so the east riverside drain is on the left and the west riverside drain is on the readers' right. Note that the vertical and horizontal scales of these plots are significantly different, so that in the Montano plots (Figures 4-5 and 4-6) although the well on the west side of the west riverside drain (the furthest right blue dot) appears to be under the drain, it is actually thirty feet to the west (right). These subtleties are lost at the wide horizontal scale.

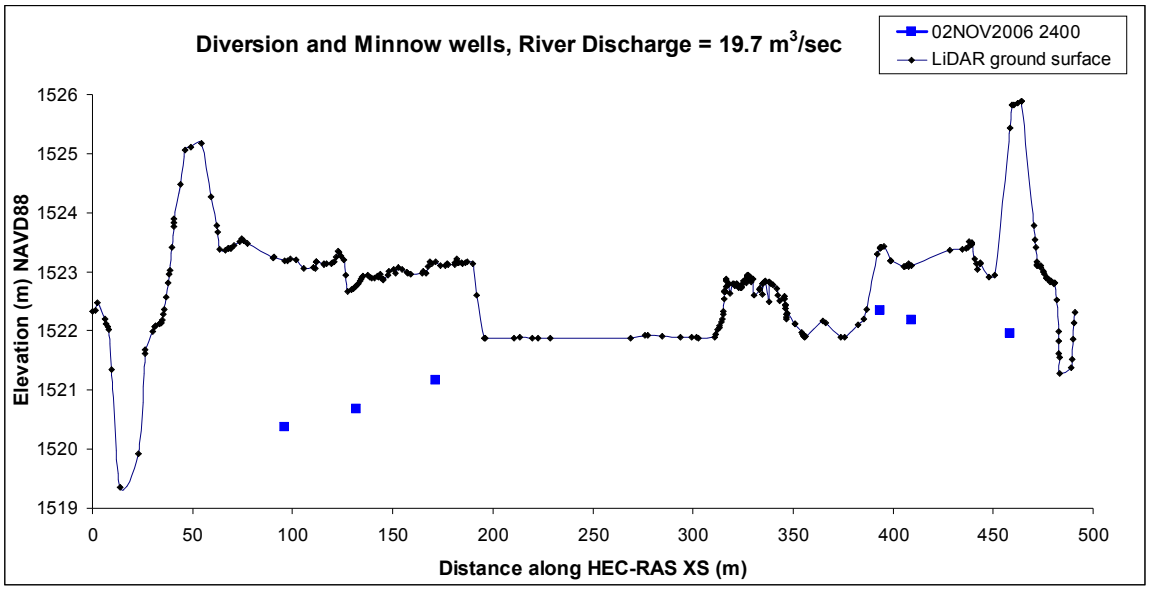

Figure 4-2 Groundwater elevation for BEMP wells at 02NOV2006 2400 with HEC-RAS ground surface

The BEMP well data plotted with the ground surface (e.g. Figure 4-2) suggest a linear gradient from the river. Figures 4-3 and 4-4 show the line (blue) described by linear regression of the groundwater elevations for two representative streamflows. On both dates, each linear groundwater gradient intersects the riverside drains above the invert elevation, which would result in water in the riverside drains. This behavior is consistent with the assumption that the riverside drains drive the groundwater gradient in the riparian corridor.

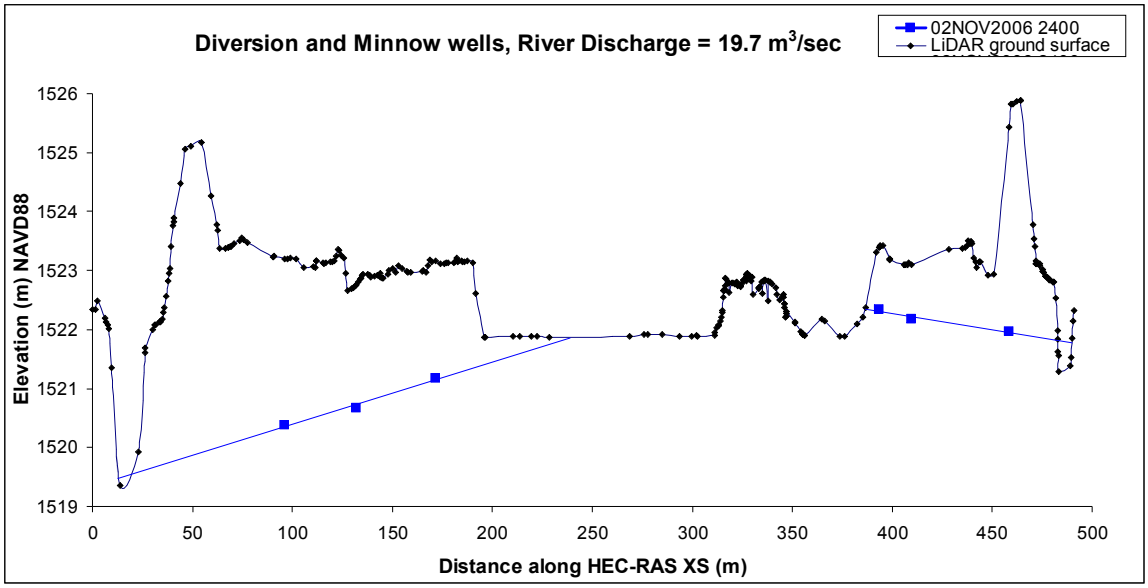

Figure 4-3 Groundwater elevation in BEMP wells at 02NOV2006 2400 with HEC-RAS ground surface

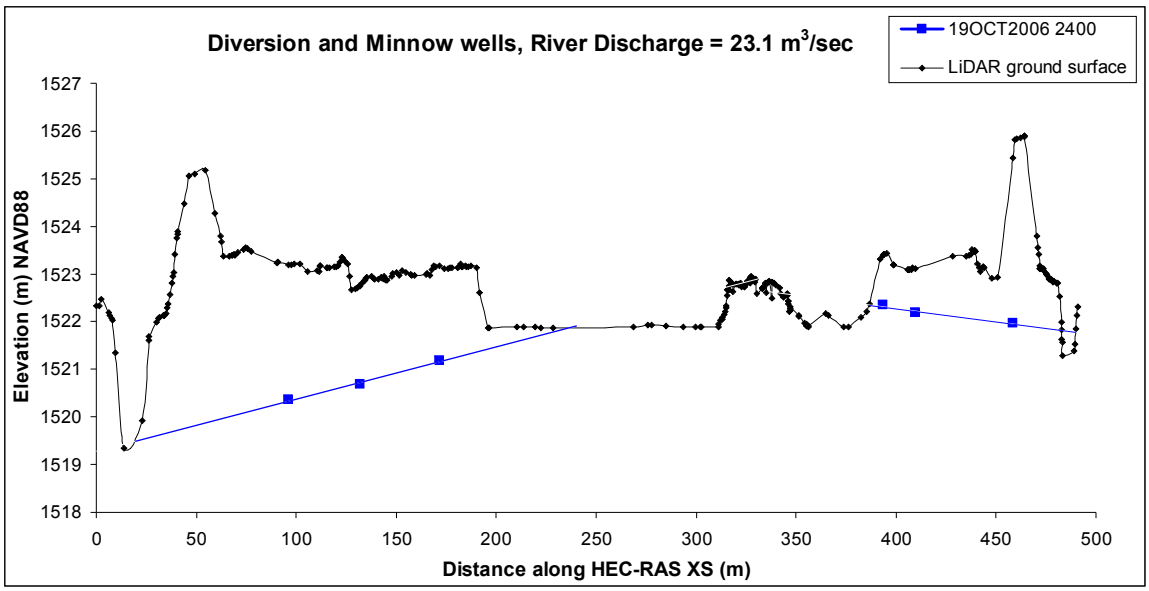

Figure 4-4 Groundwater elevation in BEMP wells at 19OCT2006 2400 with HEC-RAS ground surface

The well data at Montano was then analyzed to validate the assumption that the riverside drains drive the gradient in the riparian corridor. In Figure 4-5 at the Montano Bridge, the groundwater levels are significantly below the west riverside drain invert elevation. This indicates that that riverside drain does not appear to be significantly interacting with the groundwater at this location, much less driving the gradient from the river. This plot is taken from data in November, when irrigation diversions have ceased. Figure 4-6 shows a similar plot during irrigation season. Clearly, the west riverside drain is still not significantly interacting with the groundwater elevation at this location. This indicates that the riverside drains serve as a boundary condition is incorrect.

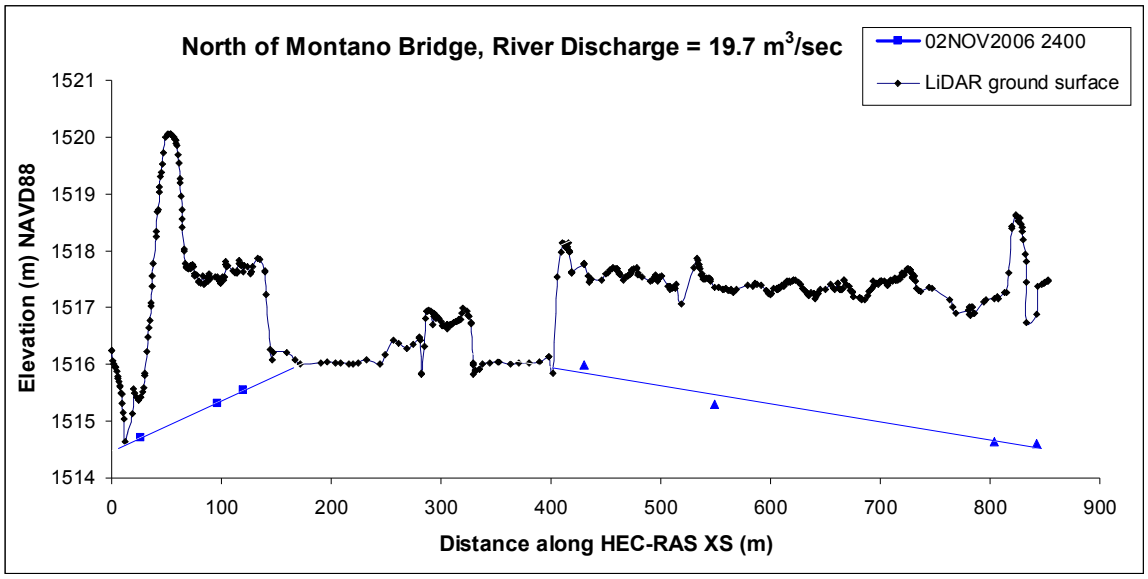

Figure 4-5 Groundwater elevation in USGS wells at 02NOV2006 2400 with HEC-RAS ground surface

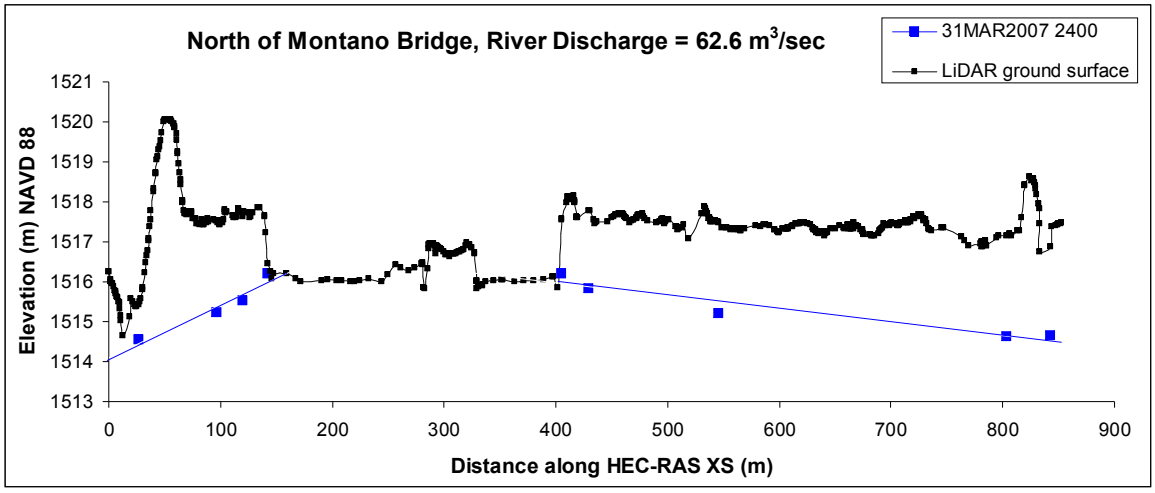

Figure 4-6 Groundwater elevation in USGS wells at 31MAR2006 2400 with HEC-RAS ground surface

This discrepancy is partly attributed to changing riverside drain invert elevation. The current purpose of the riverside drains is to capture streamflow that is infiltrating to groundwater then return it to the river. To do this, the riverside drains were constructed such that the drain invert elevation is below the river invert elevation. However, to return water to the river, at the confluence the riverside drain invert elevation must be the same as the river invert elevation. This is accomplished by gradually decreasing the slope of the riverside drain for some length upstream of the confluence. For the study reach, the west riverside drain empties into the Rio Grande 1500 meters downstream of the Montano Bridge. Therefore, as can be seen in Figure 4-6, the west riverside drain invert elevation is actually above the river invert elevation. In Figure 4-4 at the BEMP wells, the west riverside drain invert elevation is approximately one meter below the river invert elevation. This is true for most of the study reach, with the exception of when the drain returns flow to the river. For the entire study reach, the east riverside drain is cut deeper than the west riverside drain, on average three meters lower than the river invert elevation. However, the east drain returns part of its flow to the Rio Grande half way between Interstate 40 and the Central Bridge therefore it also experiences a stretch where the invert elevation is higher than the river. This variability in relative invert elevation to the river indicates that the gradient control must be something other than the water surface elevation in the riverside drains.

The USGS has four other transects similar to the one at Montano utilized in this study. The purpose of these transects is to understand the river-riverside drain interaction and what controls the gradient from the river. Discussions with the USGS about this analysis and their in-house analyses of groundwater data led to the conclusion that city pumping likely controls the gradient.

4.3.2 Gradient Analysis

For the four plots above, a linear trend line was added to the well data on each side of the river (Figure 4-7). The slope and R^2 value of each trend line are summarized in Table 4-1 below.

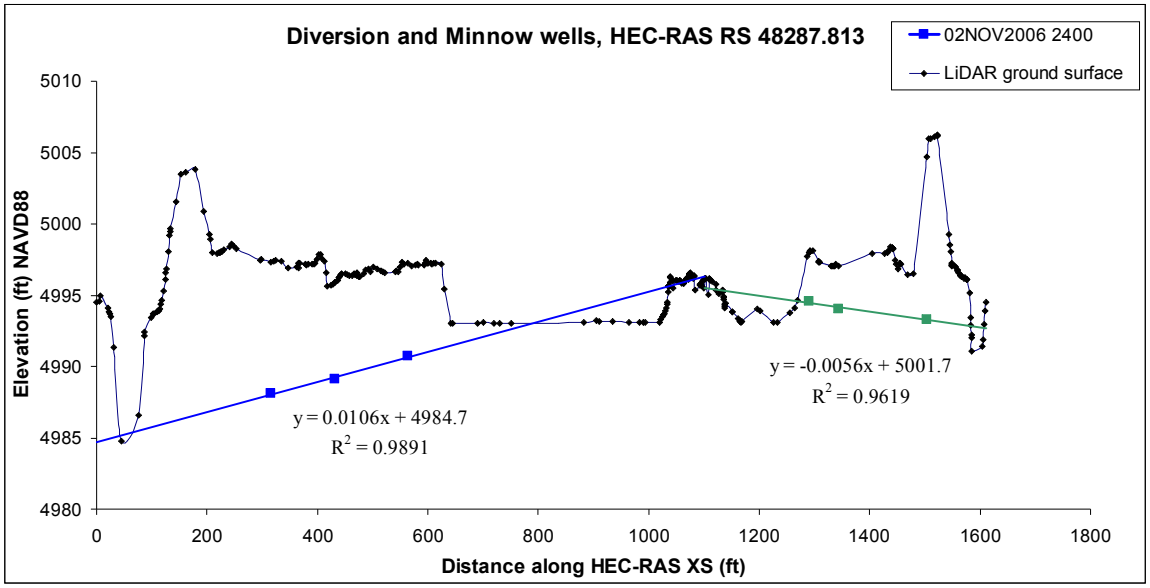

Figure 4-7 Linear gradient calculated from well data, 02NOV2006 2400

Table 4-1 Slope and gradient from linear regression of the USGS and BEMP well data

	East Wells		West Wells	
	Slope	R^2	Slope	R^2
NOV Paseo	0.0106	0.9891	0.0052	0.9619
OCT Paseo	0.0109	0.9887	0.0052	0.9901
NOV Montano	0.0088	0.9989	0.0032	0.9595
APR Montano	0.0104	0.9957	0.0028	0.9391

Several groundwater characteristics are illuminated in Table 4-1. Physically, there are most likely different soil layers around and beneath the river that cause the groundwater gradient to change as water passes through each soil type and the groundwater gradient might most appropriately be estimated by 'connecting the dots' and drawing a straight line between each well. However, the R^2 values from the linear regression indicate a linear relationship does a good job of approximating the shape of the groundwater surface between the wells. Table 4-1 shows the gradient on the east side of the river is very consistent between the two sites, Paseo and Montano. Although the gradient on the west side of the river is the same at Paseo through time, it varies slightly more between Paseo and Montano (maximum difference of 0.0024 m/m) than the east side (max difference of 0.0021 m/m). At both sites there is a steeper gradient on the east side than the west side.

When the water surface elevation in the river is added as a point in the linear regression, the R^2 value decreases across the board, although the slopes stay reasonably consistent (Table 4-2).

Table 4-2 Slope and gradient from fitting a linear equation to the USGS and BEMP well data, including the river surface

	East Wells		West Wells	
	Slope	R^2	Slope	R^2
NOV Paseo	0.0168	0.876	0.004	0.6648
OCT Paseo	0.0171	0.8795	0.0041	0.7312
NOV Montano	0.012	0.8978	0.0036	0.9525
APR Montano	0.0133	0.9276	0.0033	0.9161

The fact that the gradient remains so consistent between the two sites reinforces the idea that city pumping drives the gradient instead of the riverside drains, because on the west side the riverside drains have completely different relationships with the groundwater between the two sites, yet the gradient remains the same.

The magnitude of the eastern gradient being smaller than the western gradient also appears to be consistent with the assumption that city pumping is driving the gradient. Figure 4-8, from USGS WRI Report 03-4040, presents the locations of city well clusters. A well cluster is located just east of the river near the Montano Bridge, which would account for the increased gradient away from the river at that location. Other figures in the same report also demonstrate that the cone of depression from city pumping is much more severe on the east side of the river than the west side. This depression explains why BEMP wells also demonstrate a steeper gradient in the eastern riparian corridor than the western, not just the USGS wells at Montano.

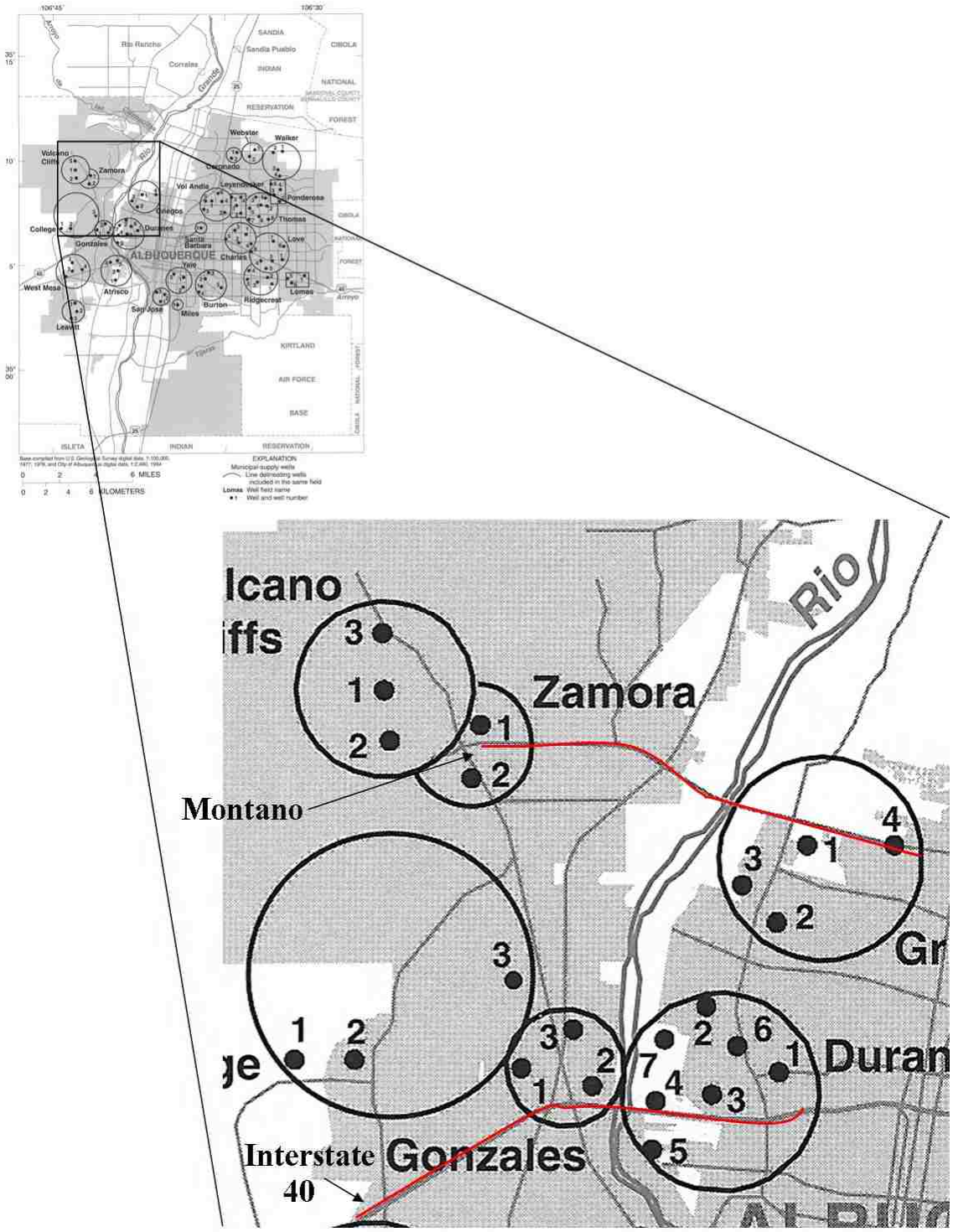

Figure 4-8 Location of well clusters in the Albuquerque area, from USGS WRI Report 03-4040, with discussed wells highlighted

Thus, neither riverside drain in the study reach serves as the boundary condition for the gradient away from the river. However, because the riverside drains provide an excellent location for assigning a boundary condition (consistently parallel to the river), the water surface elevation will be fixed at the horizontal position of the riverside drain. This does not imply that the drain is driving the gradient. The elevation of the water surface is determined from the well data, as discussed below.

4.3.3 Determining Water Surface Elevation at the Riverside Drains

In the preceding analysis, the relative stability of the water surface elevation in the wells near the riverside drains was observed, leading to speculation that water surface elevation could be assumed constant over certain periods of time (i.e. irrigation season, vs. non-irrigation season). The Montano cross sections have wells placed directly next to the riverside drain, so the USGS data was used for the following analysis. The BEMP wells are not close enough to the riverside drains.

To investigate seasonal stability, time periods from 2006 and 2007 were selected: January 1 to February 28, April 1 to May 31, June 1 to July 31, and November 1 to December 31. For each time period, the average water surface elevation in each well was calculated. As shown in Table 4-3, the standard deviation of the water surface elevation at each well for each time period is very small, indicating that the water surface elevation does not vary much. The missing data for the west riverside drain east well are because there were no data available for those dates.

Table 4-3 Average standard deviation (m) in the Montano Transect 1 Riverside Drain Wells. East RD, W = well on the west side of the east drain; West RD, E = well on the east side of the west drain; West RD, W = well on the west side of the west drain

Dates	East RD, W	West RD, E	West RD, W
01JAN-28FEB 2006	0.055	0.067	0.098
01APR-31MAY 2006	0.055	0.084	0.141
01JUN-31JUL 2006	0.069	0.057	0.054
01SEP-09SEP 2006	0.031	0.030	0.029
01NOV-31DEC 2006	0.101	0.058	0.059
01JAN-28FEB 2007	0.065	0.061	0.059
01APR-31MAY 2007	0.038		0.058
01JUN-31JUL 2007	0.034		0.109
01NOV-31DEC 2007	0.062		0.319

Table 4-4 shows the average water surface elevation for each of the time periods. The dates have been rearranged to reflect groupings based on whether the time period occurs during irrigation season (green) or not (blue), illustrating that the water surface elevation in these wells are reasonably consistent year to year (the averages differ by a maximum of 0.64 ft). There is no clear-cut difference between the two groupings, indicating there is no basis for an irrigation season – non-irrigation season delineation.

Table 4-4 Average Water Surface Elevation (m) in the Montano Transect 1 Riverside Drain Wells

Dates	East RD, W	West RD, E	West RD, W
01NOV-31DEC 2006	1514.62	1514.67	1514.63
01NOV-31DEC 2007	1514.55		1514.80
01JAN-28FEB 2006	1514.61	1514.65	1514.69
01JAN-28FEB 2007	1514.48	1514.65	1514.60
01APR-31MAY 2006	1514.67	1514.60	1514.56
01APR-31MAY 2007	1514.78		1514.76
01JUN-31JUL 2006	1514.56	1514.67	1514.57
01JUN-31JUL 2007	1514.58		1514.55

To investigate seasonal control (versus monthly above) for the water surface elevation (i.e. city pumping is higher during the summer due to increased water demand and decreases in the winter), all the water surface elevation data in the wells furthest from the river were plotted for the entire period of record. The well on the east riverside drain and the two wells on the west riverside drain were all plotted together (Figure 4-9).

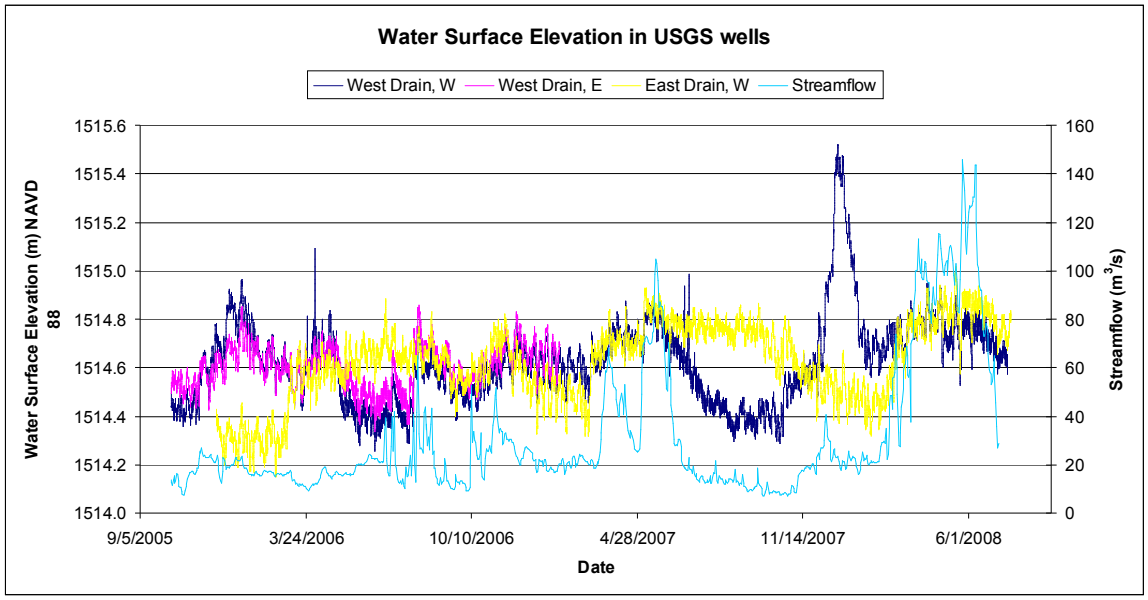

Figure 4-9 Water Surface Elevation in the USGS wells.
WDWS = West Drain West Shallow (the drain on the west side of the west riverside drain), WDES = WestDrainEastShallow (well on the east side of the west riverside drain), EDWS = East Drain West Shallow (well on the west side of the east riverside drain).

The water surface elevation appears to exhibit cyclical characteristics. However, the period of record is not long enough to establish yearly trends. The data available exhibit low flow periods that initiate and terminate at different months of the year, so a monthly average does not appear meaningful. It is also apparent from Figure 4-9 that the two west wells have extremely similar patterning, but the east drain well predominately behaves differently from the west wells. This suggests that the wells on each side of the river that are closest to the riverside drains either 1) are not strongly influenced by streamflow or 2) have extremely different stratigraphies. The daily streamflow on Figure 4-9 illuminates this relationship further. Several of the monsoonal streamflow peaks in July and early August 2006 are reflected in both the east and west drain wells. However, the east drain well does not mirror the drop in streamflow from June to October 2007 and the west drain well exhibits a significant increase in groundwater elevation that is not explained by an increase in streamflow in January 2008. While the wells exhibit similar patterns to the streamflow data, clearly they are influenced by other sources of water (i.e. water being routed through the riverside drains).

Figure 4-10 plots the sole east riverside drain well in addition to the water surface elevation in the east riverside drain and river streamflow. Figure 4-11 plots both wells on the west riverside drain with the river streamflow and the water surface elevation in the west drain. Figure 4-10 shows that the groundwater elevation in the well next to the east riverside drain follows the water surface elevation in the drain very closely unlike the west riverside drain wells (Figure 4-11) which are consistently 1.8 meters lower than the riverside drain. This discrepancy indicates that either the water surface elevation in the well on the east riverside drain has more interaction with the water in the riverside drain, or that the water surface in the drain coincides with the water table at this location. The spike in groundwater elevation in the west wells is explained by a similar peak in the west riverside drain surface water measurement, indicating that some water was moving through the system via the west riverside drain. This flow event in the west riverside drain is the cause of the abnormally high standard deviation for the 2007 November to December time period in Table 4-3.

All of the analysis presented in this section guided the final process utilized in the Methods section below.

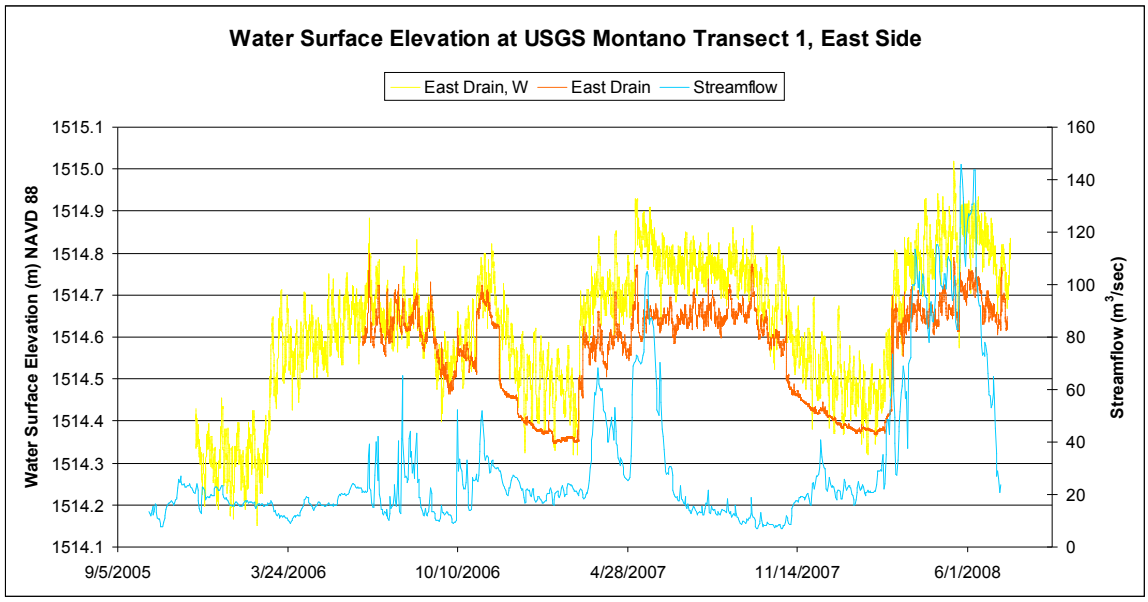

Figure 4-10 Water surface elevation in the EDWS well and the East Riverside Drain

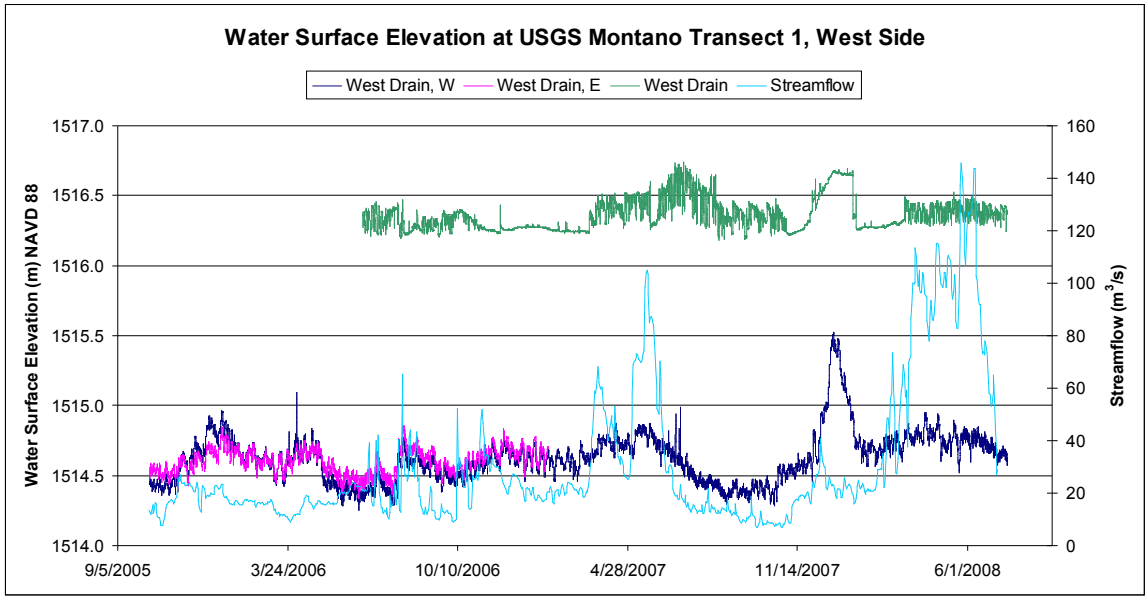

Figure 4-11 Water surface elevation in the WDWS and WDES wells and the West Riverside Drain

4.4 Methods

This study combines the terrain model building and display capabilities of ESRI's ArcGIS with the hydraulic model HEC-RAS via the tool HEC-GeoRAS. Figure 4-12 provides an overview of the process utilized.

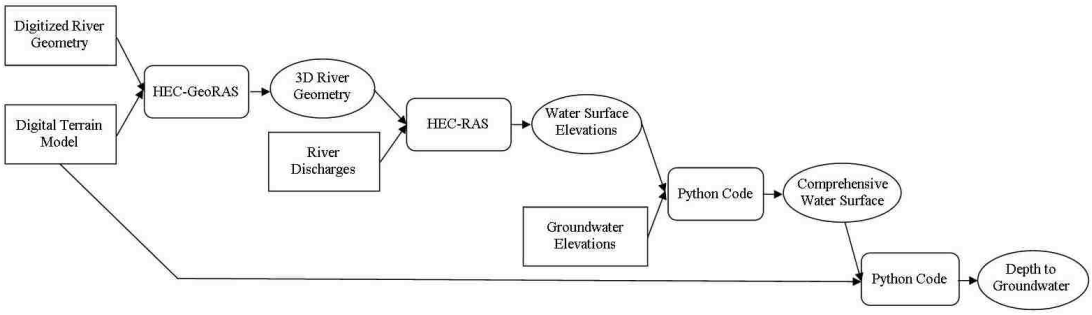

Figure 4-12 Methods overview

4.4.1 Model Geometry and Flow Files

Airborne LiDAR data flown in 1999 was used as the basis of the terrain model for the riparian corridor in ArcGIS. Multiple TINs of LiDAR data covering the study area were combined to create one TIN of the study reach. All points within the river were deleted. The channel is defined in the terrain model based on 2006 Bureau of Reclamation cross sections taken every 150 m. These cross sections were interpolated in ArcGIS with a tool that accounts for river meandering, described in Merwade et al (2008). The tool outputs an interpolated mesh derived from the cross sections. Because the LiDAR data has significantly more island detail, specifically island lengths, the TIN island points were added to the mesh of interpolated cross sections. This enhanced mesh was added to the LiDAR TIN to define the channel.

All of the HEC-RAS required geometries were delineated in ArcGIS by studying aerial photos including the river thalweg, overbank flowpaths, banklines, cross section lines, and levee locations. Initial Manning's *n* values were assigned to cross section locations by whether the area was river channel (0.03), river islands (0.05), or riparian corridor (0.08), based on a HEC-RAS model previously developed by the US Army Corp of Engineers. HEC-GeoRAS was utilized to create the HEC-RAS geometry from the terrain model and export it from ArcGIS to HEC-RAS. Some adjustments to levee locations and riparian areas were made to several cross sections in HEC-RAS based on

aerial photos. Appendix A contains detailed descriptions of how the HEC-GeoRAS layers were developed and justification for the modifications to HEC-RAS cross sections.

An unsteady HEC – RAS model was created with this geometry. USGS fifteen minute calculated discharge from the Paseo gage was used as the upstream boundary condition; the Central stage measurement was used as the downstream boundary condition at the final cross section. The final cross section is 1030 m downstream from the Central cross section, so the measured WSE at Central was adjusted to account for the drop in river channel bed elevation by subtracting the measured channel bottom slope of that reach (0.0009) times the distance between the two cross sections. The USGS measurements at the time step before the period under consideration were utilized as the initial conditions.

An unsteady model may not have been necessary for the present study because there is only minor overbanking at the flows considered so a looped rating curve to account for return overbanking flows is unnecessary. An unsteady model was developed to study other aspects of HEC-RAS modeling (i.e. HEC-RAS sensitivity to refined bathymetric data) that are not presented here.

4.4.2 Model Calibration

The HEC-RAS model was calibrated with fifteen minute USGS discharge data. The goal of this project is to correlate river stage to groundwater elevation; therefore the HEC-RAS model was calibrated to stage measurements at the three bridges instead of peak discharge and volume, although all three variables were considered. In order to calibrate to stage, control markers for the gage datum at each gage were surveyed and the actual gage datum was determined. The stage measurement was added to the gage datum to calculate the actual water surface elevation (WSE) relative to mean sea level in NAVD88. The calculated WSE for the USGS fifteen minute stage measurements was compared to the HEC-RAS calculated WSE. Manning's *n* values and geometry were adjusted to minimize the difference between the calculated (HEC-RAS) and measured (USGS) water surface elevations averaged over all the time steps. Discharge dependent travel times were accounted for in measured versus calculated comparisons. More information about model calibration is located in Appendix A.

This model is designed to represent conditions after the diversion dam was installed, so the calibration flows were selected after spring 2006. On the advice of USGS personnel (personal communication, July 2008), flows during the monsoon season were avoided due to lack of confidence in the rating curves. Dam operation, which began in January 2007, essentially invalidates the rating curves at Alameda and Paseo (see Chapter 3 for a discussion of rating curves). Therefore, calibration flows were selected from September, October, and November of 2006: after the monsoon season yet before dam operation commenced. Due to these constraints, the highest calculated discharge used in this study was only 53.5 m^3/s which occurred in November 2006 as a result of a Cochiti dam release. Table 4-5 outlines the calibration flows utilized in this study.

Table 4-5 Calibration flows characteristics

Name	Start	End	Max Q (m^3/s)	Min Q (m^3/s)	Avg Q (m^3/s)
High	07NOV2006 0015	10NOV2006 2115	60.5	34.1	48.6
Moderate	18OCT2006 1330	20OCT2006 1330	27.2	20.9	23.6
Low	09SEPT2006 1000	09SEPT2006 1900	12.5	10.3	10.9

Ultimately the Manning's *n* values were set to 0.02 for the channel, 0.05 for channel islands, and 0.08 for the riparian corridor. Nordin (1964) calculates Mannings *n* values for the Bernalillo reach of the Rio Grande to be 0.0128 to 0.0284. Although the Bernalillo reach has coarsened considerably since Cochiti Dam was closed, the Albuquerque reach has not seen as dramatic coarsening (Ortiz 2004), so Manning's *n* values in this range have been validated by previous research. Additionally, the elevations of all the cross sections were reduced by 0.076 m. The drop in elevation was necessitated by the calibration during low flows – the measured stage (which is fixed in the model) did not create enough area for the measured discharges to pass through, therefore artificial significant pooling occurred behind the final HEC-RAS section. Because the selected Manning *n* values produced good results at the other flow rates, it was determined that the geometry was not representative of the channel conditions and the elevation of the entire reach was dropped. Dropping the channel elevation can be justified by considering the data that defined the channel: the cross sections that were used to generate the bathymetric data were estimated from aerial photos with some survey validation. It is reasonable that estimation from an aerial photo may be off by 0.076 m. This elevation change improved the calibration for all flows considered.

Figures 4-13 and 4-14 show the model input discharges and calibrated outputs at the Paseo del Norte cross section. As desired, the HEC-RAS generated discharge closely tracks the input discharges. Figure 4-15 and 4-16 show a close correlation between USGS measured stage (input) and the HEC-RAS calculated stage (output) at the Paseo del Norte and Central cross sections. Central follows the pattern of the input stage closely but is on average 0.08 meters lower.

It should be noted that the model calibration presented is not a unique solution. Manning's *n* is held constant throughout the reach in this calibration, although it could have been varied from cross section to cross section. An analysis of bed sediment size would be required to justify significant variation of Manning's *n* within the study area. Cross section geometry could also be modified at various locations, instead of the uniform channel bed reduction utilized, to achieve a model with similar outputs.

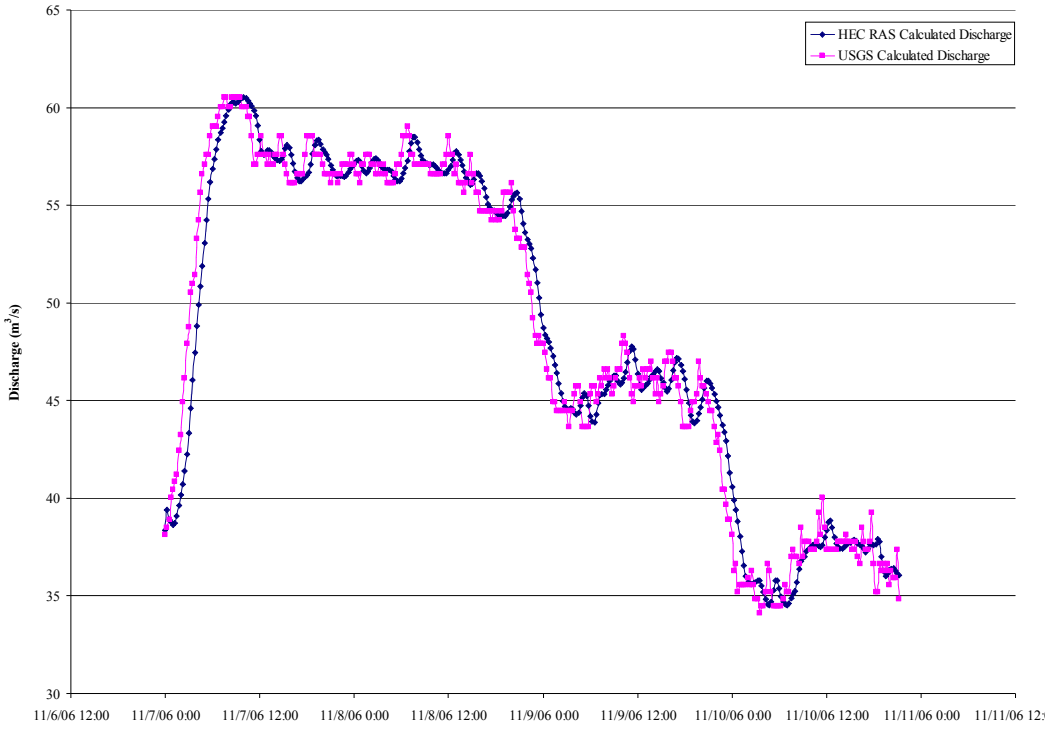

Figure 4-13 USGS Calculated Discharge (input) and HEC RAS Calculated Discharge (output) at the Paseo del Norte cross section for high flow calibration (Nov)

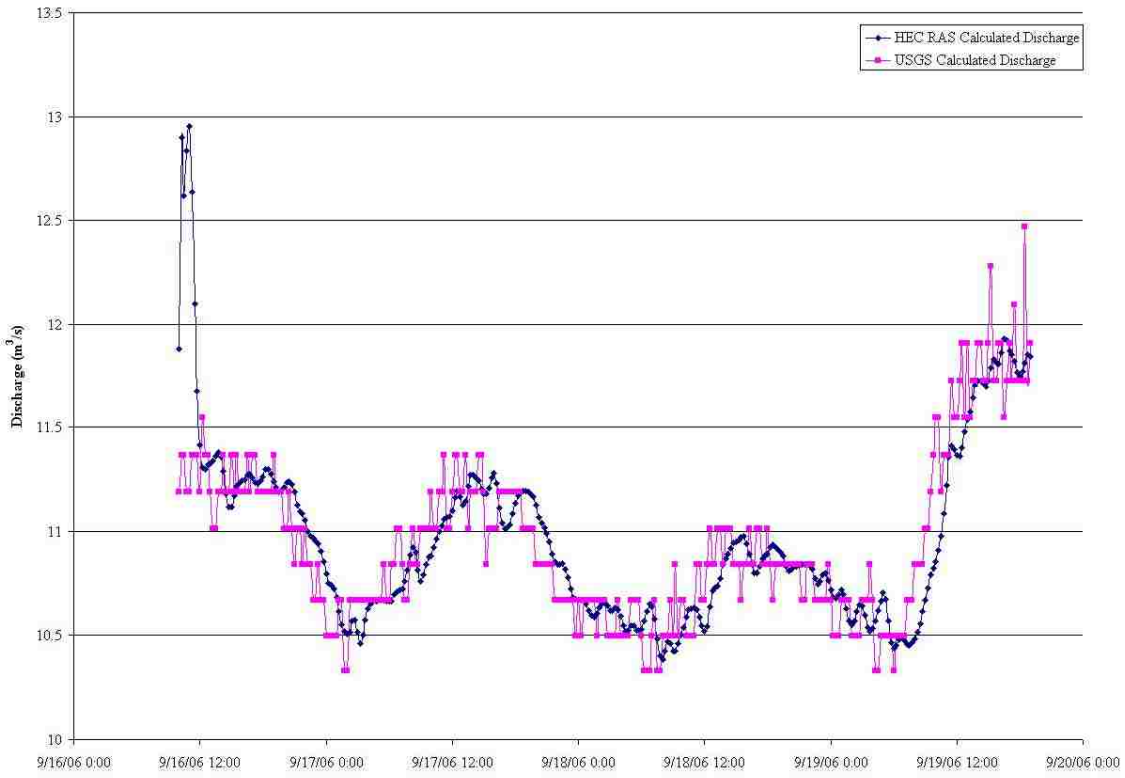

Figure 4-14 USGS Calculated Discharge (input) and HEC RAS Calculated Discharge (output) at the Paseo del Norte cross section for low flow calibration (Sept)

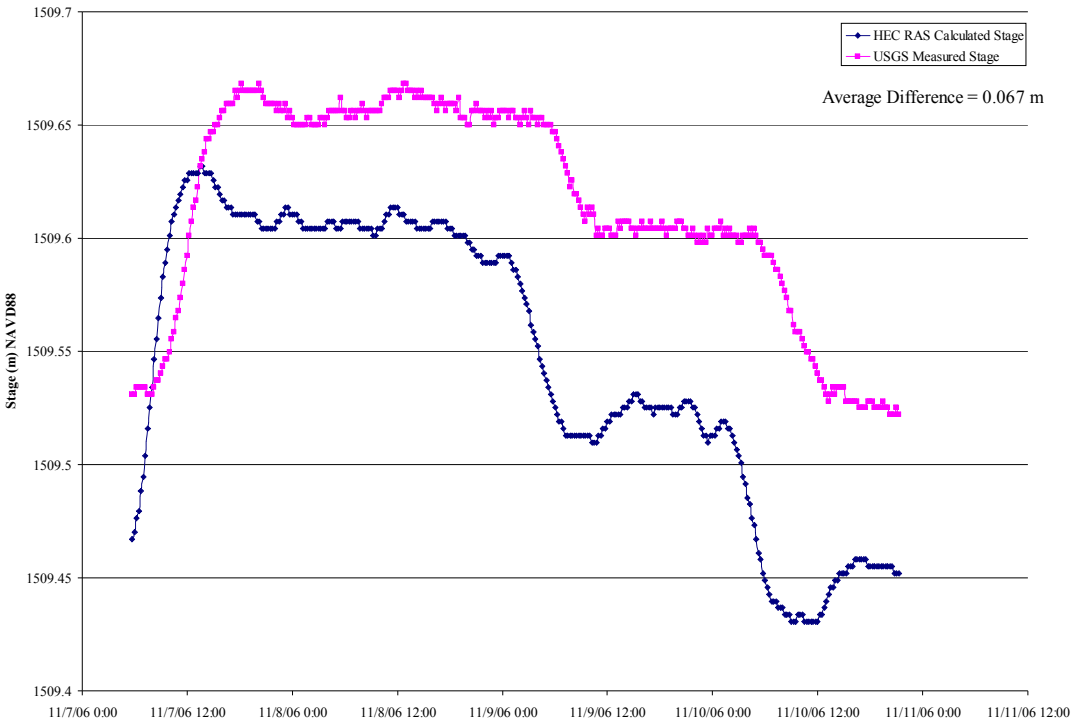

Figure 4-15 USGS measured stage (input) and HEC RAS calculated stage (output) at the Paseo del Norte cross section for low flow calibration (Nov)

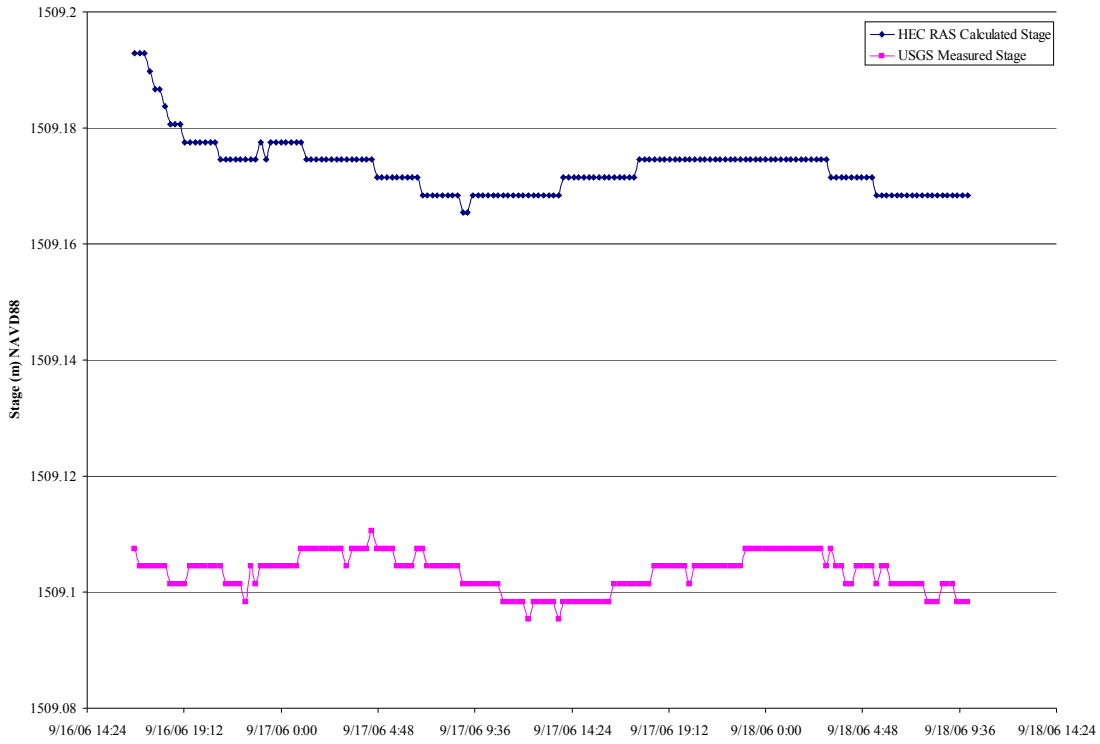

Figure 4-16 USGS measured stage (input) and HEC RAS calculated stage (output) at the Central cross section for low flow calibration (Sept)

4.4.3 Model Validation

Two flow series that meet the criteria listed above were selected to validate that the model correctly predicts water surface elevation. Again, the USGS calculated discharge at Paseo del Norte was used as the upstream boundary condition and the Central measured stage was used as the downstream boundary condition. The average of the difference between the measured and calculated water surface elevation at each gage for the two flow series is given in Table 4-6. The input and output stage at Paseo del Norte and Central are shown in Figures 4-17 and 4-18 respectively. The HEC RAS generated stage tracks the measured stage very well for both validation runs. In the first run (shown in Figure 4-17), the average difference between the input and output stage is 0.06 meters. The average difference in stage for the second run is 0.03 meters. The model output discharge at the Central cross section (Figure 4-19) does not track the input discharge as well as the input/output stages do. Both validation flows are at low discharges, therefore the differences may be explained by changing cross sectional area that is not accounted for in the rating curve. The fact that the stages match well lends credibility to the

calibration, because the discharge is a calculation and stage is an actual measurement. It is worth noting that the HEC-RAS model does not appear to be as sensitive as the streamflow gage because it undulates less.

Table 4-6 Average difference between the measured and calculated water surface elevation for the validation runs

	Measured – Calculated WSE (m)			
	Alameda	Paseo del Norte	Central	Final XS
14DEC2006 0400 to 15DEC1006 0530	0.012	-0.06	0.064	-0.003
26DEC2006 0000 to 27DEC2006 0300	0.046	-0.064	0.0335	0.00

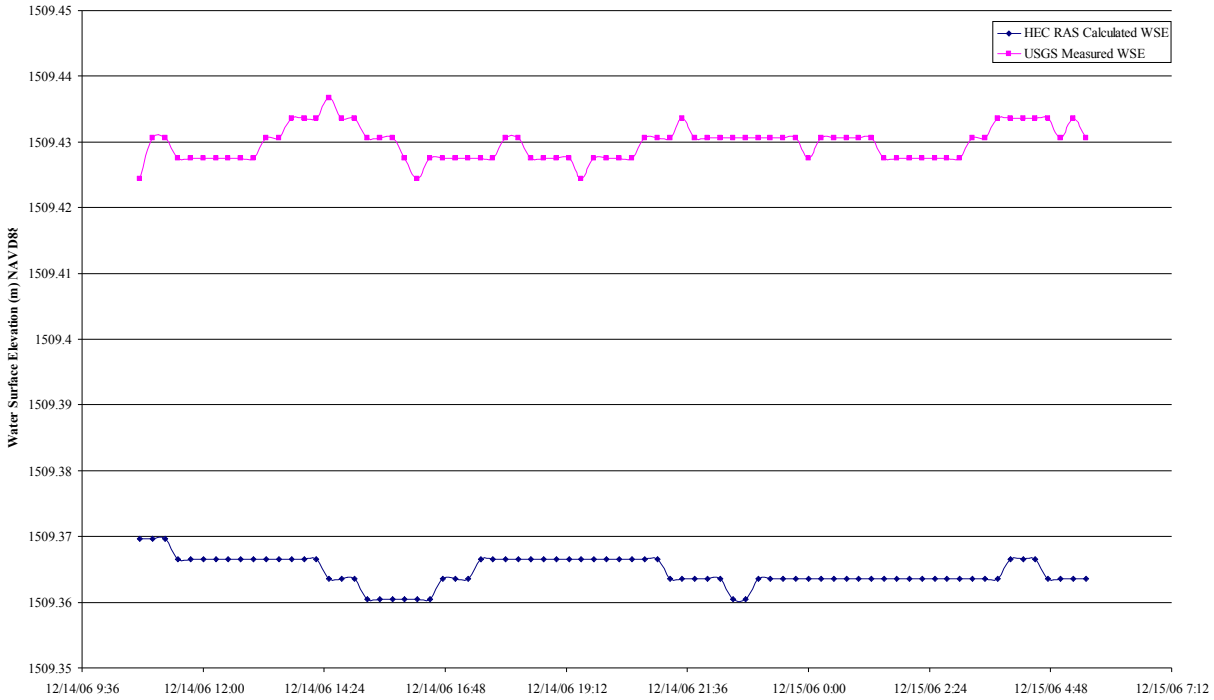

Figure 4-17 Validation run results for stage at the Paseo del Norte cross section

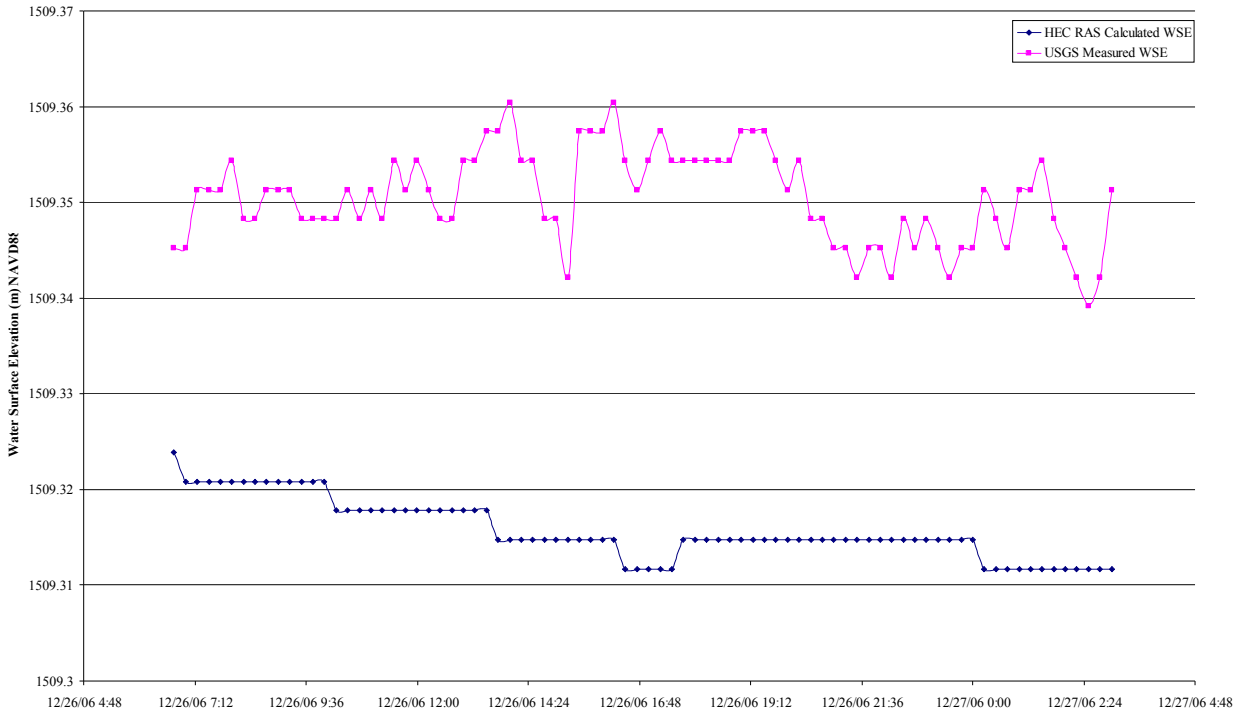

Figure 4-18 Validation run results for stage at the Central cross section

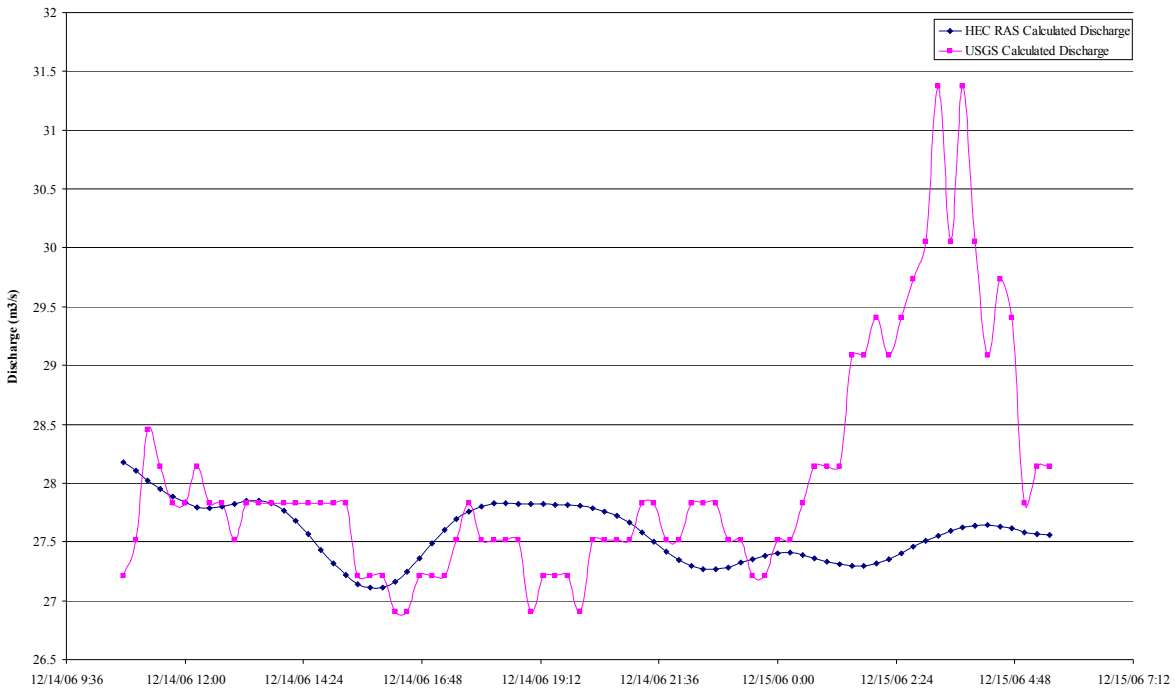

Figure 4-19 Validation run results for discharge at the Central cross section

4.4.4 Groundwater Data

Both the BEMP and USGS groundwater measurements were given as depth to groundwater. That measurement was converted to a water surface elevation by adding the elevation of the ground surface at each well. The USGS X, Y coordinates were given in WGS84 and were projected to New Mexico State Plane Central in ArcGIS. A visual basic program was used to combine the water table elevation measurements at each date-time value from all the BEMP and USGS wells into one database IV (dbf IV) file.

4.4.5 Riverside Drain Water Surface Elevation

The riverside drains were digitized as a 2D polyline in ArcGIS from aerial photographs and the LiDAR data. The 2D line was converted to a PolylineZM file via 3D Analyst > Functional Surface > Interpolate Shape. The terrain model was used as the basis of interpolation. Interpolate Shape was used to convert the 2D file to a 3D file because it causes a significant increase in the number of vertices of the line, the elevation values assigned were used as a space holder and overwritten as described below. The vertices of this PolylineZM file were converted to a 3D points shapefile with the ET GeoWizards tool (downloaded from www.ian-ko.com). The XYZ coordinates of the points shapefile were then exported to an ASCII file with 3D Analyst > Conversion > From Feature > Feature Class Z to ASCII. This ASCII file was brought into Excel. The gradient equations presented in Table 4-2 were used to calculate the water surface elevation at each riverside drain at each cross section (the red dots in Figure 4-20).

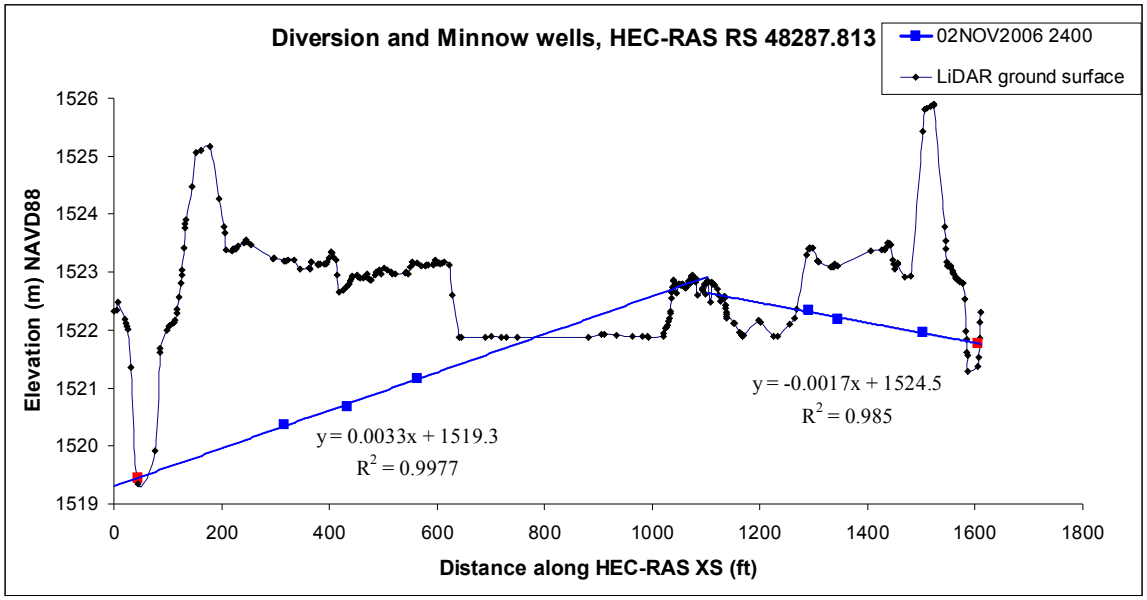

Figure 4-20 Example of water surface calculation at the riverside drains

The water surface elevation at Paseo and Montano are two points that can be used to define the line of the reach gradient on each side of the river. Figure 4-21 shows the calculated water surface elevation (red dots) from Figure 4-20 with the banklines and well locations for context. The water surface elevation at the east riverside drain at Paseo is used with the water surface elevation at the east riverside drain at Montano to calculate the downstream gradient on the east side. The same procedure is used to calculate the reachwise gradient on the west side of the river. This gradient was calculated as a function of the Y coordinate of each vertex, then applied to define the water surface elevation along each riverside drain in Excel. The Excel file was brought back into ArcGIS as XY data and converted to 3D points with 3D Analyst > Convert > Features to 3D.

The groundwater downstream gradient calculated via this process at the east riverside drain is 0.000819 m/m. The slope of the terrain model channel bottom for the study reach is 0.00094 m/m (15 % steeper than the gradient found at the riverside drain). The slope of the energy grade line for the river for a representative flow was found to be 0.001076 m/m (30% greater than the gradient at the riverside drain).

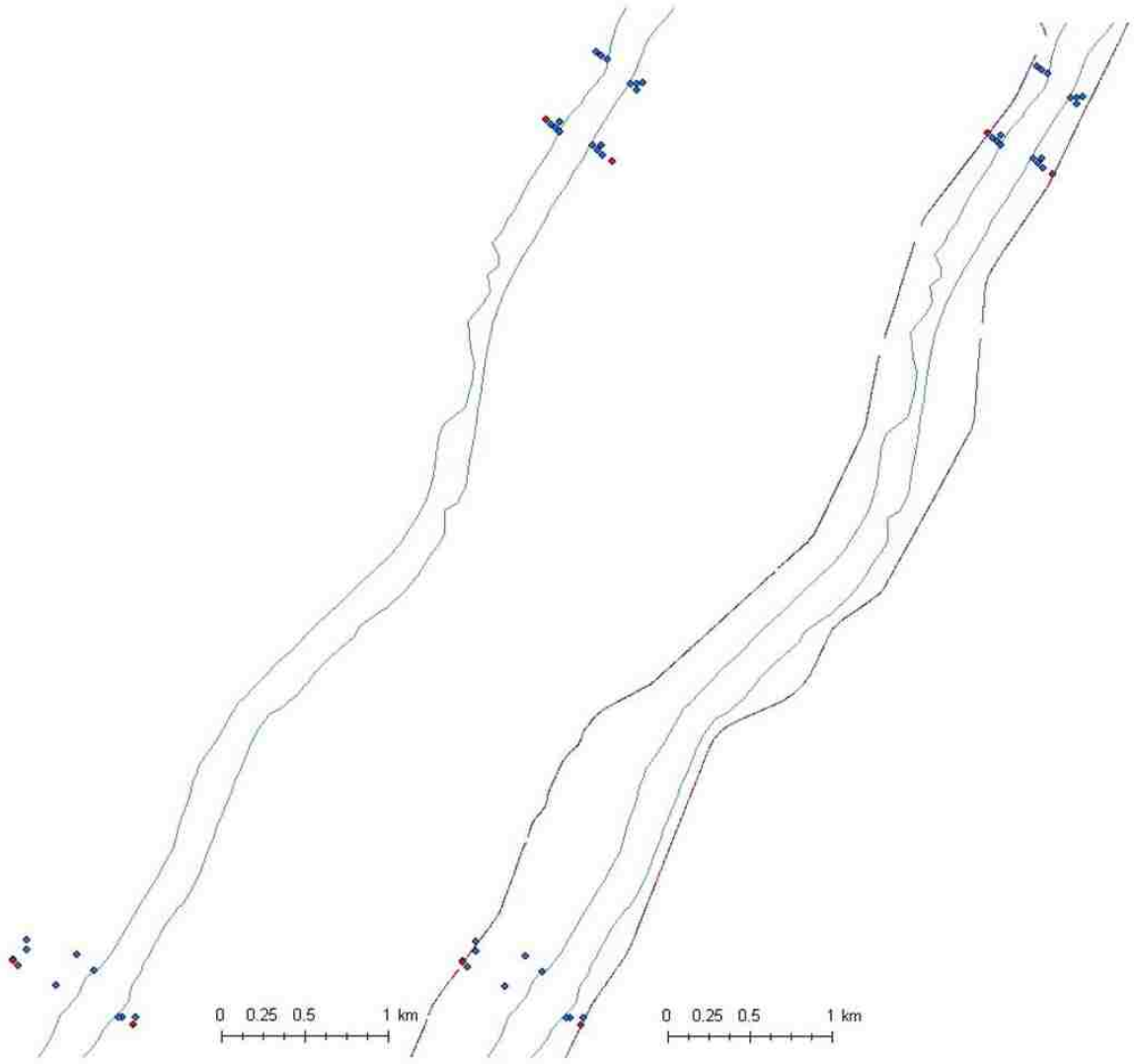

Figure 4-21 Water surface elevation assignment at riverside drains

4.4.6 Combining Groundwater and Surface Water Data

HEC RAS has the capability to export data to be read by ArcGIS. The water surfaces were exported in batches, sized such that ArcGIS could bring the entirety of each file in at one time. This data was read into ArcGIS by HEC-GeoRAS, which then generated a water surface TIN of each profile (date-time value). Figure 4-22 displays a sample HEC-RAS output water surface TIN. Figure 4-22 illustrates that the TIN has a water surface elevation defined for every point on the cross section (the light blue lines), even though none of the flows considered resulted in overbanking. This complicated utilization of the water surface, because the TIN is defining water surface elevation in the

riparian corridor, whereas the elevation in that area ought to be defined by groundwater measurements from the wells. Therefore, a shapefile of the banklines was digitized in ArcGIS and Model Builder was used to execute an Interpolate Shape to assign the water surface TIN elevation to the banklines shapefile.

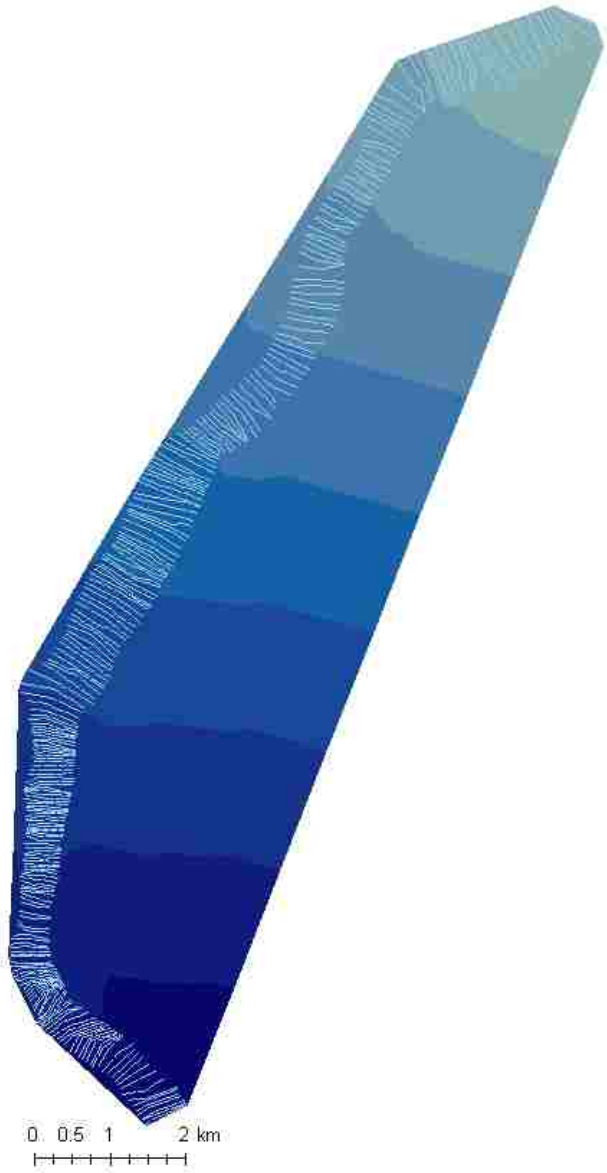

Figure 4-22 HEC-GeoRAS extracted water surface TIN

Model builder in ArcGIS was utilized to combine the groundwater and surface water elevations. XY Event layers were created from the groundwater dbfs, then model Builder finds the water surface TIN with the same date-time stamp and combines the two datasets.

The riverside drain elevation file (constant through time) was added to the TIN as masspoints. Figure 4-23 (an example resultant water surface) does an excellent job of graphically showing that the gradient from the river is steeper on the east side of the river than the west side, especially at the northern part of the study reach. In the southern part of the reach, the river has eroded its way towards the west levee (therefore also the riverside drains), so the riverside drain is closer to the river on the west side than the east side. Because this water surface is fixed at the river and at the riverside drains, the gradient looks steeper on the west side than the east side, which is not consistent with the well data. Although not perfect, the water surface is a reasonable representation of the actual water surface for the whole reach.

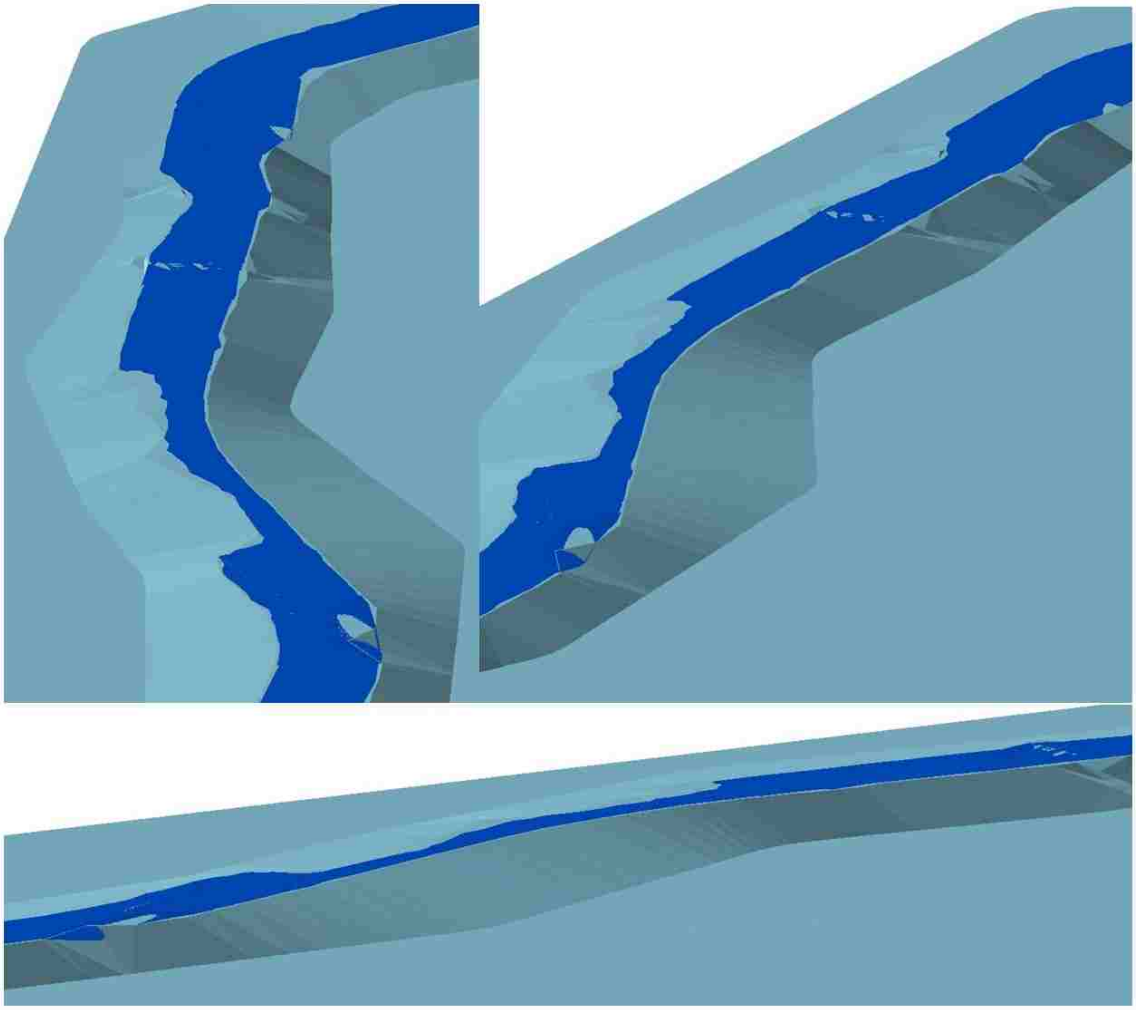

Figure 4-23 Water surface generated after combining groundwater, surface water, and riverside drain water surface elevation, with exaggerated elevation.

Because the data is combined as a TIN, ArcGIS fills in the entire extent of the dataset, which is not physically correct. Therefore, the TIN was converted to a 0.91 meter raster (Figure 4-24, left). The raster cell size was selected to balance computing time and desire for high resolution groundwater maps. Each water surface raster was clipped to the area within the levees to exclude artificial values from interpolation (Figure 4-24, right).

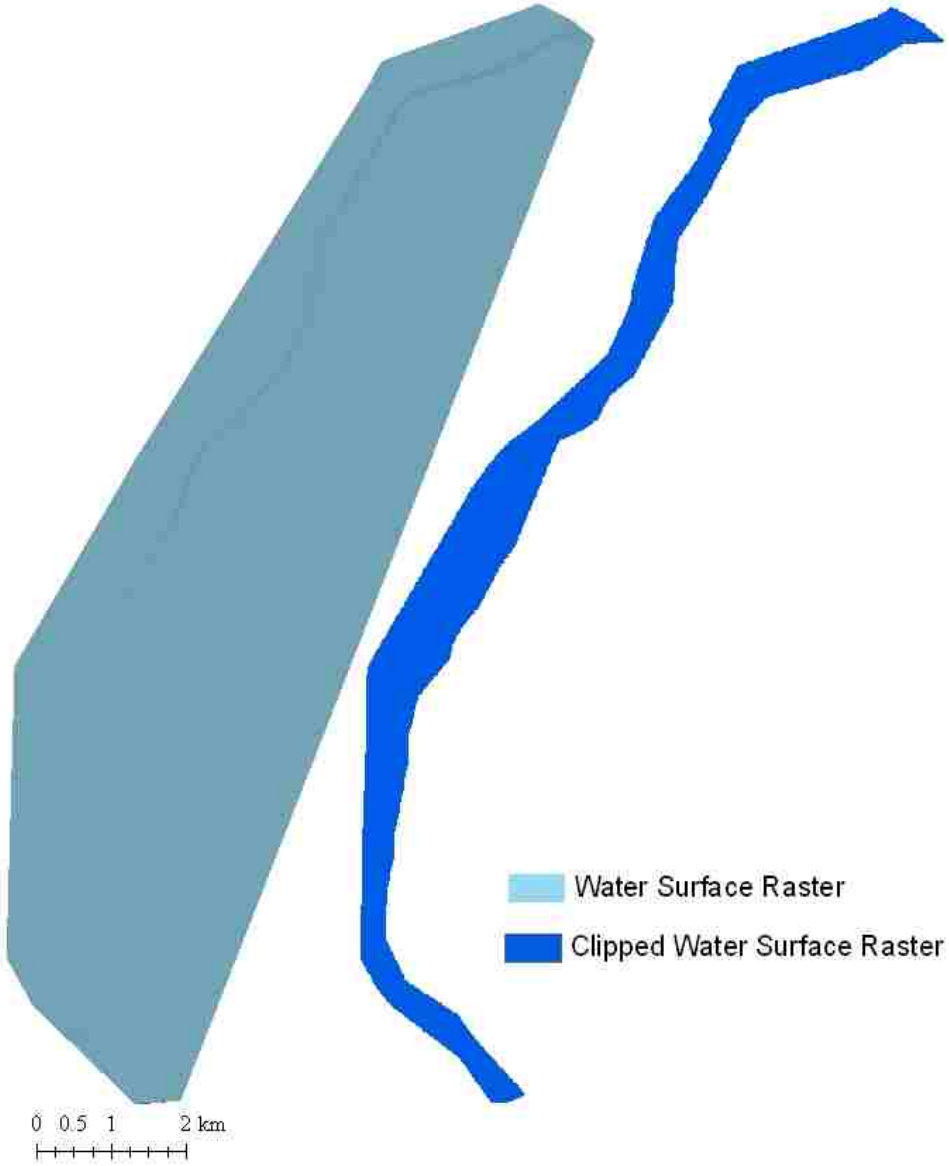

Figure 4-24 Water surface raster generated from a TIN (left), clipped to the area between levees (right)

4.5 Results: Depth to Groundwater as a Function of Discharge

The motivation for creating a HEC-RAS model developed in ArcGIS was to display surface and groundwater elevations everywhere in the reach, not just at points (wells, stream gages). This facilitates calculating depth to groundwater everywhere in the riparian corridor. The terrain model TIN was converted into a 0.91 m grid cell DEM. The water surface raster was subtracted from the land surface in ArcGIS to calculate depth to groundwater. Statistics, including maximum and average depth to groundwater may be calculated for the entire grid. Artificially extreme values of depth to groundwater are the result of the presence of bridge features and other manmade structures in the terrain model. These high values were eliminated from the data set with the SetNull function in the raster calculator. Negative depth to groundwater indicates surface water. Figure 4-25 shows depth to groundwater grids for a portion of the study reach from Alameda to Paseo del Norte for two different flow rates. For the lower flow rate (48.1 m^3/sec), the depth to groundwater grid has more red, indicating a deeper depth to groundwater than the higher flow rate. The final grid in Figure 4-25 indicates that the difference in depth to groundwater between flow rates is predominately 0.0-0.2 meters, and that the difference in depth to groundwater grids decreases with distance from the river. As the water surface elevation at the riverside drains is fixed at the same elevation for both flow rates; whereas the water surface elevation changes at the river based on discharge, the maximum difference in depth to groundwater would be expected near the river and the minimum at the riverside drains.

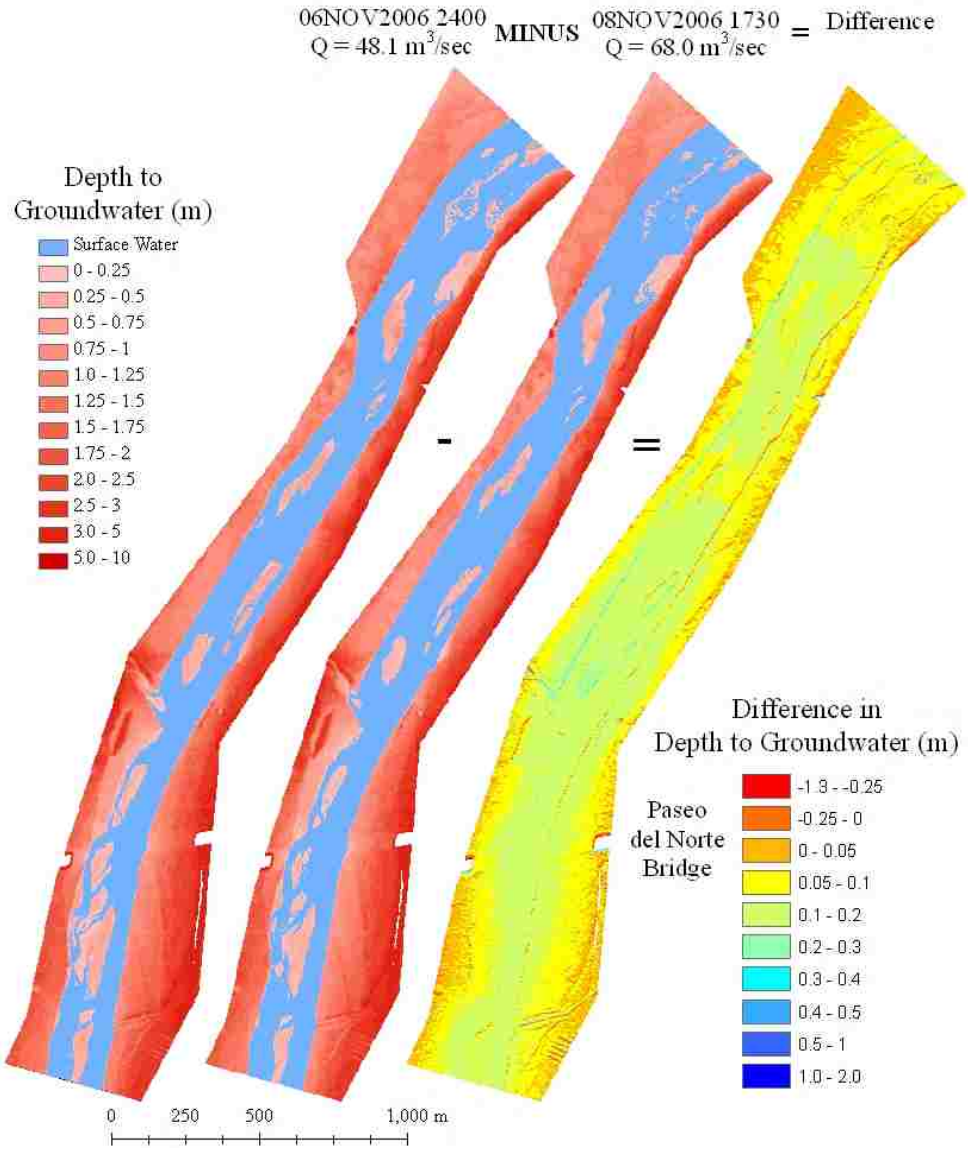

Figure 4-25 Depth to groundwater in riparian corridor for a portion of the study reach for two different flow rates

Depth to groundwater as a function of discharge is time dependent – the depth on the rising and falling sides of the hydrograph will be different because of the travel time of the water through the ground. For the November calibration flow, six points were selected that had corresponding discharges but were on opposite sides of the hydrograph. Table 4-7 shows the difference in depth to groundwater for the selected points. Figure 4-26 shows the different depth to groundwater grids for one pair of discharges. Again, the difference in depth to groundwater for the discharges decreases with distance from the river.

Table 4-7 Depth to groundwater comparison for the same flow rate

Rising	Falling	Discharge (m^3/s)	Rising avg depth to gw	Falling avg depth to gw
07NOV2006 0215	09NOV2006 0045	45.6	1.48 ± 0.92	1.44 ± 0.89
07NOV2006 0300	08NOV2006 2215	49.8	1.42 ± 0.86	1.43 ± 0.89
07NOV2006 0345	08NOV2006 2045	52.3	1.41 ± 0.86	1.39 ± 0.854

The high value of standard deviation is expected because depth to groundwater is calculated for the entire grid. The depth to groundwater is expected to increase at a cross section with distance from the river, and the groundwater gradient is expected to vary from cross section to cross section depending on the proximity of city wells.

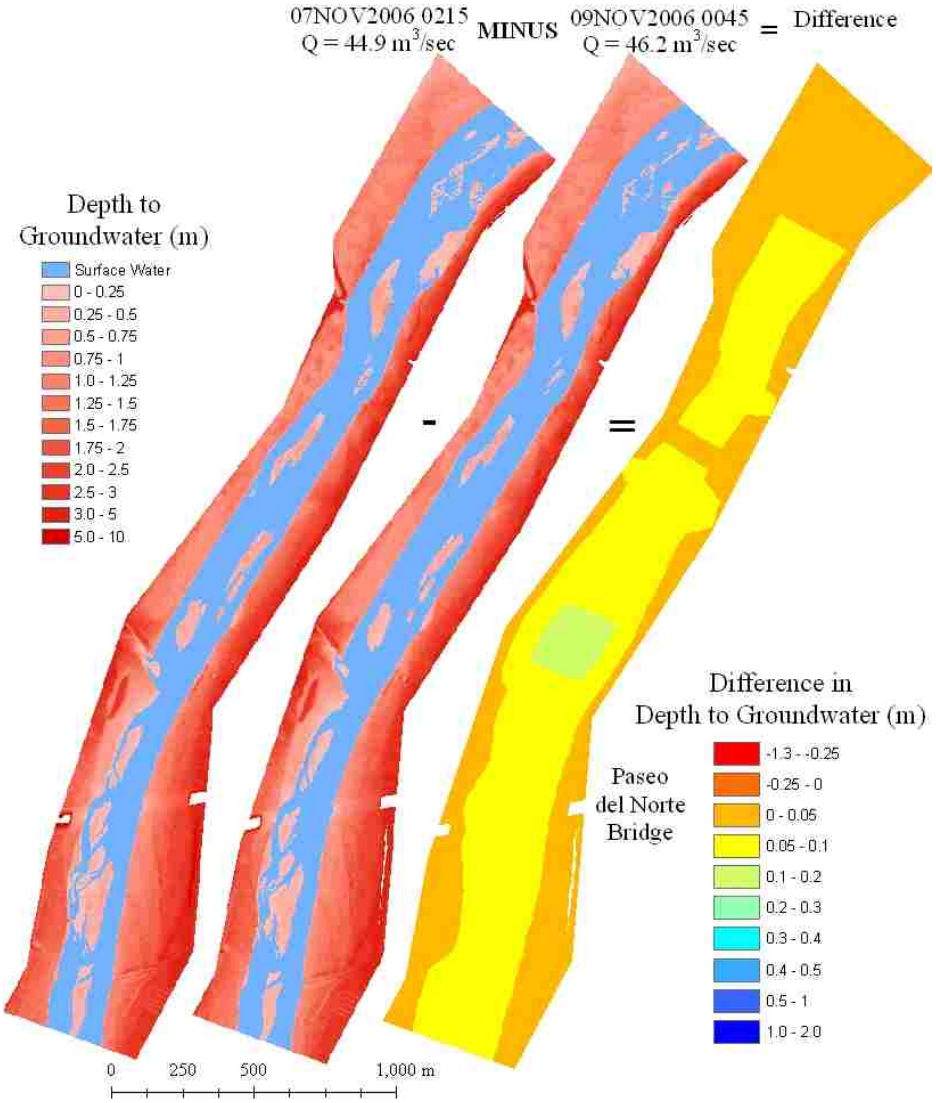

Figure 4-26 Depth to groundwater in the riparian corridor for a portion of the study reach for a similar flow rate on different sides of the hydrograph.
The 07NOV2006 0215 occurs on the rising side of the hydrograph while 09NOV2006 0045 occurs on the falling side.

4.6 Discussion

Depth to groundwater is used in several evapotranspiration (ET) equations (Jury 2004, Nichols 2000) as well as bare soil water table evaporation calculations (Gardner 1958, Stormont et al. 2009). Therefore, large scale, high resolution depth to groundwater grids such as those generated in this study may improve the calculation of ET for riparian areas by providing a more accurate depth to groundwater variable. ET equations are dependent on the type of vegetation, which is frequently determined by remote sensing (Etlantus 2007), which is also a gridded cell format. Therefore, having depth to water table grids is advantageous for refined ET estimates as the remotely sensed data can easily be combined with depth to water table via Model Builder in ArcGIS to calculate large scale ET. Improved ET estimates enable better water accounting.

Figure 4-25 demonstrates the ability of this process to show large scale groundwater – surface water interactions. For 06NOV 2006 2400, the islands are more prominent in the channel and the depth to groundwater is generally deeper than on 08NOV2006 1730, where the increased discharge is seen in smaller river island areas and the impact of this increased discharge is seen in smaller depth to groundwater values. While the pictures generated by this technique are instructive, the animations created are even more so.

Incorporating the boundary condition is very important for properly representing the water surface. Initially, the water surface was interpolated only between the surface water and groundwater points, then depth to groundwater grids were calculated. These grids had a larger cell size (3.0 meters versus 0.91 meters) and did not have the bridge areas removed. The average depth to groundwater for each of the six grids was smaller than after the boundary at the riverside drains was imposed. This is because without the additional boundary, the riparian water surface was based solely on the river surface for most of the reach. This implies that for a given cross section, the depth to groundwater was unlikely to change. The standard deviations were smaller for the same reason: most of the groundwater surface was essentially a horizontal extension of the river surface, thus deviations mostly resulted from reach-wise variation.

Incorporating some gradient boundary condition significantly improves the water surface produced by this process. While the riverside drains provide an excellent location for assigning such a boundary, the process by which the water surface elevation at that

location is assigned could use refinement. Cursory analysis of the water surface elevation in the wells nearest the riverside drains suggests a cyclical pattern. However, the current period of record is not sufficient for determining the time variability of the water surface so that it can be accounted for. A longer period of record and a Fourier transform of this data will facilitate adding the time component to the riverside drain data. Also, calculating the gradient as a function of both the x and y coordinate of each vertex could significantly improve the estimation of the water surface at the riverside drain.

The initial assumption that the riverside drains control the water surface elevation implied that the groundwater levels in the riparian corridor would never be low enough to stress cottonwoods. However, because the riverside drains do not control the gradient within the riparian corridor, it is entirely possible that city pumping could lower groundwater levels enough to stress riparian cottonwood populations. Incorporating the time-variant water surface at the riverside drains will allow the depth to groundwater grids to reflect this possibility.

5 Model Use

5.1 Visualization Tools

The other motivation for utilizing ArcGIS is to create visualization tools to generate pictures and animations that enhance understanding groundwater-surface water interaction. ArcGIS's ArcScene was utilized to create 3D pictures of the terrain and water surfaces together. Figure 5-1 shows a 2D picture of the water surface raster for 07NOV2006 0015 with the terrain model DEM being displayed in 3D. The 2D pictures created from this analysis are instructive but when the 3D images are animated in time the impact of the river water surface elevation is clearly seen.

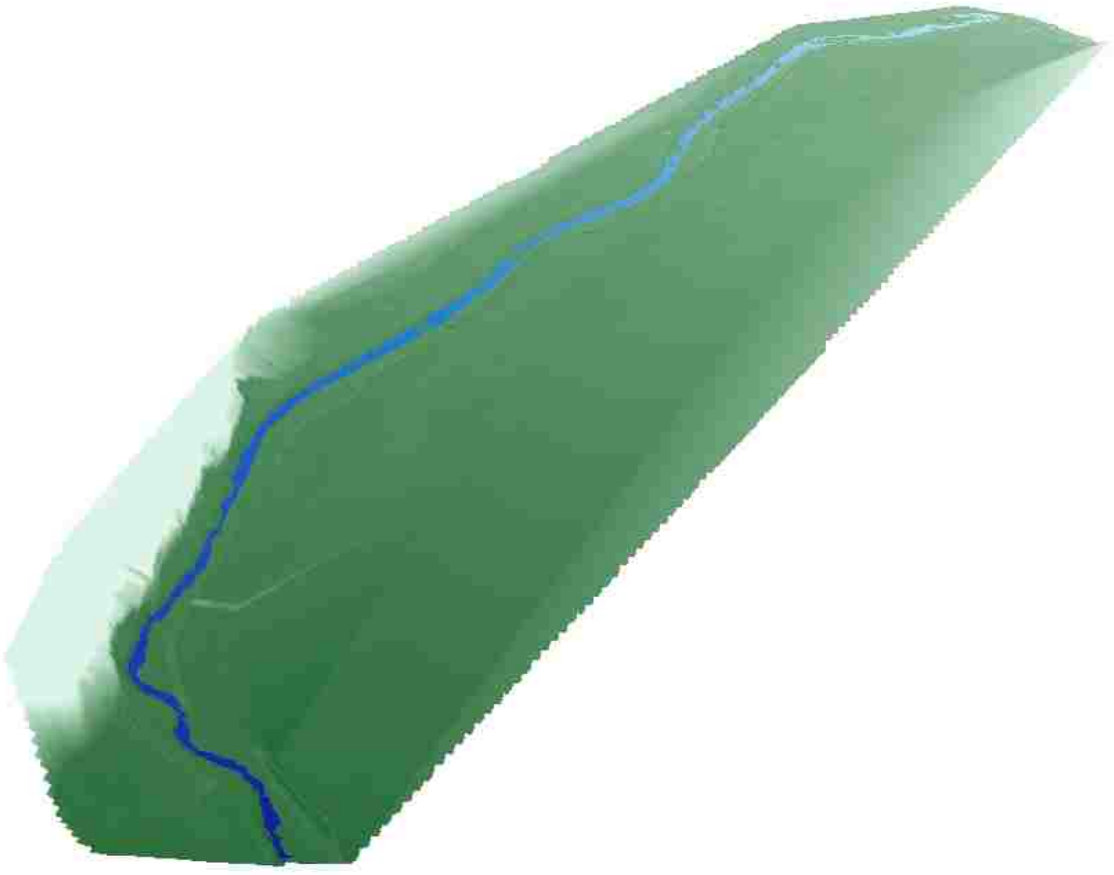

Figure 5-1 Water surface raster with the digital terrain model in 3D

5.2 Evaluation of Ecological Impacts of Hydrologic Management

River discharge is largely responsible for long term ecological health in the riparian corridor. Decreased streamflows result in increased depth to groundwater, which can stress riparian vegetation. Native and non-native riparian species have different depth to groundwater tolerances. Horton et al. (2001) studied the physiological response to groundwater depth for various vegetation types. The response to depth to groundwater of three common species, *Populus fremontii* (cottonwood), *Salix gooddingii* (willow), and *Tamarix chinensis* (salt cedar) are presented in Table 5-1. The values in Table 5-1 are interpreted from Figure 7 of Horton et al. (2001) and taken from the text of the same article. The *populus* species studied is technically different than the species present in the study reach, but is very likely to have similar responses (personal communication with Dr. James Cleverly, May 2008). The categories listed are generalizations of the data presented by Horton: "healthy" indicates that the depth to groundwater is sufficiently shallow that the vegetative type will not be negatively impacted, "stressed" means that at this magnitude of depth to groundwater there is some evidence of crown dieback. When crown dieback reaches forty percent, the depth to groundwater is classified as "crown dieback"; "mortality" indicates that at this depth to groundwater the vegetation dies. These categories are not intended to describe short term (days) but rather prolonged (months) vegetative response. Salt cedar is more efficient at extracting water from the vadose zone than the two native species; therefore its mortality is not correlated to depth to groundwater.

Table 5-1 Riparian vegetation response to depth to groundwater, interpreted from Horton et al. 2001

	Healthy	Stressed	Crown dieback	Mortality
Cottonwood	0 - 2.5	2.5 – 3.0	3.0 – 5.0	5.0
Willow	0 – 2.0	2.0 – 2.25	2.25 – 3.0	3.0
Salt cedar	0 – 2.25	2.25 – 2.5	2.5	

The depth to groundwater impact on ecological health is plotted for two river discharges: a moderate streamflow of 52.3 m^3/sec at 08NOV2006 2045 in Figure 5-2 and a low streamflow of 23.8 m^3/sec at 19OCT2006 1730 in Figure 5-3. These plots are from the same data as Figure 4-25 (depth to groundwater), the classification is now based on how that depth to groundwater impacts the vegetation on the grid cell.

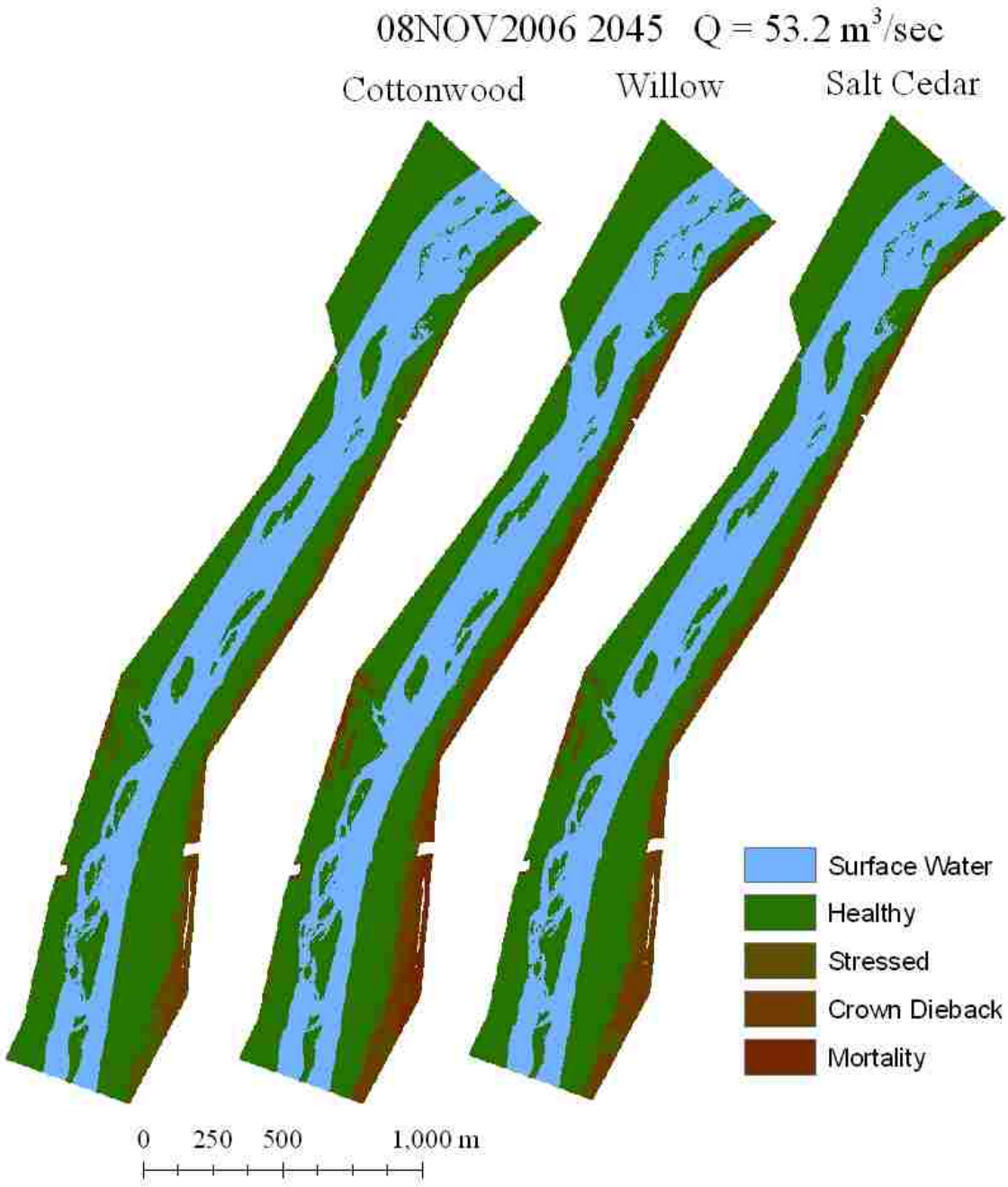

Figure 5-2 Ecological health as a function of depth to groundwater, 08NOV2006 2045

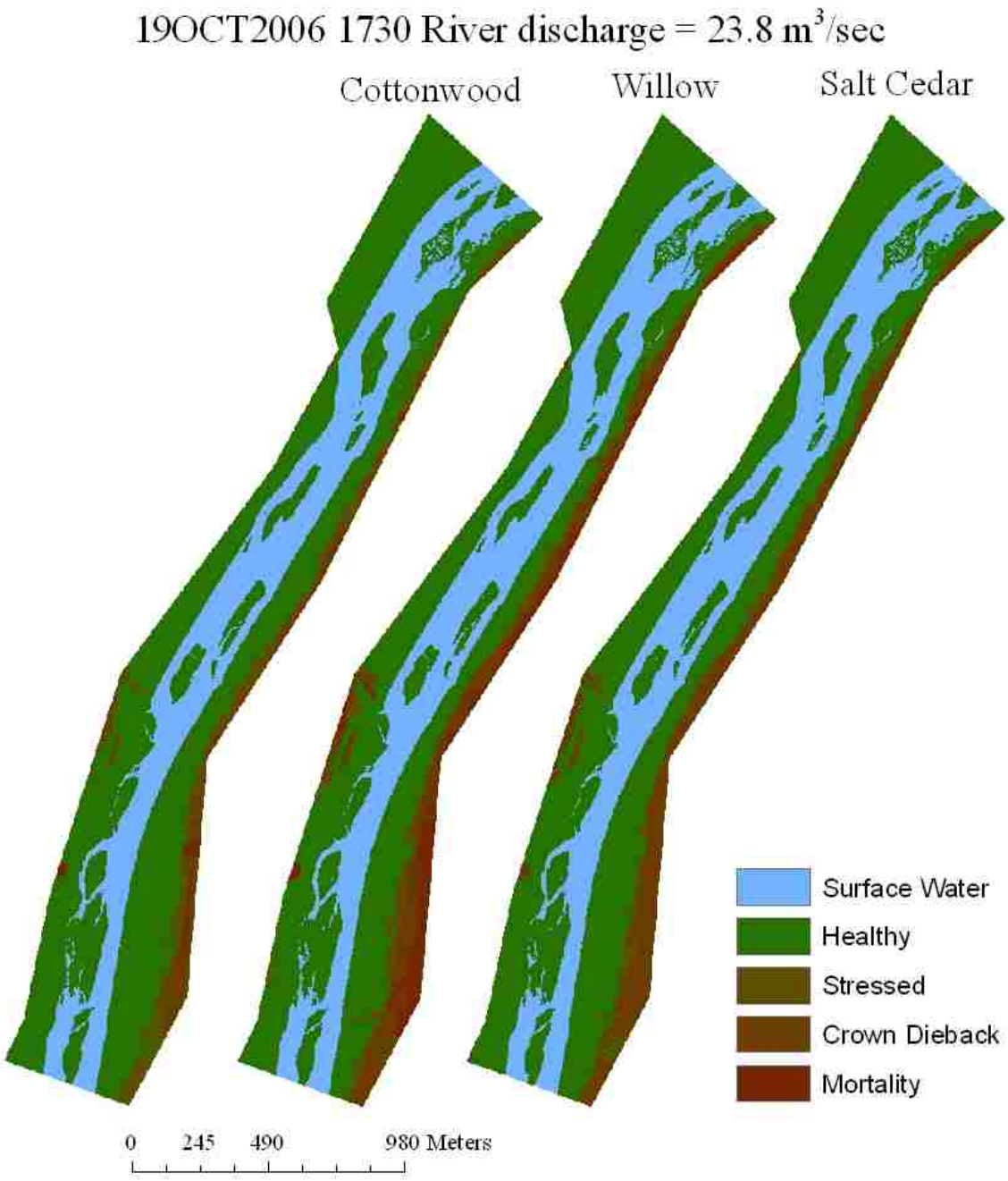

Figure 5-3 Ecological health as a function of depth to groundwater, 19OCT2006 1730

The smaller streamflow (Figure 5-3) corresponds to slightly more cottonwood and willow stress, but Figures 5-2 and 5-3 are extremely similar. Depth to groundwater values at each flowrate that cause crown dieback or mortality are primarily functions of the terrain and not due to changes in groundwater gradient. The lack of impaired areas is an expected result: the current riparian forest does not suffer from lack of groundwater.

The Horton (2001) work utilized to classify Figures 5-2 and 5-3 focused on mature riparian vegetation. As mentioned in Chapter Two, cottonwood seedlings require shallow soil moisture until they develop roots that tap the capillary fringe. Therefore, for new cottonwood trees to grow, the groundwater must be shallow for extended periods of time. The data in Figures 5-2 and 5-3 could be reclassified to show the ability of the riparian corridor to support cottonwood seedlings. This information could be used to direct restoration efforts under current streamflow management techniques.

Rio Grande streamflow in the Albuquerque Reach is primarily controlled by upstream dams and reservoirs, most notably Cochiti Dam. Cochiti Dam could be operated to encourage native species re-growth and sustenance by maintaining groundwater levels sufficient to support cottonwoods and willows through streamflow manipulation. Dam management has been shown to be an effective way to maintain established cottonwood populations (Horton et al. 2001). This model could be used to determine what magnitude dam releases are required to sustain native species populations or to encourage native species seedlings.

5.3 Diversion Dam

Cochiti Dam controls the magnitude of streamflow for the Albuquerque reach; however, the water utility diversion dam will impact water surface elevation upstream and downstream of the dam site. The impact of the upstream increase in water surface elevation can be quantified with the model presented in this thesis. The diversion dam was added as an inline structure to the HEC-RAS model, with the two easternmost gates open and the rest of the gates up. The water surface was combined with the riverside drain data and depth to groundwater was calculated. The impact of the dam is measured by comparing the groundwater depths for the same flow rate with a HEC-RAS run with the dam down (Figure 5-4). The right grid shows large areas with shallower groundwater depths (lighter colors) upstream of the diversion dam. When the dam is raised and creating a pool in the river, the average depth to groundwater is 0.2 meters higher (1.129 ± 0.72 m) than when the dam is completely lowered (1.33 ± 0.73 m).

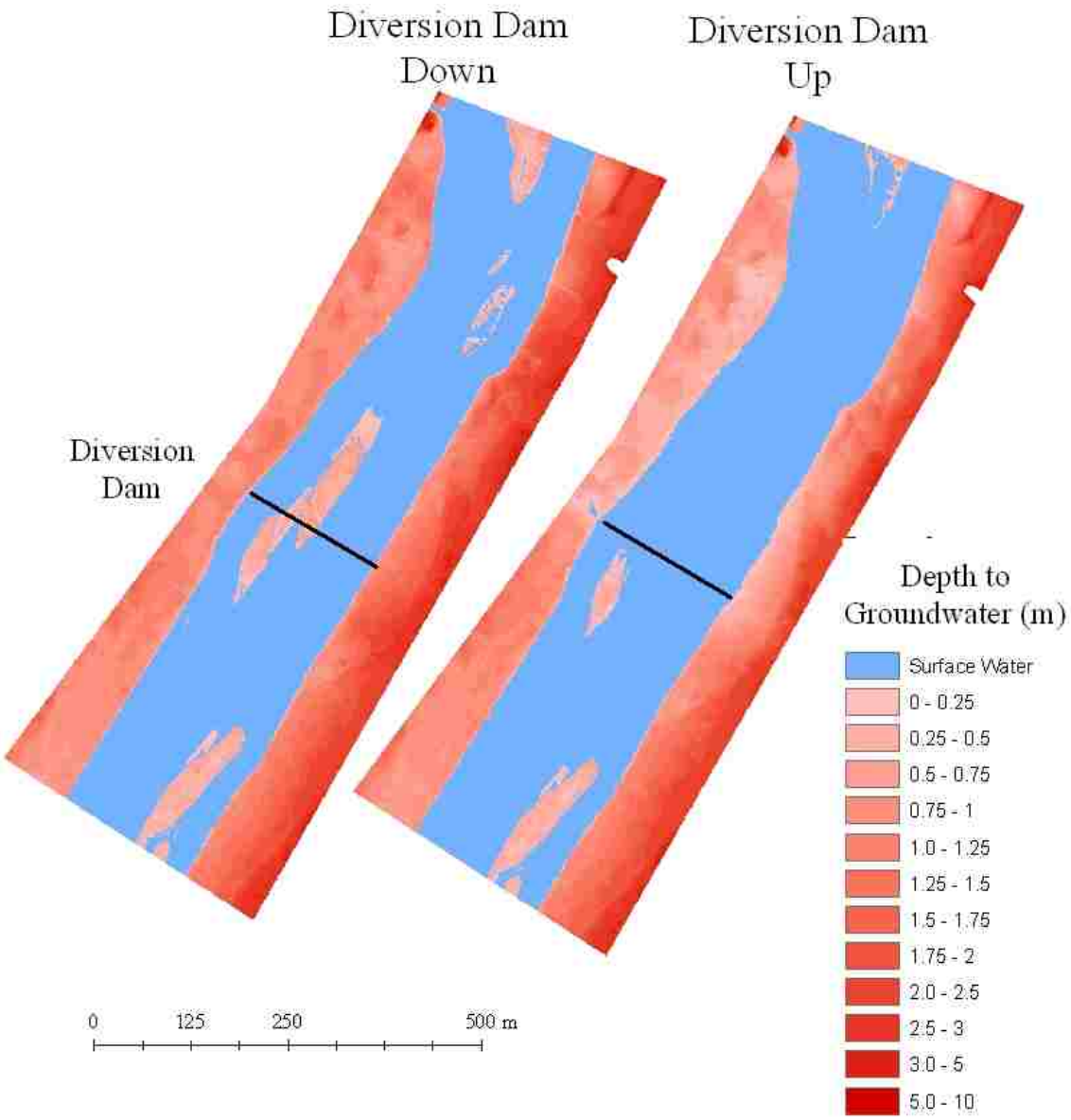

Figure 5-4 Impact of diversion dam on groundwater depth

5.4 Climate Change

AR4 reports that for the American southwest, climate change is likely to increase temperature, decrease net precipitation, cause more precipitation to fall in the spring and snow to melt sooner (AR4 2007). These combined effects would represent a significant change in hydrology for the Rio Grande basin. Coonrod and Hurd's climate change study for the Middle Rio Grande Basin (2007) indicated for a wide range of climate change scenarios the upper watersheds of the basin will likely see a decrease in river flow. The projected average decrease in June streamflow for the upstream watersheds is

sixty percent over the considered climate change scenarios. Based on USGS streamflow measurements at the Central Bridge, the average June streamflow from 1970-2000 for the study reach is 85.2 m^3/sec. Thus, the projected average June streamflow will be 36.6 m^3/sec. These two streamflows were run through the HEC-RAS model and their water surfaces were used to calculate the depth to groundwater. The results are compared in Figure 5-5.

The mean depth to groundwater for the current average June streamflow is 1.34 ± 0.84 meters; the reduced streamflow average is 1.42 ± 0.86 meters. Thus, a sixty percent reduction in streamflow corresponds to a six percent increase in depth to groundwater. The magnitude of the increase is not as substantial as might be expected because the water surface elevation is fixed to be the same value at the riverside drains for both flow rates. Therefore, the change in depth to groundwater is exclusively a result of the decreased water surface elevation in the river. This demonstrates that the tool is impacted by river water surface elevation. This analysis can be used to identify areas of the riparian corridor that are particularly vulnerable to reduced water tables as a result of changing streamflow.

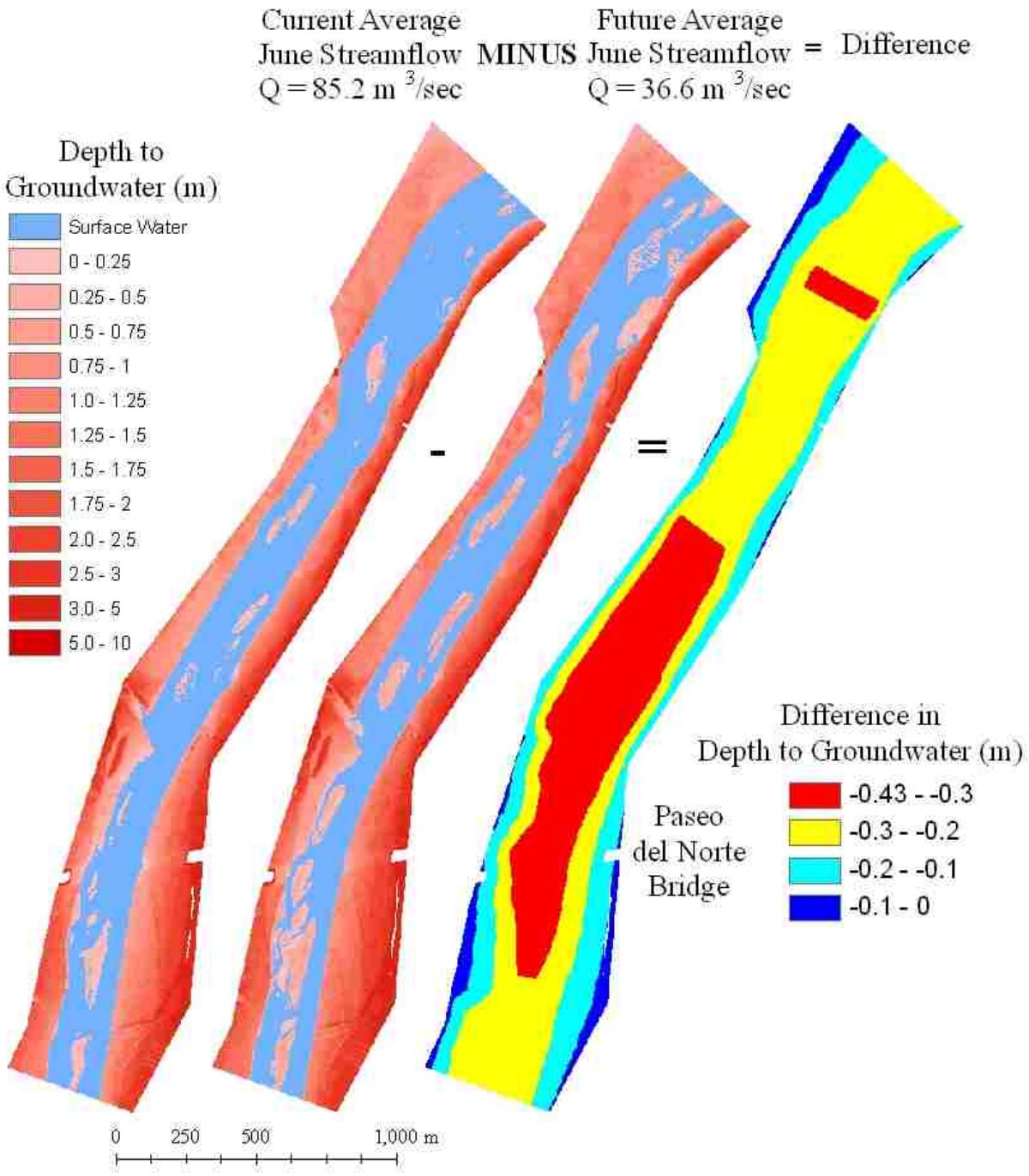

Figure 5-5 Climate changed depth to groundwater for July

6 Conclusions

The Albuquerque reach of the Rio Grande is an excellent area for studying the connection between the groundwater and surface water due to the high density of streamflow, groundwater elevation, and riverside drain water surface elevation measurements available from various agencies, including the USGS and the University of New Mexico.

HEC-GeoRAS is an effective program to simplify and expedite HEC-RAS model creation. The terrain model used with HEC-GeoRAS must be of sufficient resolution that the river features are captured. The use of LiDAR data to create HEC-RAS geometry facilitates modeling longer HEC-RAS cross sections and provides flexibility in changing HEC-RAS cross section location because a survey team is not required each time a new cross section is desired. Combining interpolated bathymetric data with LiDAR data to capture the actual river bottom is successfully demonstrated.

USGS streamflow data must be used with caution when calibrating hydraulic and hydrologic models. High streamflow measurements have an inherent significant uncertainty that must be acknowledged when modeling large streamflow events. Understanding the limitations of the streamflow measurement process will assist in model calibration and correctly assessing the quality of input data and model results. The water surface elevation calculated by hydraulic models should be compared to the measured water surface elevation whenever possible to ensure correct model calibration.

This thesis presents a viable method for creating comprehensive river water - groundwater surfaces. The intricacies of generating these surfaces are presented, including the importance of identifying what process is controlling the groundwater gradient from the river. The water surfaces produced by this tool enable high resolution mapping of groundwater depth for the entire riparian corridor. The resolution of the groundwater map is controlled by the terrain model resolution, not the water surface.

The current depth to groundwater in the riparian corridor is shown to be sufficient to support mature cottonwood, willow, and salt cedar populations. One method to quantify the impact of climate change reduced streamflows is presented, although the model could be used to study climate change impacted groundwater depth at various time intervals: yearly, monthly, daily. Although not presented, similar ecological impact

studies could be conducted under a variety of climate change scenarios. The tool may be used to identify vulnerable areas of mature cottonwoods and willows as well as ideal locations for restoration projects.

This model is demonstrated for the study reach in Albuquerque, NM. However, the process outlined and programs developed could be used to study other systems with similar datasets. The current model is weak for representing overbanking, but otherwise can be applied to gaining or losing reaches. Identification of groundwater gradient control and selection of the boundary location are key in utilizing the tool. If groundwater movement is primarily gravity driven (not influenced by pumping), the boundary location may be effectively infinity and could simply be defined at a specified distance from each bank. Bedrock outcrops or manmade structures may be appropriate boundary conditions. The gradient control will likely determine the appropriate boundary location.

7 Future Work

The next step for the model is to improve the estimation of the water surface at the riverside drains. Currently, the gradient at each drain is applied as a function of the latitude of the location. It would be more precise to apply the gradient as a function of river station. Incorporating river station values to the riverside drain shapefiles would improve the application of the reachwise gradient.

An important component of the model is application of the groundwater gradient derived from the wells to assign the water surface elevation at the riverside drains. This process defines the groundwater gradient from the river at each cross section as well as the reachwise groundwater gradient. For the study reach, the gradient from the river is primarily driven by city pumping. The impact of city pumping is not accounted for in the model because the water surface elevation is fixed at the riverside drains throughout time. Assigning the water surface elevation at the riverside drains as a function of time of year would account for the impacts of city pumping. With more data, Fourier transforms may provide insight into seasonal patterns that could be utilized to assign the water surface with respect to time.

The new surface water drinking project means a temporary reduction in city groundwater pumping. This reduction will be more pronounced in the winter months when water demand is lower. As data becomes available, the impact of reduced city pumping can be quantified with the model, if elevation as a function of time can be quantified. However, the current water plan for the city includes a return to the same quantities of groundwater withdrawals within the next thirty years. The gradient is also influenced by evapotraspiration from riparian vegetation. Thus, in thirty years when groundwater pumping has returned to current demand and evapotranspiration rates are elevated due to an increase in air temperature from climate change, the gradient from the river is likely to increase. While streamflow rates and groundwater pumping demand are currently balanced to support riparian vegetation, the future groundwater levels can not be guaranteed to do so. Predictions made with this tool about future groundwater levels must be considered conservative because they do not account for increased ET rates.

Appendices

Appendix A: Detailed Methods

Appendix B: Data Sources

Appendix C: Program Codes

Appendix A: Detailed Methods

Terrain Model

LiDAR data

LiDAR data is available for the entirety of Bernalillo County as TINs. The LiDAR data points and lines were created from 1:5000 photoscale photography and 1m LiDAR survey. LiDAR does not penetrate water well; therefore, the channel is estimated as a rectangular channel with a flat bottom in the LiDAR data set. Twenty two grid cells that covered the Rio Grande and its floodplain to at least the levees were obtained. The TINs did not have the projection defined, although the projection information was available in the documentation that came with the TINs, so the projection New Mexico State Plane NAD83 Central Zone FIPS 3002 (Feet) was assigned in ArcCatalog to each file.

In ArcGIS 9.1, new TINs may be created only from a set of point or by adding new features (lines or points) to an already existing TIN. Therefore, all TINs were deconstructed into point shapefiles using 3D Analyst > Convert > TIN to Features > Nodes to points (data nodes only). Any points within the channel were then deleted, including islands. The points were then re-combined into a TIN using 3D Analyst > Create/Modify TIN > Create TIN from features. The points were recombined as mass points using the z values from the original data. This produced one TIN that encompassed the entire study area.

Bathymetry data

Bathymetry data was obtained from the Bureau of Reclamation. In 2006, the Bureau of Reclamation acquired a series of aerial photos of the Rio Grande while the river flow was low. From these photos, cross sections of the Rio Grande were determined. Where the channel bottom was not visible it was estimated as a trapezoidal channel. These cross sections were taken approximately every 150m along the river.

Additional bathymetry data was collected from Alameda Bridge to the diversion dam. A Trimble DSM 232 GPS Receiver (Trimble Navigation Limited, Sunnyvale CA) and an Ohmex Instruments SonarLite Portable Echo Sounder System (Ohmex

Instruments, Lymington UK) were connected to simultaneously record water depths and location. In addition to acting as the control and signal generator for the depth sounder, the SonarLite served as the data logger for the GPS and depth soundings. The measurements were downloaded using the SonarLite software and converted from text files to Excel files. The data was processed to remove erroneous data and consolidated to just the columns required for this study. Data processing was performed by Dr. Jungseok Ho at the University of New Mexico and provided to the author. Sonar readings were taken in two sets: one that focused on the western half of the river and one that covered the east side. When the east side was measured, the water surface elevation was measured to be 1.15 meters on the PLC screen (from the cement base of the dam). When the west side was measured, the gate configuration had been changed thus the water surface elevation was measured at 1.09 meters. The depth readings were subtracted from the appropriate measured water surface elevation to create the channel bottom. The points were brought into ArcGIS by converting them to a database file IV (DBF IV) in Excel. The DBF IV file was brought into Excel and a XY Events layer created from it, which was then converted to a shapefile. To project these points, a two step process was required. First, the points were converted from the original coordinate system WGS 1984 to NAD 1983. Then they were projected to State Plane New Mexico Central Zone.

A third set of bathymetric data was obtained from URS Engineering Corp. Cross sections between Alameda Bridge and just downstream of the diversion dam were measured by the URS survey team. These points were processed similarly to the SonarLite data to create shapefiles. In February there were some outliers so those points were deleted from the attribute table using the Editor toolbar.

Combining bathymetry data with terrain model

The Bureau of Reclamation cross sections were interpolated using the method outlined in Merwade et al. (2008). A channel boundary polygon was digitized in ArcGIS by tracing the banklines and connecting the banklines at the top and bottom. This was used in the channel bathymetry tool to determine the extent of the interpolation. The cross section points were obtained from the Bureau of Reclamation as a text file that contained Northing, Easting, and Elevation columns. These xyz points were converted to

a DBF IV in Microsoft Excel and brought into ArcGIS where they were converted to a TIN using 3D Analyst. A shapefile of 2D lines that displayed where the cross sections were taken was obtained from the Bureau of Reclamation. 3D Analyst > Convert > Features to 3D was used to extract the elevation data from the xyz point TIN to the polyline file. This resulted in a file of 3D lines to be used with the bathymetry interpolation tool. Three columns were added to this file, StationNo, XS and Reach because these fields are hard coded into the bathymetry interpolation tool. XS was populated by copying the values from the original polyline file. StationNo and Reach were populated using HEC-GeoRAS.

Dr. Venkatesh Merwade's tool (described in Merwade et al. 2008) was used to interpolate the Bureau of Reclamation cross sections and create a mesh of interpolated cross sections. This mesh was added to the TIN derived from the LiDAR as hard lines.

HEC-GeoRAS Component

HEC-GeoRAS was utilized to create the HEC-RAS geometry from the terrain model. HEC-RAS requires a minimum of four files to be delineated in ArcGIS: river centerline, cross section cut lines (where you want cross sections), river banklines, and left overbank, right overbank, and center flowpath centerlines (where the discharge will flow, especially if it overbanks). Additionally, a levee shapefile (delineating levee locations) was created to import into HEC-RAS.

The river centerline was sketched in ArcGIS using aerial photos and the LiDAR data. The cross section cut lines were also sketched in ArcGIS to be perpendicular to the flowpath centerlines with approximately sixty one meters between cross sections. Levee locations were outlined in ArcGIS from the LiDAR data.

For each original LiDAR TIN, the TIN Edge tool was utilized to extract triangle edges with the "Data Produced" option selected, which gives all of the lines in the TIN. Then the banklines were selected using the Selection tool in the Tools toolbar. This process required decisions about the distinction between sandbars and banklines. After a continuous bankline for each bank had been selected, all the lines from all the different TINs were brought into one file using Data Management Tools >General > Merge. Then Data Management > Generalization > Dissolve was used to make one file with one

feature in it. Shapefiles that outlined the extent of the west/east banklines were used to extract an EastBank shapefile and a WestBank shapefile.

The stream centerline was assigned as the center flowpath line. To create the overbank flowpath lines, Editor > Buffer was used to buffer the east and west banklines by 3 meters. This created a continuous line around the entire bankline that was trimmed with the split tool. Buffer was found to be better than move because it ensured that the banklines and flowpath lines did not cross.

A polygon shapefile titled Land Use was created to assign Manning's *n* values. Two fields were added to this file, Land Use and ManningN. Using the Editor toolbar, the polygon was delinated in ArcGIS to encompass the cross section lines. A landuse of Riparian Forest and a ManningN of 0.08 was assigned to the entire polygon. The same two fields were added to the channel boundary polygon utilized in the bathymetry interpolation tool. LandUse was designated as river channel and ManningN was assigned as 0.03. These n values are typical for natural streams that are "clean, straight, full stage, no rifts or deep pools" (0.03), and a flood plain with trees and a "heavy growth of sprouts" (0.08) (Sturm, 2001). Data Management Tools > General > Merge was used to combine these two polygons into one polygon. The polygon of channel islands (taken from the LiDAR data) was added to this polygon to assign a Manning *n* value of 0.05 to channel islands. The channel Manning *n* values of 0.03 and 0.08 for overbanking are consistent with a Rio Grande HEC-RAS model previously developed by the United States Army Corp of Engineers.

The LiDAR TIN of the study area was used as input to HEC-GeoRAS to assign elevations to each of the cross sections, river centerline, banklines, and levees. HEC-GeoRAS also calculated downstream reach lengths for each cross sections, assigned bank station values at the intersection of banklines and cross section lines, and assigned river and reach names to each cross section. All of this information was then compiled into one file by HEC-GeoRAS and converted to a HEC-RAS readable format in the HEC-GeoRAS Toolbar > RAS Geometry > Extract GIS data.

HEC-RAS Model

A new HEC-RAS project was created. The Geometric Data Editor was opened and File > Import Geometry Data > GIS Format was used to bring in the HEC-GeoRAS compiled file.

The banklines selected from the TINs turned out to be the edges of the river bottom so the bank stations were shifted in the Graphic XS Editor in HEC-RAS to be at the top of the bank instead of the bottom.

The cross section points filter was applied to cross sections that had more than 496 points. "Minimize Area Change" was selected and points were removed so that each cross section had a maximum of 496 points. Artificial channels in the riparian corridor were removed after consulting the LiDAR data and aerial photos to determine the source of the low spot. A significant portion of the cross sections were modified to remove such channels.

HEC-GeoRAS incorrectly assigned some levee locations. For nine cross sections (Rivers Station Number 59710, 51712, 49047, 48822, 47359, 46462, 35960, 34746, 34323), one levee point needed to be added, and was added in the levee table (Geometry Editor > Tables > Levees). Multiple other cross sections that only had one levee point (as they should), had the correct levee location but that location was incorrectly labeled (usually as the west levee when the location was actually the east levee). This problem was also corrected in the levee table.

HEC-RAS Model Calibration

After the geometry was established, the model was calibrated. Three series of streamflows were selected as calibration flows: a high, moderate, and low flow whose characteristics are outlined in Table 4-5 in Chapter 4.

The models were calibrated to water surface elevation instead of peak discharge, because the point of this study is to correlate river water surface elevation to groundwater depth. HEC-RAS outputs a lengthy list of parameters at each cross section, including water surface elevation. The coordinate system of the elevation is the same as the input geometry. After each run, a profile summary table was created that included the water surface elevation at five cross sections: the initial cross section (where the upstream

boundary condition of the Paseo hydrograph was applied), the cross section at the Alameda, Paseo, and Central bridges, and the final cross section where the downstream boundary condition. The upstream boundary condition was the Paseo computed discharge hydrograph. The downstream boundary condition was the Central stage measurement, converted to water surface elevation. Because the boundary condition is applied at the very last cross section located twelve hundred meters downstream from the Central bridge, the slope of the ground surface between the Central cross section and the final cross section was measured from the terrain model. The slope was used with the downstream reach length to calculate the difference in channel bottom elevation between the two cross sections, 0.97 meters. Therefore, 0.97 meters was subtracted from the water surface elevation measured at Central to calculate the water surface elevation at the final cross section.

The USGS selects an arbitrary location under the stream as the gage datum from which stage is measured; therefore, stage datum is where stage = 0. The location is identified by assigning various object an elevation in the gage datum. For example, for the Central gage, a USGS survey marker with a north arrow has been placed in the north sidewalk on the west side of the river. That survey marker has an elevation of 5.41 meters in the gage datum. There are three other markers for the Central gage that have elevations assigned to the gage datum in case one of the markers is destroyed. As described in Chapter Three, the elevation of several of these markers was surveyed in order to calculate the elevation of the gage datum in NAVD88. The elevation of the gage datums are listed in Table 3-2. The water surface elevation at each gage is then calculated by adding the stage measurement to the gage datum.

A series of Excel spreadsheets were developed to compare the HEC-RAS calculated water surface elevation with the measured water surface elevation. Because the Paseo hydrograph was utilized at the initial cross section, the travel time between the initial cross section and each gaging site was calculated (as a function of streamflow). The profile summary table from HEC-RAS is copied to the clipboard and pasted into one sheet of the appropriate Excel file. The Excel file calculates the difference between the HEC-RAS and USGS water surface elevations at each fifteen minute time step

(accounting for travel time), then averages the difference over all of the time steps. The model was calibrated to minimize the average difference at each cross section.

Appendix B: Data Sources

Bernalillo County has aerial photos of the entire county available online as SID files at http://www.bernco.gov/stage/departments.asp?dept=11410&submenuid=15992. A shapefile map of Bernalillo County was downloaded from the same website and brought into ArcGIS. The shapefile of the Rio Grande from the HEC-RAS model was brought into ArcGIS over the map. Then, the grid cells on the map that covered the river were selected with the selection tool. The grid cells included A14_SE, A15_SE, A15_SW, A16_NW, A16_SW, B14_NE, B14_SE, B14_SW, B15_NW, C14_NE, C14_NW, C14_SW, D13_NE, D13_SE, D13_SW, D14_NW, E12_SE, E13_NW, E13_SW, F12_NE, F12_NW, F12_SW, G12_NW, G12_SW, H11_SE, H12_NW, H12_SW, J11_NE, J12_NW, J12_SE, J12_SW, K12_NE, K13_NW, A16_NW. The SID files for these grid cells were downloaded from the Bernalillo County GIS ftp site (http://ims.bernco.gov/website/sid/06sid/). A16_NW was only downloaded once even though it was listed twice.

Appendix C: Program Codes

Visual Basic Program

This program was written by Steven Isaacson and is run from Excel. The user is asked for Excel workbooks. After all workbooks have been added, the user is asked to identify which sheets within the workbooks are to be used. The program creates an Excel sheet for temporarily storing the data; sheet info is copied into the workbook. The workbook searches all of the sheets data for unique date-time stamps (in a specific column) and outputs dbf or csv files with all the data for each time stamp. The output file is named the date-time stamp.

```
Dim DataFolderPath As String, TempHldgWbk As Workbook, WbkName As String
Dim CurrHldgSht As Worksheet, HldgShtCnt As Integer, HldgShtRowCnt As Long,
vrtHldgShtList() As Variant, Sht As Variant
Dim HldgDateListSht As Worksheet, HldgPivotSht As Worksheet, PTCol As Integer,
HldgPvtTbl As PivotTable, PvtName As String
Dim CurrDataSht As Worksheet, CurrDataShtRows As Long, PvtRng As Variant,
PvtRngCnt As Integer, DateListRng As Range
Dim FileDateList() As String, FileDateCnt As Integer, iDateCnt As Integer, FileDateCol
As Integer, DateNotFound As Boolean
Dim FirstRow As Long, LastRow As Long, LastShtRow As Long, iRow As Long, iCol
As Integer, iCnt As Integer, HldgShtCurrLn() As Long
Dim LblInfo() As Variant, C As Variant, DateColName As String, HldgShtTotRowCnt()
As Long
Dim DTFileWbk As Workbook, DTFileSht As Worksheet, DTFileLastRow As Integer,
DTFilePathName As String, DTFileFmt As String

Dim RC As Variant


Sub GenerateDateFiles()
```

```
Dim fd As FileDialog, fs As Object
Dim vrtSelectedItem As Variant

'   Remember the starting workbook
Set HomeWbk = ActiveWorkbook

'Create a FileDialog object as a File Picker dialog box.
Set fd = Application.FileDialog(msoFileDialogFilePicker)
Set fs = CreateObject("Scripting.FileSystemObject")

'  Get the list of workbooks to look in
NumBks = 0
Do
   fd.Filters.Clear
   With fd
      .Title = "Select Workbooks with Data Sheets"
      .Filters.Add "All Files", "*.*", 1
      .Filters.Add "Excel Workbooks", "*.xls", 2
      'Sets the initial file filter to number 2.
      .FilterIndex = 2
      .AllowMultiSelect = True
      If .Show = -1 Then
         'Step through each string in the FileDialogSelectedItems collection.
         For Each vrtSelectedItem In .SelectedItems
            'ScriptPath = vrtSelectedItem
            'MsgBox "The path is: " & vrtSelectedItem
            'Workbooks.Open (vrtSelectedItem)
            NumBks = NumBks + 1
            ReDim Preserve OpenWorkbooks(NumBks)
            Set OpenWorkbooks(NumBks) = Workbooks.Open(vrtSelectedItem)
```

```
            Next vrtSelectedItem
        'The user pressed Cancel.
        Else
            End
        End If
    End With

    RC = MsgBox("Look for more Workbooks?", vbYesNoCancel, "Find More
Workbooks")
    If RC = vbCancel Then          '  Stop the program
        End
    ElseIf RC = vbNo Then      '  Stop looking for workbooks
        Exit Do
    End If
  Loop       '  End of loop to find workbooks with data
  'Set the object variable to nothing.
  Set fd = Nothing


  '  Determine location for data files
  'Create a FileDialog object as a Folder Picker dialog box.
  Set fd = Application.FileDialog(msoFileDialogFolderPicker)

  fd.Filters.Clear
  With fd
    .Title = "Select Folder to Store Data (Date Files)"
    .AllowMultiSelect = False
    If .Show = -1 Then
      'Step through each string in the FileDialogSelectedItems collection.
      For Each vrtSelectedItem In .SelectedItems
```

```
            'MsgBox "The path is: " & vrtSelectedItem
            DataFolderPath = vrtSelectedItem
        Next vrtSelectedItem

    Else    '  The user pressed Cancel.
        End     '  Stop the program
    End If
End With

'  ----------------------------------------
'  Load Label info from the SetupInfo sheet
'     1st dim - Column
'     2nd dim -   1 = Column Letter
'                 2 = Column Number
'                 3 = Column Label
'                 4 = Include in output (boolean)
'                 5 = DateTime Key Field (boolean)
'  ----------------------------------------
HomeWbk.Activate
HomeWbk.Sheets("SetupInfo").Activate
Application.Goto Reference:="ColLayout"
HomeWbk.Sheets("SetupInfo").Range("ColLayout").Activate
iRow = ActiveCell.Row - 1

ReDim LblInfo(Range("ColLayout").Rows.Count,
Range("ColLayout").Columns.Count)
For Each C In Range("ColLayout")
    LblInfo(C.Row - iRow, C.Column) = C.Value
Next C
```

```
    '  ---------------------------------------
    '  Create the TempHldgWbk
    '  ---------------------------------------
    ChDir DataFolderPath
    WbkName = "TempData " & Format(Date, "ddmmmyyyy") & Format(Time, "HhNn")
    Set TempHldgWbk = Workbooks.Add
    With TempHldgWbk
       .Title = WbkName
       .Subject = "Temp Holding Workbook"
       .SaveAs Filename:=WbkName & ".xls"
    End With

    '  ---------------------------------------
    '  Process each data workbook
    '  ---------------------------------------
    HldgShtCnt = 0
    HldgShtRowCnt = 75000   '  Initialize value to cause sheet creation on first pass
    For Each WorkBk In OpenWorkbooks
       WorkBk.Activate

       '  Go through each sheet and verify if it is to be used
       For Each CurrDataSht In WorkBk.Sheets
          RC = MsgBox("Use sheet:  " & CurrDataSht.Name & Chr(10) & "From:  " &
WorkBk.Name, vbYesNoCancel, "Verify Data Sheet")
          If RC = vbCancel Then          '  Stop the program
             End
          ElseIf RC = vbYes Then      '  Process the sheet to copy the data to the holding
sheet
             CurrDataSht.Activate    '  Activate the data sheet to process
             CurrDataShtRows = Range("A3").SpecialCells(xlCellTypeLastCell).Row
```

```
        '  Check to see if CurrHldgSht can hold the data
        If HldgShtRowCnt + CurrDataShtRows - 2 > 65530 Then     ' 65530  Need to
create new holding sheet
            HldgShtCnt = HldgShtCnt + 1
            Set CurrHldgSht = TempHldgWbk.Sheets.Add
            With CurrHldgSht
                .Name = "HoldingSheet" & HldgShtCnt
            End With
            '  Add it to the list of holding sheets
            ReDim Preserve vrtHldgShtList(HldgShtCnt)
            Set vrtHldgShtList(HldgShtCnt) = CurrHldgSht

            '  Initialize HldgShtCurrLn array
            ReDim Preserve HldgShtCurrLn(HldgShtCnt)
            HldgShtCurrLn(HldgShtCnt) = 2
            ReDim HldgShtTotRowCnt(HldgShtCnt)

            '  Add labels to the new holding sheet
            CurrHldgSht.Activate
            For iCol = 1 To UBound(LblInfo, 1)
                Cells(1, iCol).Value = LblInfo(iCol, 3)
            Next iCol
            HldgShtRowCnt = 1   '  Reset the row count
        End If      '  Done creating new holding sheet

        CurrDataSht.Activate    '  Activate the data sheet to process
        Range(Cells(3, 1), Cells(CurrDataShtRows, 1)).EntireRow.Select
        Selection.Copy

        '  Paste in Holding Sheet
        CurrHldgSht.Activate
```

```
            Range(Cells(HldgShtRowCnt + 1, 1), Cells(HldgShtRowCnt + 1,
1)).EntireRow.Select

            'Selection.Insert Shift:=xlDown
            Selection.PasteSpecial Paste:=xlPasteValues, Operation:=xlNone, SkipBlanks
_
               :=False, Transpose:=False
            Selection.PasteSpecial Paste:=xlPasteFormats, Operation:=xlNone, _
               SkipBlanks:=False, Transpose:=False

            HldgShtRowCnt = HldgShtRowCnt + CurrDataShtRows - 2
         End If
      Next CurrDataSht    '  Finished with this data sheet

      WorkBk.Close SaveChanges:=False    '  Close the data workbook when done with
it
   Next WorkBk

   Application.ScreenUpdating = False     '  Turn off screen updating to speed up the
macro

   '  ---------------------------------------
   '  Process the data in the holding sheets
   '  ---------------------------------------

   '  First collect a list of FileDates from all the dates in the sheets
   FileDateCnt = 0

   TempHldgWbk.Activate
   Set HldgDateListSht = TempHldgWbk.Sheets.Add
   HldgDateListSht.Name = "DateList"
```

```
    Set HldgPivotSht = TempHldgWbk.Sheets.Add
    HldgPivotSht.Name = "PivotHoldingSht"
    PTCol = 1
    '   Find key date column name from label info
    For iCol = 1 To UBound(LblInfo, 1)
        If LblInfo(iCol, 5) = True Then
            DateColName = LblInfo(iCol, 3)
            FileDateCol = LblInfo(iCol, 2)
            Exit For
         End If
    Next iCol
    If DateColName = "" Then
        Application.ScreenUpdating = True      '   Turn on screen updating
        RC = MsgBox("No 'Key DateTime Field' was marked as TRUE on the SetupInfo
sheet.  The column to use as the key field must be marked.", _
            vbExclamation, "Key DateTime Field Unknown ")
        End
    End If

    PvtRngCnt = 1
    Set PvtRng = Nothing

    For Each Sht In vrtHldgShtList
        Sht.Activate
        LastShtRow = Range("A1").SpecialCells(xlCellTypeLastCell).Row
        PvtName = Sht.Name & "Pvt"

        Range("A1").Select
        Range(Selection, ActiveCell.SpecialCells(xlLastCell)).Select
        Set PvtRng = Selection
```

```
TempHldgWbk.PivotCaches.Add(SourceType:=xlDatabase, SourceData:= _
    PvtRng).CreatePivotTable TableDestination:=HldgPivotSht.Cells(3, PTCol), _
    TableName:=PvtName, DefaultVersion:=xlPivotTableVersion10
Set HldgPvtTbl = HldgPivotSht.PivotTables(PvtName)
HldgPvtTbl.AddFields RowFields:=DateColName
HldgPvtTbl.PivotFields("DateTime").Orientation = xlDataField

HldgPivotSht.Activate
'  Copy the DateTime list
HldgPvtTbl.RowRange.Select
Selection.Copy

'  Add the new holding sheet datetime list to the master list
HldgDateListSht.Activate
Range("A1").Select
If ActiveCell.Value = "" Then
    ActiveSheet.Paste
    Range("A1").Select
    Selection.End(xlDown).Select
    ActiveCell.EntireRow.Delete     '  Delete the Grand Total Line
Else
    Selection.End(xlDown).Select
    'ActiveCell.SpecialCells(xlLastCell).Select
    ActiveCell.Offset(1, 0).Select
    iRow = ActiveCell.Row

    ActiveSheet.Paste
    Range("A1").Select
    Selection.End(xlDown).Select
    ActiveCell.EntireRow.Delete     '  Delete the Grand Total Line
```

```
        Cells(iRow, 1).Select
        ActiveCell.EntireRow.Delete     '   Delete the extra Header
    End If
    PTCol = PTCol + 4   '   Increment offset column for placing pivot tables
Next Sht


'   Do a final pivot to get the final list
PTCol = 4
HldgDateListSht.Activate
PvtName = "FinalDateList"

Range("A1").Select
Range(Selection, Selection.End(xlDown)).Select
Set PvtRng = Selection

TempHldgWbk.PivotCaches.Add(SourceType:=xlDatabase, SourceData:= _
    PvtRng).CreatePivotTable TableDestination:=HldgDateListSht.Cells(3, PTCol), _
    TableName:=PvtName, DefaultVersion:=xlPivotTableVersion10
Set HldgPvtTbl = HldgDateListSht.PivotTables(PvtName)
HldgPvtTbl.AddFields RowFields:=DateColName
HldgPvtTbl.PivotFields("DateTime").Orientation = xlDataField

HldgPvtTbl.RowRange.Select
Set DateListRng = Selection

'   Store the DateList in the array
iRow = ActiveCell.Row

ReDim FileDateList(DateListRng.Rows.Count - 2)
For Each C In DateListRng
```

```
    If C.Row <> iRow And C.Row <> (iRow + DateListRng.Rows.Count - 1) Then
        FileDateList(C.Row - iRow) = C.Value

        'FileDateCnt = FileDateCnt + 1
    End If
Next C



'   ----------------------------------------
'   Load FileFormat info from the SetupInfo sheet
'       1st dim - Column
'       2nd dim -   1 = Format Text
'                   2 = Use in output (boolean)
'   ----------------------------------------
HomeWbk.Activate
HomeWbk.Sheets("SetupInfo").Activate
' Application.Goto Reference:="ExpFileFormat"
HomeWbk.Sheets("SetupInfo").Range("ExpFileFormat").Activate

For Each C In Range("ExpFileFormat")
    If C.Value = True Then
        DTFileFmt = Cells(C.Row, 1).Value
        Exit For
    End If
Next C



'   ------------------------------------------------
'   Sort the sheets by the key field
'   ------------------------------------------------
```

```
    For Each Sht In vrtHldgShtList
        Sht.Activate
        HldgShtCnt = Right(Sht.Name, Len(Sht.Name) - 12)

        Range("A1").Select
        Range(Selection, ActiveCell.SpecialCells(xlLastCell)).Select
        Selection.Sort Key1:=Range(Cells(1, FileDateCol), Cells(1, FileDateCol)),
Order1:=xlAscending, Header:=xlYes, _
            OrderCustom:=1, MatchCase:=False, Orientation:=xlTopToBottom, _
            DataOption1:=xlSortNormal

        Range("A1").Select
        ActiveCell.SpecialCells(xlLastCell).Select
        HldgShtTotRowCnt(HldgShtCnt) = Selection.Row

    Next Sht

    '  ---------------------------------------------------
    '  Process the list of FileDates, writing each file
    '  ---------------------------------------------------
    ChDir DataFolderPath        '  Make sure data folder is the current path
    For FileDateCnt = 1 To UBound(FileDateList)

        WbkName = FileDateList(FileDateCnt)
        Set DTFileWbk = Workbooks.Add

        Set DTFileSht = DTFileWbk.Sheets.Add
            With DTFileSht
                .Name = FileDateList(FileDateCnt)
            End With
```

```
    '   Add labels to the new holding sheet
    DTFileSht.Activate
    For iCol = 1 To UBound(LblInfo, 1)
       Cells(1, iCol).Value = LblInfo(iCol, 3)
    Next iCol
    DTFileLastRow = 1   '   Reset the row count

    '   Process each holding sheet to copy matching rows
    For Each Sht In vrtHldgShtList
       Sht.Activate
       HldgShtCnt = Right(Sht.Name, Len(Sht.Name) - 12)
       'Range("A1").End(xlDown).Select
       'LastShtRow = Selection.Row

       For iRow = HldgShtCurrLn(HldgShtCnt) To HldgShtTotRowCnt(HldgShtCnt)
          Sht.Activate
          If Sht.Cells(iRow, FileDateCol).Value = FileDateList(FileDateCnt) Then      '
Row is a match

             Sht.Cells(iRow, FileDateCol).EntireRow.Select
             Selection.Copy

             '   Paste in Date File Sheet
             DTFileSht.Activate
             Range(Cells(DTFileLastRow + 1, 1), Cells(DTFileLastRow + 1,
1)).EntireRow.Select

             Selection.PasteSpecial Paste:=xlPasteValues, Operation:=xlNone,
SkipBlanks _
                :=False, Transpose:=False
             Selection.PasteSpecial Paste:=xlPasteFormats, Operation:=xlNone, _
```

```
                SkipBlanks:=False, Transpose:=False

                DTFileLastRow = DTFileLastRow + 1
            ElseIf Sht.Cells(iRow, FileDateCol).Value > FileDateList(FileDateCnt) Then
'   Row is higher than data file date
                HldgShtCurrLn(HldgShtCnt) = iRow
                Exit For        '   Go to the next sheet
            End If

        Next iRow
    Next Sht    '   Data additions complete

    '   Delete Unneeded Columns
    For iCol = UBound(LblInfo, 1) To 1 Step -1
        DTFileSht.Activate

        If LblInfo(iCol, 4) = False Then    '   Do not keep column
            Cells(1, iCol).EntireColumn.Select
            Selection.Delete
        End If
    Next iCol
    '   To change the selection and widen the columns to fit for dbf
    Range("A1").Select
    Range(Selection, ActiveCell.SpecialCells(xlLastCell)).Columns.AutoFit
    Range("A1").Select


    '   Save and close the date file
    If DTFileFmt = "CSV" Then
        DTFilePathName = DataFolderPath & "\" & WbkName & ".csv"
```

```
            DTFileWbk.SaveAs Filename:=DTFilePathName, FileFormat:=xlCSV,
CreateBackup:=False
            DTFileWbk.Close SaveChanges:=True
        ElseIf DTFileFmt = "DBF4" Then
            DTFilePathName = DataFolderPath & "\" & WbkName & ".dbf"
            DTFileWbk.SaveAs Filename:=DTFilePathName, FileFormat:=xlDBF4,
CreateBackup:=False
            DTFileWbk.Close SaveChanges:=False
        End If
    Next FileDateCnt



    Application.ScreenUpdating = True


    '   Close data workbooks
    TempHldgWbk.Close SaveChanges:=True


End Sub
```

Python Codes

These python codes are used to combine the groundwater, surface water, and riverside drains. Because of a file-sharing problem with Arc, the first code interpolates banklines from the HEC-RAS surfaces and creates a TIN from the groundwater and riverside drain data. The second code adds the banklines to the TIN. TINs are named based on the date-time stamp.

Python Code I

```
#!c:\Python24\python.exe
"""Documentation HERE"""

__author__ = 'Kelly Isaacson <kisaac@unm.edu>'
__date__ = 'October 22, 2008'
__version__ = '1.0'
```

```
# Import system modules
import sys
import os
import tempfile

# Import ArcGIS module
import arcgisscripting

try:
    # Create the Geoprocessor object
    gp = arcgisscripting.create()

    # Check out any necessary licenses
    gp.CheckOutExtension("3D")

    # Script arguments...
    tin_dir = sys.argv[1]
    gw_dir = sys.argv[2]
    output_dir = sys.argv[3]
    banklines = sys.argv[4]
    riverside_drains = sys.argv[5]


    # Setup ouput subdirectories.
    tin_out = os.path.join(output_dir, 'tins')
    raster_out = os.path.join(output_dir, 'raster')
    bank_out = os.path.join(output_dir, 'banklines_3d')
    gw_out = os.path.join(output_dir, 'gw_out')

    sub_dirs = [tin_out, raster_out, bank_out, gw_out]
    for sdir in sub_dirs:
        if not os.path.isdir(sdir):
            os.mkdir(sdir)

    # Constants
    Spatial_Reference =
"PROJCS['NAD_1983_StatePlane_New_Mexico_Central_FIPS_3002_Feet',GEOGCS['
GCS_North_American_1983',DATUM['D_North_American_1983',SPHEROID['GRS_1
980',6378137.0,298.257222101]],PRIMEM['Greenwich',0.0],UNIT['Degree',0.01745329
25199433]],PROJECTION['Transverse_Mercator'],PARAMETER['False_Easting',16404
16.666666667],PARAMETER['False_Northing',0.0],PARAMETER['Central_Meridian',-
106.25],PARAMETER['Scale_Factor',0.9999],PARAMETER['Latitude_Of_Origin',31.0]
,UNIT['Foot_US',0.3048006096012192]]"


    # Output files will be silently overwriten, unless locked by an Arc*
```

```
# instance.
gp.overwriteoutput = True

gp.workspace = tin_dir

# Iterate Process
input_tins = gp.ListDatasets("*", "TIN")
tin = input_tins.next()
while tin:
   # Get timestamp
   base_name = '_'.join(tin.split())
   base_name = ''.join([base_name[:5], base_name[-7:]])

   # Local variables...
   gw_dbf = os.path.join(gw_dir, '.'.join([base_name, 'dbf']))
   output_raster = os.path.join(raster_out,
                                ''.join([base_name, 'r']))
   output_tin = os.path.join(tin_out,
                             '_'.join([base_name, 'tin']))

   # Setup temp files.
   bank_lines_3d = os.path.join(bank_out,
                                '_'.join([base_name, 'bl3d']))
   gw_points = "gw_points"
   gw_output_points = os.path.join(gw_out,

      '_'.join([base_name, 'gw']))

   # Create new tin.
   gp.createtin_3d(output_tin,
               Spatial_Reference)

   # Process: Make XY Event Layer...
   gp.MakeXYEventLayer_management(gw_dbf,
                                  "EASTING", "NORTHING",
                                  gw_points, Spatial_Reference)
   gp.SaveToLayerFile(gw_points, gw_output_points)

   # Process: Interpolate Shape...
   gp.interpolateshape_3d(tin, banklines, bank_lines_3d, "", "", "LINEAR", "true")


   # Process: Edit TIN...
   gp.edittin_3d(output_tin, "%s WSE <None> masspoints" % gw_points)
   gp.edittin_3d(output_tin, "%s Shape <None> hardline true" % riverside_drains)
   gp.edittin_3d(output_tin, "%s Shape <None> hardline true" % bank_lines_3d)
```

```
        # Process: TIN to Raster...
        gp.tinraster_3d(output_tin, output_raster,
                        "FLOAT",
                        "LINEAR", "CELLSIZE 10", "")


        tin = input_tins.next()
except:
    print gp.GetMessages()
    raise
```

Python Code II

```
#!c:\Python24\python.exe
"""This is a model built by Jed Frechette and Kelly Isaacson at the University of New
Mexico to combine groundwater well points, river surface water elevations, and riverside
drain elevation data.
A model was built in ArcMap's Model Builder that incorporated the major functions of
the program, which was then exported to a Python Script.  It has been modified for two
primary purposes:
1) to iterate through a folder of input water surface tins
2) to name output files based on input files names
The model combines surface water and groundwater data based on the names of the input
files, which should both be named in the format [DDMMMYYYY HHMM].
Presently, the riverside drains component of the surface water is a constant variable in the
model, although this will like change as data about the water level in the riverside drains
is obtained."""

__author__ = 'Kelly Isaacson <kisaac@unm.edu>'
__date__ = 'October 22, 2008'
__version__ = '1.0'

# Import system modules
import sys
import os
# Import ArcGIS module
import arcgisscripting

def prepare_data(tin_dir, gw_dir, output_dir, banklines, riverside_drains):


        # Setup ouput subdirectories.
    tin_out = os.path.join(output_dir, 'tins')
    raster_out1 = os.path.join(output_dir, 'WSraster')
    raster_out2 = os.path.join(output_dir, 'ClippedWSraster')
```

```
raster_out3 = os.path.join(output_dir, 'D2GWraster')
bank_out = os.path.join(output_dir, 'banklines_3d')
gw_out = os.path.join(output_dir, 'gw_out')

sub_dirs = [tin_out, raster_out1, raster_out2, raster_out3, bank_out, gw_out]
for sdir in sub_dirs:
    if not os.path.isdir(sdir):
        os.mkdir(sdir)

try:
    # Create the Geoprocessor object
    gp = arcgisscripting.create()
    # Check out any necessary licenses
    gp.CheckOutExtension("3D")
    gp.CheckOutExtension("Spatial")

    # Output files will be silently overwriten, unless locked by an Arc*
    # instance.
    gp.overwriteoutput = True

    gp.workspace = tin_dir

    # Get list of input TINS.
    input_tins = gp.ListDatasets("*", "TIN")
    tin = input_tins.next()
    output_list = []
    while tin:
        # Get timestamp
        base_name = '_'.join(tin.split())
        base_name = ''.join([base_name[:5], base_name[-7:]])

        # Local variables...
        gw_dbf = os.path.join(gw_dir, '.'.join([tin, 'dbf']))
        output_raster = os.path.join(raster_out1,
                                     ''.join([base_name, 'r']))
        output_tin = os.path.join(tin_out,
                                  '_'.join([base_name, 'tin']))
        clip_raster = os.path.join(raster_out2,
                                   ''.join([base_name, 'c']))
        d2gw_raster = os.path.join(raster_out3,
                                   ''.join([base_name, 'd']))
        d2gw_m_raster = os.path.join(raster_out3,
                                   ''.join([base_name, 'm']))
        d2gw_mSN_raster = os.path.join(raster_out3,
                                   ''.join([base_name, 's']))
```

```
            # Setup temp files.
            bank_lines_3d = os.path.join(bank_out,
                                 '_'.join([base_name, 'bl3d']))
            gw_points = base_name
            gw_output_points = os.path.join(gw_out,
                                  '_'.join([base_name, 'gw']))

            # Process: Interpolate Shape...
            gp.OutputMFlag = "DISABLED"
            gp.interpolateshape_3d(tin, banklines, bank_lines_3d, "", "1", "LINEAR",
"DENSIFY", "0")

            # Process: Make XY Event Layer...
            gp.MakeXYEventLayer_management(gw_dbf,
                                  "EASTING", "NORTHING",
                                  gw_points, SPATIAL_REFERENCE)
            gp.SaveToLayerFile(gw_points, gw_output_points)

            output_list.append((output_tin,
                        gw_output_points,
                        riverside_drains,
                        bank_lines_3d,
                        output_raster,
                        clip_raster,
                        d2gw_raster,
                        d2gw_m_raster,
                        d2gw_mSN_raster,
                        base_name))
            tin = input_tins.next()
        except:
            print gp.GetMessages()
            raise
        return output_list

def create_dtms(tin_dir,
                output_tin,
                gw_points,
                riverside_drains,
                bank_lines_3d,
                output_raster,
                clip_raster,
                d2gw_raster,
                d2gw_m_raster,
                d2gw_mSN_raster,
                clip_area,
                terrain_model):
```

```
try:
    # Create the Geoprocessor object
    gp = arcgisscripting.create()

    # Check out any necessary licenses
    gp.CheckOutExtension("3D")
    gp.CheckOutExtension("Spatial")

    # Output files will be silently overwriten, unless locked by an Arc*
    # instance.
    gp.overwriteoutput = True

    gp.workspace = tin_dir

    # Create new tin.
    gp.createtin_3d(output_tin,
                    SPATIAL_REFERENCE)

    # Process: Edit TIN...
    gp.edittin_3d(output_tin, "%s.lyr WSE <None> masspoints" % gw_points)
    gp.edittin_3d(output_tin, "%s Shape <None> masspoints true" % riverside_drains)
    gp.edittin_3d(output_tin, "%s.shp Shape <None> hardline true" % bank_lines_3d)

    # Process: TIN to Raster...
    # This is by far the slowest part of the script.
    gp.tinraster_3d(output_tin, output_raster,
                    "FLOAT",
                    "LINEAR", "CELLSIZE 3", "")

    #Process: Clip raster by levees
    gp.ExtractbyMask_sa(output_raster, clip_area, clip_raster)

    #Process: Calculate depth to groundwater by subtracting water surface from terrain
model
    gp.Minus_sa(terrain_model, clip_raster, d2gw_raster)

    #Process: Convert depth to groundwater to meters
    gp.Times_sa(d2gw_raster, 0.3048, d2gw_m_raster)

    #Process: Set Null artificial high values of depth to groundwater
    gp.setnull_sa(output_raster, output_raster, d2gw_mSN_raster, VALUE > 10 )



    #Process:
```

```
    except:
        print gp.GetMessages()
        raise

def get_depth2gw(base_name, gw_surface, riparian, terrain):
    # gw_surface2 = clip(gw_surface, raparian)
    # depth2gw = terrain - gw_surface2
    # return depth2gw
    pass

# Constants
SPATIAL_REFERENCE =
"PROJCS['NAD_1983_StatePlane_New_Mexico_Central_FIPS_3002_Feet'"\

",GEOGCS['GCS_North_American_1983',DATUM['D_North_American_1983'"\

",SPHEROID['GRS_1980',6378137.0,298.257222101]],PRIMEM['Greenwich'"\
                ",0.0],UNIT['Degree',0.0174532925199433]],PROJECTION["\
                "'Transverse_Mercator'],PARAMETER['False_Easting',"\
                "1640416.666666667],PARAMETER['False_Northing',0.0]"\
                ",PARAMETER['Central_Meridian',-106.25],PARAMETER['"\
                "Scale_Factor',0.9999],PARAMETER['Latitude_Of_Origin'"\
                ",31.0],UNIT['Foot_US',0.3048006096012192]]"

OUTPUT_VARS = prepare_data(sys.argv[1],
                    sys.argv[2],
                    sys.argv[3],
                    sys.argv[4],
                    sys.argv[5])

for OUTPUT_TIN, GW_OUTPUT_POINTS, RIVERSIDE_DRAINS,
BANK_LINES_3D, OUTPUT_RASTER, CLIP_RASTER, D2GW_RASTER,
D2GW_M_RASTER, D2GW_MSN_RASTER, BASE_NAME\
    in OUTPUT_VARS:
    create_dtms(sys.argv[1],
            OUTPUT_TIN,
            GW_OUTPUT_POINTS,
            RIVERSIDE_DRAINS,
            BANK_LINES_3D,
            OUTPUT_RASTER,
            CLIP_RASTER,
            D2GW_RASTER,
            D2GW_M_RASTER,
            D2GW_MSN_RASTER,
            sys.argv[6],
            sys.argv[7])
```

```
#get_depth2gw(BASE_NAME, OUTPUT_RASTER, sys.argv[6], sys.argv[7])

print "Finished processing %s" % OUTPUT_TIN
```

References Cited

Bari, M, Smetten KRJ. (2004). Modelling monthly runoff generation processes following land use changes: groundwater-surface runoff interactions. Hydrology and Earth Systems Sciences, 8(5), 903-922.

Bates, P.D. (2004). Computationally efficient modeling of flood inundation Extent. Hydrological risk, A. Brath, A. Montanari, and E. Toth, eds., Cosenza, I: BIOS, 285–301.

Beauchamp, Vanessa, Stromberg, Juliet. (2007). Flow regulation of the Verde River, Arizona encourages Tamarix recruitment but has minimal effect on Populus and Salix stand density. Wetlands, 27(2), 381-389.

Bexfield, Laura M, McAda, Douglas. (2003). Simulated Effects of Ground-Water Management Scenarios on the Santa Fe Group Aquifer System, Middle Rio Grande Basin, New Mexico. USGS Water-Resources Investigations Report 03-4040.

Bhattacharjee, Joydeep, Taylor, John, Smith, Loren. (2006). Controlled flooding and staged drawdown for restoration of native Cottonwoods in the Middle Rio Grande Valley, New Mexico, USA. Wetlands, 26(3), 691-702.

Buckley, S. J., Howell, J. A., Enge, H. D., & Kurz, T. H. (2008). Terrestrial laser scanning in geology; data acquisition, processing and accuracy considerations. Journal of the Geological Society of London, 165(3), 625-638.

Burt, C.M., Mutzinger, A.J., Allen, R.G., Howell, T.A. (2005). Evaporation Research: Review and Interpretation. Journal of Irrigation and Drainage Engineering, 131(1), 37-58.

Camp Dresser and McKee. (2001). Evaluation of Integrated Surface Water and Groundwater Modeling Tools. Report for CDM Water Resources Research and Development Program.

Castellarin A., Di Baldassarre, G., Bates, P.D., Brath, A. (2009). Optimal Cross-Sectional Spacing in Preissmann Scheme 1D Hydrodynamic Models. Journal of Hydraulic Engineering, 135(2), 96-105.

Courault, Dominique, Seguin, Bernard, Olioso, Albert. (2005). Review on estimation of evapotranspiration from remote sensing data: From empirical to numerical modeling approaches. Irrigation and Drainage Systems, 19(3-4), 223-249.

Ellis, Lisa, Molles, Manuel, Crawford, Clifford. (1999). Influence of experimental flooding on litter dynamics in a Rio Grande riparian forest, New Mexio. Restoration Ecology, 7(2), 193-204.

Etlantus, Alandren. (2007). Comparison of remote sensing methods to estimate evapotranspiration, Middle Rio Grande riparian corridor, New Mexico. M.S. Thesis, University of New Mexico.

Gardner, W.R. (1958). Some steady-state solutions of the unsaturated moisture flow equation with application to evaporation from a water table. Soil Science, 85, 228-232.

Gavilán, Pedro, Estévez, Javier, Berengena Joaquín. (2008). Comparison of standardized reference evapotranspiration equations in southern Spain. Journal of Irrigation and Drainage Engineering, 134(1), 1-12.

Hurd, Brian, Coonrod, Julie. (2007). Climate change and its implications for New Mexico's water resources and economic opportunities. Prepared for the National Commission on Energy Policy.

Horton, Jonathan, Kolb, Thomas, Hart, Stephen (2001). Physiological response to groundwater depth varies among species and with river flow regulation. Ecological Applications, 11(4), 1046-1069.

Hughes, Joseph, Liu, Jie. (2008). MIKE SHE: Software for Integrated Surface Water/Groundwater Modeling. Groundwater, 46 (6), 797-802.

Illangasekare, Tissa, Prucha, Robert. (2001). MIKE SHE Code Verification and Validation for RFETS Site-wide Water Balance Model. Report for Kaiser-Hill Company, L.L.C.

Intergovernmental Panel on Climate Change. Climate Change Report 2007: Synthesis Report. AR4. (2007).

Ivkovic, KM, Letcher, RA, and Croke, BFW. (2009). Use of a simple surface-groundwater interaction model to inform water management. Australian Journal of Earth Sciences, 56, 71-80.

Jackson, Robert, Carpenter, Stephen, Dahm, Clifford, McKnight, Diane, Naiman Robert, Postel, Sandra, Running, Steven. (2001). Issues in Ecology Technical Report: Water in a changing world. Ecological Applications, 11(4), 1027-1045.

Jury, William, Horton, Robert. (2004). Soil Physics. John Wiley & Sons: New Jersey. Pg 96.

Kinzel, Paul J, Wright, C Wayne, Nelson, Jonathan M., Burman, Aaron R. (2007). Evaluation of an experimental LiDAR for surveying a shallow, braided, sand-bedded river. Journal of Hydraulic Engineering, 133(7), 838-842.

Lines, Gregory. (1999). Health of native riparian vegetation and its relation to hydrologic conditions along the Mojave River, Southern California. USGS 99-4112.

Marks, JS. (2006). Taking the public seriously: the case of potable and non potable reuse Presented at the International Conference on Integrated Concepts on Water Recycling, Wollongong, NSW Australia, 14-17 February 2005. Desalination, 187 (1-3), 137-147.

MacClune, Karen L., Barth, Gilbert, Shafike, Nabil, Hathaway, Deborah. (2006). High-Resolution Groundwater Models for the Assessment of Riparian Restoration Options and River Conveyance Efficiency. MODFLOW and More 2006: Managing Ground-Water Systems - Conference Proceedings Paper. www.mines.edu/igwmc

McAda, Douglas, Barroll, Peggy. (2002). Simulation of Groundwater flow in the Middle Rio Grande Basin between Cochiti and San Acacia, New Mexico. USGS Water Resources Investigations Report 02-4200.

Merwade, Venkatesh, Cook, A, Coonrod Julie. (2008). GIS techniques for creating river terrain models for hydrodynamic modeling and flood inundation mapping. Environmental Modelling & Software, 23(10-11), 1300-1311.

Merwade, Venkatesh, Maidment, David, Goff, John. (2006). Anisotropic considerations while interpolating river channel bathymetry. Journal of Hydrology, 331, 731-741.

Merwade, Venkatesh, Maidment, David, Hodges, Ben. (2005). Geospatial Representation of River Channels. Journal of Hydrologic Engineering, 10(3), 243-251.

Nichols, William. (2000). Regional Groundwater Evapotranspiration and Groundwater Budgets, Great Basin, Nevada. US Geological Survey Professional Paper 1628.

Nordin, Carl. (1964). Aspects of Flow Resistance and Sediment Transport Rio Grande Near Bernalillo New Mexico. USGS WSP 1498-H

Ortiz, Richard (2004). A River in Transition: Geomorphic and Bed Sediment Response to Cochiti Dam on the Middle Rio Grande, Bernalillo to Albuquerque, NM. M.S Thesis. University of New Mexico.

Postel, Sandra. (2000). Entering an era of water scarcity: the challenges ahead. Ecological Applications, 10(4), 941-948.

Rantz, S.E. (1982). Measurement and Computation of Streamflow. USGS Water Supply Paper 2175. Washington D.C.

Rassam, D, Pagendam, D, Hunter H. (2008). Conceptualisation and application of models for groundwater-surface water interactions and nitrate attenuation potential in riparian zones. Environmental Modeling & Software, 23, 859-875.

Rodriguez, Leticia, Cello, Pablo, Vionnet, Carlos. (2008). Fully conservative coupling of HEC-RAS with MODFLOW to simulate stream-aquifer interactions in a drainage basin. Journal of Hydrology, 353, 129-142.

Sahoo, G.B and Ray, C. (2006). Flow forecasting for a Hawaii stream using rating curves and neural networks. Journal of Hydrology, 317, 63-80.

Seiber, George and Roark, Mike. Personal communication. July 2008 – Oct 2008.

SS Papadopulous & Associates. Assessment of flow conditions and seepage on the Rio Grande and adjacent channels, Isleta to San Marcial, Summer 2001. S.S Papadopulous & Associates, Inc. Boulder, CO.

Stormont, John, Farfan, Enrique, and Coonrod, Julie. Total soil water evaporation in a riparian environment: model development and application. Journal of Hydrologic Engineering, posted ahead of print at ascelibrary.aip.org

Stromberg, Julie, Chew M.K. (2002). Flood Pulses and Restoration of Riparian Vegetation in the American Southwest. Middleton, Beth ed. Flood Pulsing in Wetlands. John Wiley & Sons Inc. New York. 11-42.

Sturm, Terry. (2001). Open Channel Hydraulics. McGraw-Hill Water Resources and Environmental Engineering Series, New York. 512 pages.

Tetra Tech, Inc. (2004). Upper Rio Grande Water Operations Review FEIS Appendix J: FLO-2D and Surface Water/ Groundwater Model. 102 pages.

Torrez, Hugo Enrique Farfan. (2007). Estimating Soil Water Evaporation Using Nonlinear Inverse Theory. PhD Dissertation, University of New Mexico.

Webb, Robert, Leake, Stanley, Turner, Raymond. (2007). The Ribbon of Green: Change in Riparian Vegetation in the Southwestern United States. The University of Arizona Press: Tuscon, AZ.

Werner, Adrian, Gallagher, Mark, Weeks, Scott. (2006). Regional-scale, fully coupled modeling of stream-aquifer interaction in a tropical catchment. Journal of Hydrology, 328, 497-510.

Wilcox, Laura Jean, Bowman, Robert S., Shafike, Nabil G. (2007). Evaluation of Rio Grande Management Alternatives Using a Surface-Water/Groundwater Model. Journal of the American Water Resources Association, 43 (6), 1595-1603.

Wright, C Wayne, Brock, John C. (2002). EAARL: A LiDAR for mapping shallow coral reefs and other coastal environments. Seventh International Conference on Remote Sensing for Marine and Coastal Environments. Miami FL

Vörösmarty, Charles, Green, Pamela, Salisbury, Joseph, Lammers, Richard. (2000). Global Water Resources: Vulnerability from Climate Change and Population Growth. Science, 289, 284-288.

Yan, Z., Lu W, Long Y, Li, P. (2009). Application and comparison of two prediction models for groundwater levels: A case study in Western Jilin Province, China. Journal of Arid Environments, 73, 487-492.

Yang, Jie, Townsend, Ronald, Daneshfar, Bahram. (2006). Applying the HEC-RAS model and GIS techniques in river network floodplain delineation. Canadian Journal of Civil Engineering, 33, 19-28.